Hydrochemical Signatures of Glacial Meltwater on Volcán Chimborazo, Ecuador

A Thesis
SUBMITTED TO THE FACULTY OF
UNIVERSITY OF MINNESOTA
BY

Rachel T. McLaughlin

IN PARTIAL FULFILLMENT OF THE REQUIREMENTS
FOR THE DEGREE OF
Masters of Science

Gene-Hua Crystal Ng, Andrew Wickert

November 2017

Acknowledgements

While a thesis may stand as a piece of individual research, no research is accomplished in a vacuum. As such I would like to express my sincere gratitude to the numerous people who have contributed to and supported my Masters work.

To all three of my advisers on this project— Crystal (Gene-Hua) Ng, Andy Wickert, and Jeff La Frenierre— I would like to say thank you for your unending patience and encouragement. To Jeff, our fearless leader in the field, thank you for taking me to new heights (literally) and challenging me both physically and intellectually. Andy, I never thought I would learn to solder in grad school. Thank you for broadening my experience in countless ways and helping me overcome many GIS challenges. Lastly (but not least-ly), Crystal, I am incredibly grateful for your compassionate guidance, moral and academic support, and trust in my capabilities. Your input and feedback have been invaluable to my learning and research.

I would additionally like to thank Michel Baraer, for not only sharing his model with me, but also providing a great deal of technical and academic support.

Many thanks to Helen Thompson for sharing her water samples, Casey Decker and Abigail Michels for their field assistance, Jeff Jeremiason and Chris Harmes for laboratory analysis training and support, Scott Alexander for laboratory support, and Chad Sandell for field and laboratory assistance. Thank you to Josh Zoellmer for his many contributions to the landcover mapping enterprise. Also, I would like to acknowledge the University of Minnesota and the Walter H. Judd Fellowship for providing financial support for this project.

Finally, thank you to my friends in the Department of Earth Sciences for being an amazing community, to my parents for their love and well considered advice, and to my partner, Robert Zwirner, who has been unwavering in his support of all my endeavors.

Abstract

Glacier recession in the tropical Andes is generating significant concern over future water availability for domestic use, irrigation, and hydropower. Sparse data sets, extreme heterogeneity in climate patterns, and the limited understanding of groundwater and ecohydrological processes in these catchments make predicting the hydrologic response to glacier retreat difficult. Here I examine a glaciated watershed on Volcán Chimborazo, Ecuador. I use geospatial analysis and recent geologic studies to evaluate the vegetation and geologic factors that influence the hydrologic response of the watershed. Additionally, I utilize hydrochemical and stable isotope signatures to investigate how melt and groundwater contributions to streamflow have changed over time along with possible meltwater-groundwater connections. A new landcover map of Volcán Chimborazo, generated using object based image analysis, reveals a significant increase in the upper limit of vegetation on the mountain and expansion of crop and pasture land since 1978. Geologic cross-sections, based on recent studies, show that near surface geology is dominated by glacial deposits and underlain by relatively young volcanic bedrock. Results from a hydrochemical mixing model (HBCM) combined with discharge measurements reveal spatial variability in groundwater discharge and suggest that groundwater discharge during the dry season has decreased from 2012-2017. Short time scale variability is clearly influenced by precipitation, but long-term discharge trends remain uncertain. Lastly, stable isotope and solute concentrations in samples suggest groundwater in the study watershed is recharged by precipitation falling at high elevations where ice and snow may dominate the hydrologic system.

Table of Contents

List of Figures

List of Tables

List of Appendices

Chapter 1: Introduction

Mountain watersheds are an important source of fresh water (Messerli et al. 2004; Barnett et al. 2005; Kaser et al. 2010) acting as headwaters to rivers serving over 700 million people worldwide (Messerli et al. 2004). These watersheds are particularly key in the semi-arid to arid tropical regions, where up to 80% of freshwater supplies originate in the mountains (Messerli 2001; Vuille et al. 2008). In alpine catchments, snowpack and glaciers tend to dominate the hydrology and help buffer the hydrologic system on interannual time scales, but these water stores are sensitive to climate change (Lemke et al. 2007). In response warming temperatures and shifting precipitation patterns mountain glaciers are receding at accelerated rates (Bradley 2006; IPCC 2014) and nowhere is this truer than the tropics. Tropical glaciers are especially sensitive to climate change (Hastenrath 1994; Kaser & Ostmaston 2002) and at high risk, with some climate models predicting the greatest warming to occur at low-latitudes and high elevations (Bradley 2006). 99% of all tropical glaciers are located in the Andes (Kaser 1999), concentrated in the countries of Bolivia (20%), Peru (70%), Ecuador (4%), and Columbia and Venezuela (combined 4%) (Rabatel et al. 2013). Many studies have already documented pronounced melting of Andean glaciers (Ramírez et al. 2001; Wagnon et al. 2001; Rhoades et al. 2008; Rabatel et al. 2013; La Frenierre & Mark 2017) and observed decreasing discharge from their catchments (Mark & Seltzer 2003; Baraer et al. 2012; Rabatel et al. 2013). It is predicted that mountain glacier recession and the resulting hydrologic changes will have negative societal, economic, and ecological impacts (Braun et al. 2000; Bradley 2006;

Vergara et al. 2007; Vuille et al. 2008; Chevallier et al. 2011; Baraer et al. 2012; Polk et al. 2017; Carey et al. 2017). Being the most vulnerable, tropical glaciers therefore provide a window into the hydrologic perturbations that other glaciated, mountain catchments may experience in the future.

In the tropical Andes, where precipitation is highly seasonal, glaciers play a crucial role as hydrologic buffers. By storing a portion of precipitation as snow and ice and then slowly releasing it, mountain glaciers help to regulate streamflow and guarantee a dependable water supply during dry seasons and periods of extended drought (Mark & Seltzer 2003; Juen et al. 2007; Baraer et al. 2012; La Frenierre & Mark 2014). This hydrologic impact has been extensively studied in glaciated catchments in Peru and Bolivia. For example, in the glaciated Querococha watershed in Peru, discharge during the dry season was shown to consist of 30-45% meltwater and, year-round, to be less variable than runoff from nearby, non-glaciated catchments (Mark & Seltzer 2003). In Bolivia, it was estimated that the retreat and potential disappearance of the Chacaltaya glacier would lead to a 30% loss of stream discharge (Ramírez et al. 2001). Initially, as glaciers retreat, stream discharge increases, until a tipping point is reached where glacier volume becomes too small to sustain streamflow, and dry-season discharge consequently decreases (Braun et al. 2000; Mark 2008; Polk et al. 2017). Conceptualized as "peak water," (Carey et al. 2014), this loss of melt contributions leads to a decrease in mean annual discharge as well as an increase in discharge variability (Huss et al. 2008; Collins 2008; Baraer et al. 2012). Peak water has already occurred for some glacially fed streams in Peru's Cordillera Blanca (Baraer et al. 2012) and with many other Andean nations depending on water from

glaciated catchments for hydropower generation, irrigation for agriculture, and water for domestic use (Kaser 1999) there is a clear need to understand how these hydrologic systems will evolve with continued climate change.

Tropical glaciers are especially sensitive to climate change owing to their low latitude-high altitude positions (Hastenrath 1994; Kaser & Ostmaston 2002; Rabatel et al. 2013). The equilibrium line altitude (ELA) is the elevation at which net balance on a glacier is zero, meaning the annual accumulation of snow equals the net annual melting (ablation). On tropical mountain glaciers, the ELA is closely related to the 0˚C isotherm, or freezing line. At higher latitudes the ELA will shift seasonally with temperature changes, expanding and shrinking the ablation zone (region of melting) on a glacier. In the tropics, however, where there is little annual temperature variability, the elevation of the 0˚C isotherm is usually relatively stable and thus tropical glaciers ablate steadily year-round (Kaser & Ostmaston 2002). Consequently, minor increases in temperature with climate change can have large effects on ablation rates of these glaciers, as they shift the freezing line upslope thereby expanding the ablation zone as well as changing the phase of precipitation. Rainfall on a glacier reduces snow cover which negatively effects surface albedo and further induces melting (Francou 2004; Favier 2004a). In the tropical Andes, the regional temperature has increased by 0.7 ˚C since 1939 (Vuille et al. 2008) and since 1970, there has been a 20-50% (depending on location) decrease in glacierized area in the Andes (Mark & Seltzer 2005; Raup et al. 2007; Morris et al. 2006; Poveda & Pineda 2009; Cáceres 2010). Rabatel et al. (2013), using NCAR reanalysis climate data, determined that between 1955-2011 increases in mean monthly temperature had caused the freezing line to shift

upward by 60 m in the inner tropics and 160 m in the outer tropics. Currently, it is estimated that the glaciated area in the tropical Andes is decreasing by 1.2% -2% yr^{-1}; with IPCC scenaRíos predicting as much as 4 ˚C of warming in the 21st century, many of these glaciers could disappear by the end of this century (Rabatel et al. 2013).

For meltwater dependent communities to adapt their water management practices in the face of climate change, it is important to know how the hydrology of glaciated catchments will change with continued retreat. Modeling these catchments can be challenging, however, as physical monitoring networks are sparse and data sets often discontinuous, leading to a relatively poor understanding of hydrological processes in these remote areas (Mark 2008; Baraer et al. 2009). Many studies have focused on understanding tropical glacier dynamics(Francou 2004; Sicart et al. 2011; Manciati et al. 2014) and modeling gross, surficial runoff (Wagnon et al. 1999; Juen et al. 2007; Huss et al. 2008; Kaser et al. 2010), but such research leads to an oversimplification of the hydrologic processes in these catchments (Hood et al. 2006; Baraer et al. 2009; Rabatel et al. 2013). In addition to surface discharge networks, melt and precipitation may be partitioned between groundwater and evapotranspiration pathways.

Within the last decade, multiple studies have found significant groundwater contributions to discharge in alpine watersheds (Hood et al. 2006; Baraer et al. 2009; Andermann et al. 2012; Crossman et al. 2011; Godsey et al. 2014; Baraer et al. 2015; Markovich et al. 2016). In the Peruvian Andes, Baraer et al. (2015) even found that groundwater contributions in glacierized catchments could exceed 75% during the dry season. On Volcán Chimborazo in Ecuador, La Frenierre (2014) similarly found

groundwater to comprise ~60-70% of dry season discharge from a glacierized catchment. Clearly groundwater plays a key role in discharge, so understanding recharge mechanisms and subsurface flow systems is necessary to predict watershed hydrologic change. Recent evidence has suggested a possible melt recharge source for groundwater in tropical glaciated catchments. On the glaciated Volcán Antizana, in Ecuador, Favier et al. (2008) determined a significant portion of melt to be infiltrating at the base of the glacier and becoming recharge. Cauvy-Fraunie et al (2013) additionally discovered on Antizana meltwater resurgence in a spring from a non-glaciated catchment, suggesting melt recharge and groundwater flow that does not follow surface watershed boundaries. Melt signatures have also been identified in springs in the Cordillera Blanca, Peru (Baraer et al. 2015). On Volcán Chimborazo in Ecuador, reduced discharge from springs in recent years has forced local communities to develop new potable water sources (La Frenierre 2014; La Frenierre & Mark 2017). Local perceptions would suggest this reflects a decrease in effective rainfall not captured by local meteorological instruments (La Frenierre & Mark 2017). However, a melt recharge source could imply decreasing spring (groundwater) discharge is due to declining glacial inputs from a receding glacier past "peak water." Thus, further resolution of the subsurface hydrology in Andean catchments is necessary.

In mountain watersheds, evapotranspiration (ET) can significantly influence the amount of water becoming streamflow, especially from shallow groundwater reservoirs. With climate change, losses to ET are likely to have an even greater impact on water availability, as warming temperatures across the globe are changing local vegetation boundaries, generally shifting species distributions both upslope in elevation and poleward

in latitude (Walther et al. 2005; Morueta-holme et al. 2015). In Ecuador, new vegetation surveys on Volcán Chimborazo, compared to those originally done by Humboldt in 1802, revealed an upslope shift in plant taxa of over 500 meters. This expansion in vegetated area is largely contributed to warming temperatures in the region and glacier recession opening new habit for plant colonization (Morueta-holme et al. 2015). In addition to climate driven change, there is significant human driven vegetation and land cover change in the tropical Andes. High Andean páramo ecosystems-- comprised of peat bogs, grasslands, and patches of shrubs and low trees—are considered key shallow groundwater reservoirs that provide high contributions to baseflow even in glaciated catchments (Buytaert et al. 2006; Luteyn 1992; Buytaert et al. 2011). In recent decades, burning to improve grass quality and livestock grazing have intensified in the páramo and large sections of grassland have been converted to agricultural fields, which are drained and cultivated intensely. This activity has strong impacts on catchment hydrology, as it may change soil properties, thereby affecting groundwater storage potential, and the changes in or removal of vegetation affect ET rates (Buytaert et al. 2006). Clearly, climate and human-driven vegetation shifts are currently impacting ET rates and mechanisms the high Andes. When combined with predictions of higher temperatures that will likely increase ET rates, all this has the potential to alter available soil moisture, groundwater storage, and streamflow in glaciated watersheds (Buytaert et al. 2009; Buytaert et al. 2010).

Modeling ET in high Andean settings is difficult, as standard ET estimation methods require parameters—such as temperature, wind speed, humidity, solar radiation—that are poorly constrained in these systems as measurements are often sparse and

discontinuous (Garcia et al. 2004; Buytaert et al. 2010). Substitutions and estimations are commonly used, but in the tropical Andes this can lead to errors in ET predictions as large as 30% (Wohl et al. 2012; Cordova et al. 2015). Plant community dynamics strongly impact ET and runoff generation, but lack of spatial resolution on land cover and outdated maps make accounting for such heterogeneity difficult. Geospatial analysis of vegetation for inclusion in models, along with accurate climate variable data, is needed to constrain the water budget evolution in tropical catchments in response to climate change (Gerten et al. 2004; Cordova et al. 2015).

Although Ecuador's glaciated area is small compared to that of Peru or Bolivia, vulnerability to glacier change is still a large concern as the capital city of Quito (population 2.2 million; INEC, 2010) and much of the inter-Andean plateau rely on flow from these catchments for hydropower and domestic water supplies (Favier et al. 2008). Moreover, the majority of glaciers in Peru and Bolivia are in the outer tropics, while Ecuador's reside in the inner tropics and between these two regions, climatic and glaciologic conditions differ. Though both experience minimal intra-annual temperature variability, the outer tropics experience more pronounced precipitation seasonality, with one distinct dry season and one wet season (Favier 2004a). The inner tropics on the other hand are more humid and, though two wet seasons (long and short) with corresponding dry seasons are identified, experience year-round precipitation (Kaser 2001). Additionally, in the inner tropics the ELA is closely associated with the freezing line, while in the outer tropics moisture limitations often cause the ELA to be above the freezing line (Rabatel et al. 2013). Current climate research indicates that shifts in temperature and precipitation along with the effect

on glaciers will also differ between in the inner and outer tropics. The outer tropics have seen a drying trend in recent decades, and its glaciers are more likely to be affected by accumulation losses due to changes in precipitation than they are due to warming temperatures. On the other hand, the inner tropics appear to be getting slightly wetter and higher temperatures will have the larger impact on glaciers by raising the freezing line (thereby the ELA) and increasing the amount of rainfall (rather than snow) that falls on the glacier surface (Francou 2003; Favier 2004a; Vuille et al. 2008). There is uncertainty in these predictions (Buytaert et al. 2010) and some evidence for heterogeneity in these climatic responses (La Frenierre & Mark 2017). Studying glaciers in the inner tropics (e.g. Ecuador) offers an opportunity to examine hydrologic perturbations to glacial melt under different climatic conditions in order to generalize glacial melt impacts.

Glaciers in Ecuador exist only above 4400 m elevation; an altitude requirement that confines the major ice bodies to the stratovolcanoes of Antizana, Chimborazo, Cayambe, and Cotopaxi (Hastenrath 1981). Though there has been extensive study across glaciated watersheds in the outer tropics (Wagnon et al. 2001; Ramírez et al. 2001; Mark & Seltzer 2003; Francou 2003; Vimeux et al. 2005; Baraer et al. 2009; Baraer et al. 2012; Somers et al. 2016; Polk et al. 2017), inner tropical glaciershed studies have been largely limited to the highly instrumented glaciers on Volcán Antizana (Francou 2004; Caceres et al. 2006; Favier 2004b; Favier et al. 2008; Manciati et al. 2014; Williams et al. 2002; Maldonado 2016; Sicart et al. 2007). Glacier energy and mass balances and glacial melt discharge patterns are well-known for Antizana's glaciers, yet knowledge of Ecuador's other glaciated peaks is minimal. Research on other Ecuadorian glaciers is needed to not only

corroborate findings at Antizana about how inner tropical watersheds are responding to climate change, but also to compare across climatic conditions within the Ecuadorian Andes. Antizana resides on the eastern cordillera, and is exposed directly to moist easterly winds coming off the Amazon basin. Chimborazo, however, is on the western cordillera, receiving moisture from the Pacific as well as more highly evaporated moisture from the Amazon. Mean monthly precipitation rates differ between the two mountains, with lower rates on Chimborazo, as do patterns in precipitation anomalies in response to the El Niño Southern Oscillation (Veettil et al. 2014).

Here, I focus my study on Volcán Chimborazo, a glaciated stratovolcano whose glaciers serve as the headwaters for four major river systems (La Frenierre 2014) that supply water to a population of over 200,000 (INEC 2010). For a glaciated watershed on Chimborazo, La Frenierre (2014) used a combination of quantitative data-- meteorological and hydrological measurements, hydrochemical analyses and modeling, and analysis of remotely sensed imagery—and qualitative data – household surveys and focus groups—to measure glaciological and hydrological changes. He found that between 1986 and 2013, Chimborazo's glacier surface area decreased by 21%, and since 2000 has been decreasing at a rate of 1.2% yr^{-1}. In addition, the mean elevation for clean ice on all glaciers has increased by 180 m asl (meters above sea level) since 1986 (to 5,320 m) and eight of the 17 glaciers now feature detached tongues. National meteorological station data does not show a statistically significant change in precipitation, though there is near unanimous agreement among the surveyed local population that precipitation, along with streams,

springs, and pond levels, have decreased. Many local residents also perceive that the climate has become more variable and less predictable (La Frenierre & Mark 2017).

Research on Chimborazo has focused on a single glaciated watershed, the Upper Río Mocha catchment, because it contains the largest glacier on Chimborazo and it supplies water to the largest and most glacially dependent irrigation system on the mountain. Using the hydrochemical mixing model HBCM (Hydrochemical Basin Characterization Method), La Frenierre (2014) determined that the Upper Río Mocha is a groundwater-dominated hydrological system, with surficial glacier melt contributing only ~5% of total discharge during the dry season. However, the absence of perennial meltwater streams, despite continued glacier mass loss, along with unexpectedly low specific discharge from upper glacierized subcatchments suggest that some meltwater may not be fully accounted for in surficial streams. This leads to the hypothesis that a substantial amount of meltwater may be recharging to groundwater, which may contribute to discharge at the catchment outlet farther downstream. Understanding meltwater infiltration is important for correctly quantifying melt contributions to total discharge and predict how glacier recession might affect discharge. Furthermore, meltwater passing through groundwater systems will likely have a spatiotemporal characteristic, distinct from its contributions to surface runoff, which influences both where and when it can contribute to accessible water resources.

This thesis documents an evaluation of the relationships between meltwater, groundwater, and stream flow to address the following questions:

1. Have the proportions of meltwater runoff and groundwater discharge in streamflow changed over 2012-2017?

2. How is glacial meltwater partitioned between surface water and groundwater sources within a glaciated catchment on Volcán Chimborazo?
3. What are the climatic, hydrogeologic, and vegetation factors that affect the hydrologic response to glacial melt?

To examine these questions, I have used a combination of field methods, hydrogeochemical modeling, and geospatial analysis. Through two field campaigns, I have deployed sensor networks for measuring climate variables, stream discharge, and glacier change, and I have collected two sets, and acquired a third, of water chemistry samples for tracing water sources. To address the first research question, I utilized the HBCM hydrochemical mixing model with the collected water chemistry data to quantify relative sources of surficial meltwater and groundwater to discharge for distinct time periods. I compare results spanning 2012 to 2017, including different seasons as well as one strong El Niño year. To address the second research question, stable water isotope data were further examined to infer possible surface water versus groundwater pathways of meltwater using distinct isotope signatures. The third research question is addressed by compiling both observed and reanalysis climate data, generating geologic GIS data along with theoretical hydrogeologic cross-sections, and creating a new land cover map using object based image analysis (OBIA) of aerial and remotely sensed imagery.

Chapter 2: Geographic, Geologic, and Ecologic Characterization of Volcán Chimborazo

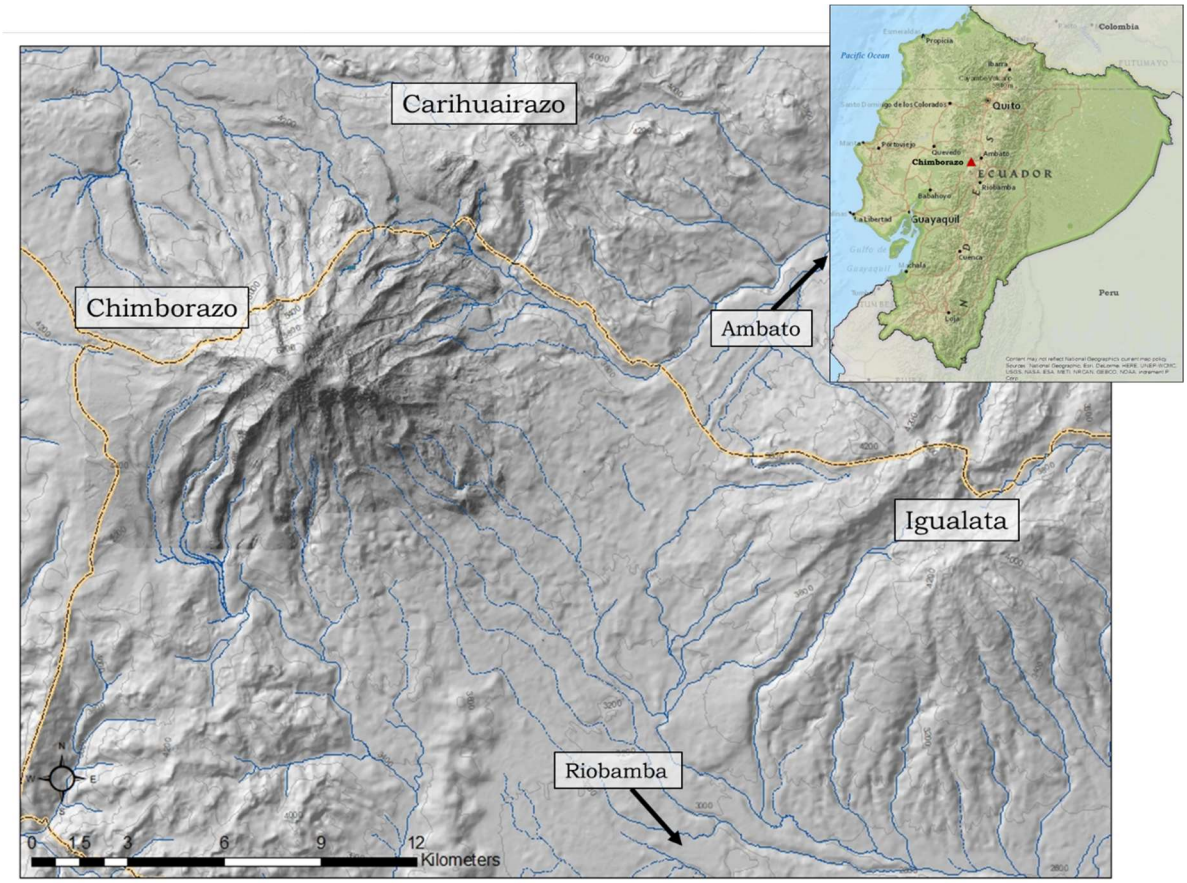

Figure 2.1 Geographic location of Volcán Chimborazo.

2.1 Study Region Overview

2.1.1 Geographic Location

The Ecuadorian Andes are composed of two parallel mountain ranges, the western Cordillera Occidental and the eastern Cordillera Oriental, separated by the Inter-Andean Valley. The two ranges' average 4000-4500 m in elevation and are punctuated by a series of stratovolcanoes that rise to 5000 m and above. Of these, only eight are still glaciated

(Cáceres 2010), the highest of which is Volcán Chimborazo (6268 m asl). Located approximately 150 km south of Quito, near the border of the Chimborazo and Tungurahua provinces, Volcán Chimborazo (1.47˚S, 78.82˚W) is the southernmost glaciated peak of the Cordillera Occidental. The mountain is a faunal preserve above 4000 m, while below that the hillslopes are heavily farmed, particularly to the southeast, by primarily indigenous communities. The capital and largest city of Chimborazo Province, Riobamba (~150,000; INEC 2010), is located 25 km southeast of the mountain (Figure 2.1).

2.1.2 Geology

Chimborazo is considered a dormant volcano, with its most recent eruptive event occurring sometime between 420 and 700 CE (Barba et al. 2008). Its geologic history (Section 2.2.2) consists of successive cone building stages that gave rise to its three main peaks: Whymper (6268 m asl), Politécnica (5850 m asl), and Martínez (5650 m asl). The three peaks are roughly aligned WNW-ESE, giving the volcano an elliptical shape (Figure 2.2). The primary geology consists of layered lava and pyroclastic flows around the mountain, along with thick ash fall deposits on the western side (Barba et al. 2008; Samaniego et al. 2012). Additionally, two major debris avalanche deposits have been identified—a younger, smaller one in the Río Colorado watershed on the northern side, and an older, massive one on the southern flank that flowed out to fill much of the Riobamba basin (Samaniego et al. 2012). The morphology of the mountain has been strongly influenced by recent glaciations, with glacial deposits and moraines from the Last Glacial Maximum (LGM; ~33-14 ka), the Younger Dryas (or Late Glacial; ~13-15 ka), and the

Neo-Glacial period (<5 ka). Deposits from the LGM extend as far down on the eastern side as 3500-3600 m asl, and on the western side to 4300-4400 m asl (Clapperton 1990; Samaniego et al. 2012). Large glacial valleys in-filled with collapsed morainic material and colluvium are present on all sides of the mountain (Clapperton & McEwan 1985; Clapperton 1990; Samaniego et al. 2012).

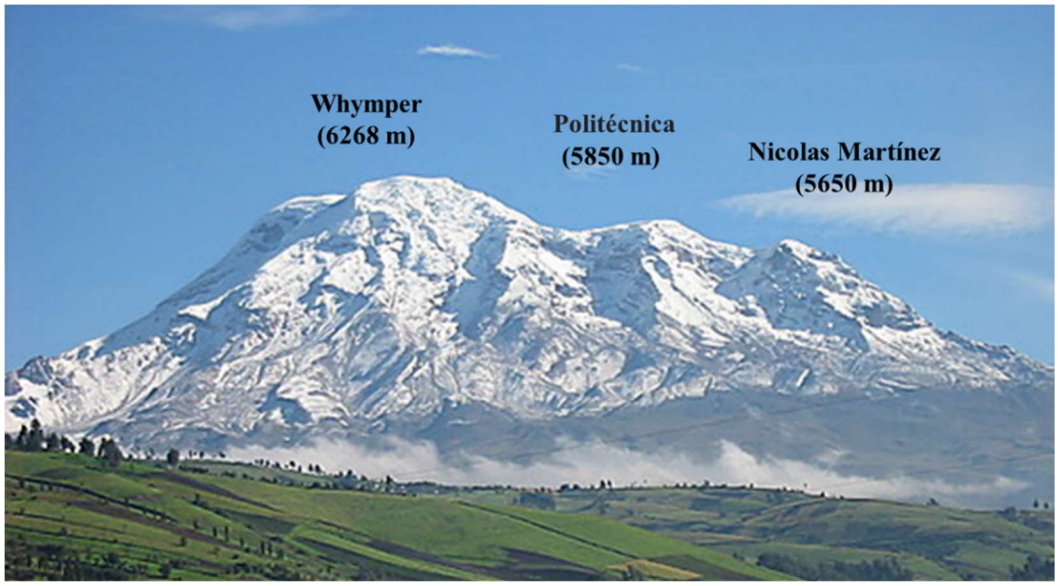

Figure 2.2 View from the south showing all three summits. Photo credit: American Alpine Institute. http://www.alpineinstitute.com/catalog/ecuador-chimborazo-climb/

2.1.3 Climate

Located in the inner tropics, Chimborazo's climate is characterized by minimal intra-annual temperature variation (~2˚C) and precipitation seasonality (La Frenierre 2014). There are typically two wet seasons, a longer one spanning February- May and one shorter one spanning October-November, that are separated by corresponding long and short dry seasons (June-September and December- January, respectively). The majority of precipitation comes from the Amazon Basin to the east, arriving on seasonal northeasterly

winds (Smith et al. 2008; Vuille & Keimig 2004) and producing a steep northeast (up to 2000 mm/yr) to southwest (<500 mm/yr) precipitation gradient across the mountain, which results in distinct wet and dry sides (Figure 2.3)(La Frenierre 2014). Locally, topography creates extreme heterogeneity in precipitation patterns, while the El Nino-Southern Oscillation (ENSO) drives interannual climatic variability at the regional scale. Generally, ENSO impacts precipitation and temperature, with El Niño (La Niña) years bringing drier, hotter (wetter, cooler) conditions (Vuille et al. 2000; Wagnon et al. 2001; Francou 2003; Bradley et al. 2003; Vuille & Keimig 2004; Smith et al. 2008). These changing conditions strongly influence glacier mass balance, with El Niño periods enhancing ablation (Wagnon et al. 2001; Favier 2004a; Francou 2004; Veettil et al. 2014). ENSO's effect on precipitation and glacier mass balance has a direct impact on stream discharge in Andean catchments.

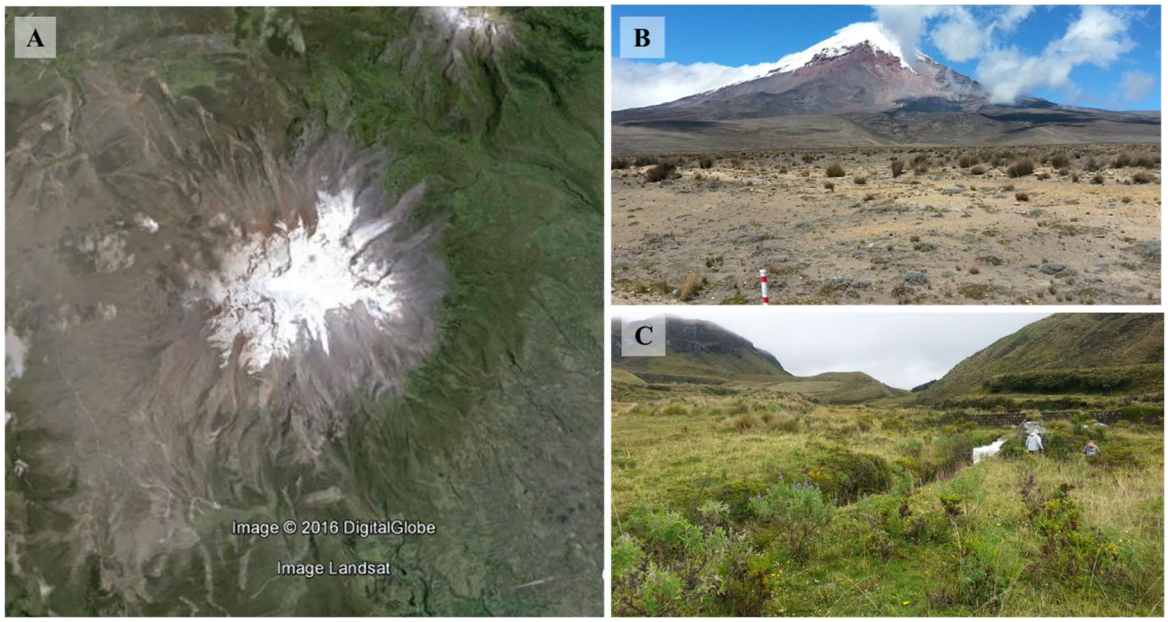

Figure 2.3 Comparison of dry (West) and wet (East) sides of Chimborazo. A) Satellite view showing sparsely vegetated western side and heavily vegetated eastern side. B) Picture of western flank landscape. C) Picture eastern flank landscape.

Chimborazo's extreme elevation along with the local precipitation patterns result in four distinct climatic zones on the mountain (Pourrut et al. 1995; La Frenierre 2014). On all sides, above ~4500 m asl, an alpine climate dominates with mean annual temperatures below freezing and snowfall as the main form of precipitation. On the eastern and northern slopes, the climate is more humid owing to the prevailing winds from the Amazon. On these sides at higher elevations, an equatorial high mountain climate exists, with temperatures ranging from 0˚-12˚ C, which moving downslope transitions into an equatorial semi-humid temperate zone, where temperatures range from 12˚-22˚ C. Mean annual precipitation in these zones is typically greater than 600 mm. To the southwest, in the rain shadow of the mountain, there is a semi-arid equatorial dry temperate climate where temperatures also range from 12˚-22˚ C, but mean annual precipitation is typically less than 600 mm with a potential moisture deficit of 600 mm.

2.1.4 Ecology

Though climatic conditions vary greatly around the mountain, most of the landscape is covered in "páramo" grasslands (Figure 2.4C) native to the high-elevation tropical Andes. The term páramo often refers to a collection of neotropical ecosystems that exist within the grassland biome, and can be subdivided into three altitudinal zones based on physiognomy and vegetation structure: subpáramo, páramo, and superpáramo (Buytaert et al. 2006; Bustamante et al. 2011). The subpáramo is the lowest zone (300-3500 m asl) and usually consists of shrubs and small trees alternating with grassland. The páramo proper (3500-4500 m asl) is largely dominated by grasslands, though woody species, like

Polylepis, can be found along stream valleys. Lastly, the superpáramo constitutes the sparsely vegetated area between the true páramo grasslands and the snowline. In all zones, saturated, low gradient wetlands can develop, which are locally referred to as bofedales (Figure 2.4A**,** singular: bofedal) (Buytaert et al. 2006; Luteyn 1999). Ecologically, the páramo has high plant diversity (>5000 species), but its vegetation mainly consists of tussock grasses, cushion plants, dwarf shrubs, ground rosettes, and giant rosettas. Páramo soils are rich in organics and can be characterized by their high infiltration rates and storage capacity, which are considered to be key in sustaining river discharge throughout the year (Podwojewski et al. 2002; Buytaert et al. 2004; Buytaert et al. 2006). The páramo and its associated wetlands that exist on the eastern and southern flank of Chimborazo are of particular importance since many communities rely on the water discharged from catchments there (Bustamante et al. 2011).

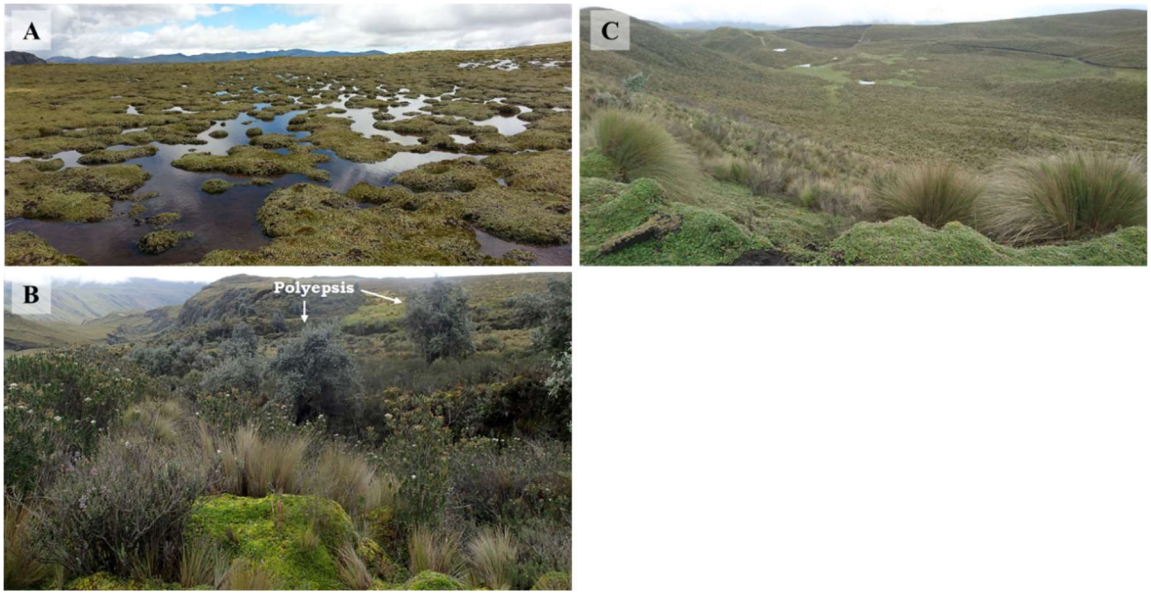

Figure 2.4 A) Bofedal in Hans Meyer watershed on northern flank B) Woody shrubs and *polyepsis* trees (indicated) near stream in Gavilan Machay subcatchment. C) Typical páramo grassland in Upper Rio Mocha Catchment.

2.1.5 Glaciology

Covering the summit of Chimborazo is a ~55 m thick mantle of ice with 17 glaciers radiating out from it (Ginot et al. 2010). On the eastern, more humid side, the glaciers extend down to 4800-5000 m asl, and on the drier western side, down to 5500-6000 m asl. Similar to all tropical glaciers, those on Chimborazo are highly sensitive to climate change and have experienced significant mass loss within recent decades. Between 1962 and 1997 there was an overall 59.8% reduction in ice surface area, from 27.7 km^2 to 11.82 km^2 (Cáceres 2010), though there is uncertainty in this value owing to the presence of snow in the aerial images used to obtain it (La Frenierre 2014). La Frenierre & Mark (2017) show that by 2013, ice surface area had shrunk to 11.1 km^2, while mean annual temperature for the area increased 0.26˚C from 1986 to 2011, which is consistent with overall temperature trends in the tropical Andes (Vuille et al. 2008). Rain gauges in the Chimborazo region show no significant change in mean annual precipitation totals over the same time period, but surveys of local residents around the mountain indicate a consistent perception that rainfall is less frequent and less predictable (La Frenierre & Mark 2017). Glacier behavior on Chimborazo supports local perceptions, as the retreat rates and rise in the mean elevation of clean ice exceed what can be explained by temperature and topographic effects alone.

2.1.6 Hydrology

Chimborazo and its glaciers serve as the headwaters of four different river systems: the Río Colorado (NW), the Río Mocha (NE), the Río Guano (SE) and the Río Chimborazo (SW). The Mocha and Colorado rivers flow north into Tungurahua Province, while the Guano

and Chimborazo flow south into Chimborazo Province, but all eventually drain into the Amazon River basin (Figure 2.5)**.** The mountain's two largest glaciers, Reschreiter (2.55 km^2) and Hans Meyer (1.33 km^2), along with two others are the only ones to produce year-round surficial discharge. Nearly all of this water drains into the Río Mocha, except a small lobe of Hans Meyer that drains into the Río Colorado. All other glaciers very seldom produce surface runoff, with the exception of one in the Río Colorado watershed and two in Río Chimborazo that produce surface meltwater only after multi-day, warm, sunny periods (La Frenierre 2014).

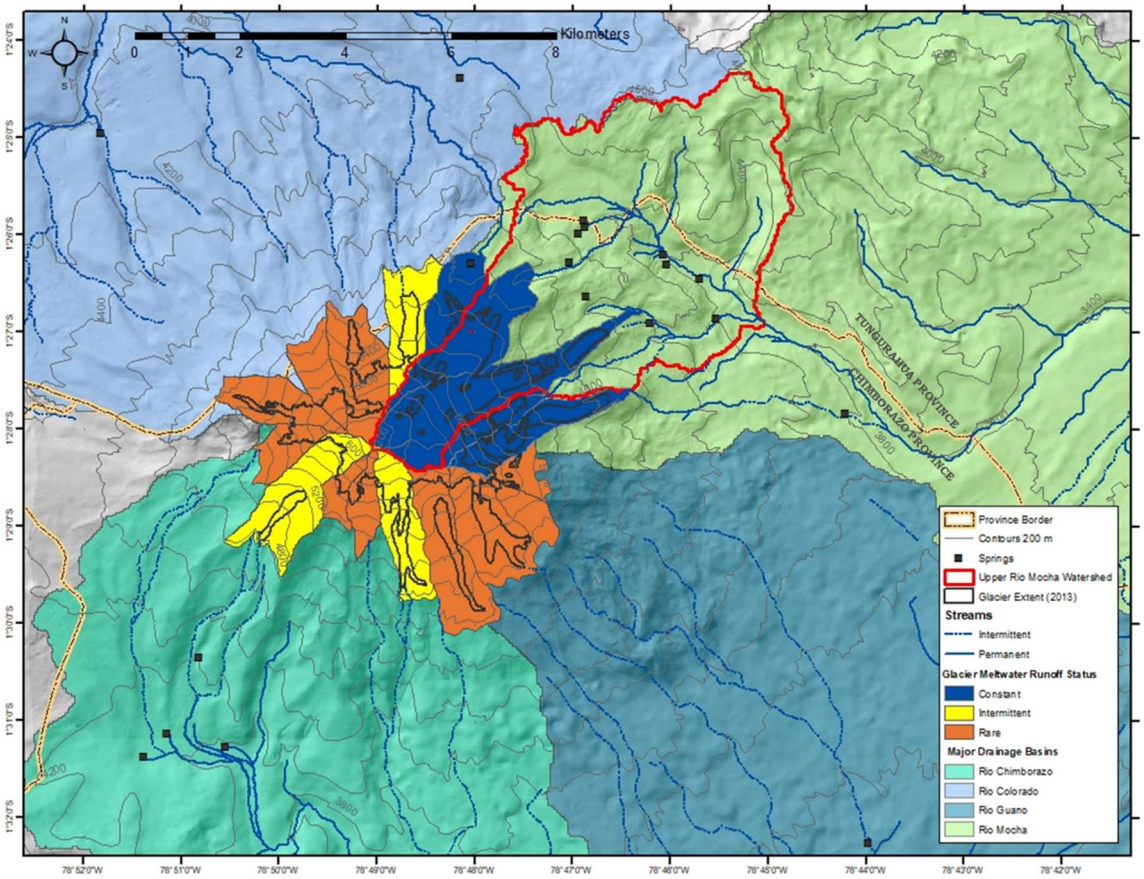

Figure 2.5 Map showing the 4 major drainage basins, spring locations, and meltwater runoff status in each of the 17 glaciersheds. Map adapted from La Frenierre (2014).

Below 4500 m asl, natural springs are common around the mountain and in the southern watersheds (Guano and Chimborazo) continuous streamflow only begins below them. Many of these springs, particularly in the eastern watersheds, are captured for either domestic or agricultural use. Half the domestic water supply for the city of Riobamba comes from the largest spring in the Río Guano watershed (La Frenierre 2014). A study of the Río Guano aquifers revealed that the primary source of the springs is likely a shallow, unconfined aquifer, 30- 100 m in depth, that exists within the Riobamba debris-avalanche deposit (Bigo 2013). Deuterium analyses indicate that this water likely infiltrates between 3500-4000 m asl. The remainder of the city water supply comes from wells drilled into a second, deeper, confined aquifer that may be a fossil resource (possibly 8000 years old), according to ^{14}C-dating results.

2.1.7 Upper Río Mocha Watershed

This study examines the Upper Río Mocha catchment and focuses mostly on the Gavilan Machay subcatchment (Figure 2.6). The Upper Río Mocha is the 30.4 km^2 watershed area upstream of Boca Toma, the diversion point for the largest irrigation system on Volcán Chimborazo. Approximately 13% of the watershed is glacierized, with meltwater from both the Reschreiter glacier and a majority of the Hans Meyer glacier flowing into it. Elevations range from 3895 m asl on the valley floor at Boca Toma, to 6268 m asl on the peak of Chimborazo. The northern side the watershed is defined by the peak of neighboring Volcán Carihuairazo (5018 m asl). Carihuairazo, once fully glaciated, now has only minimal remnants of glacier ice (<1% watershed area) that are not considered

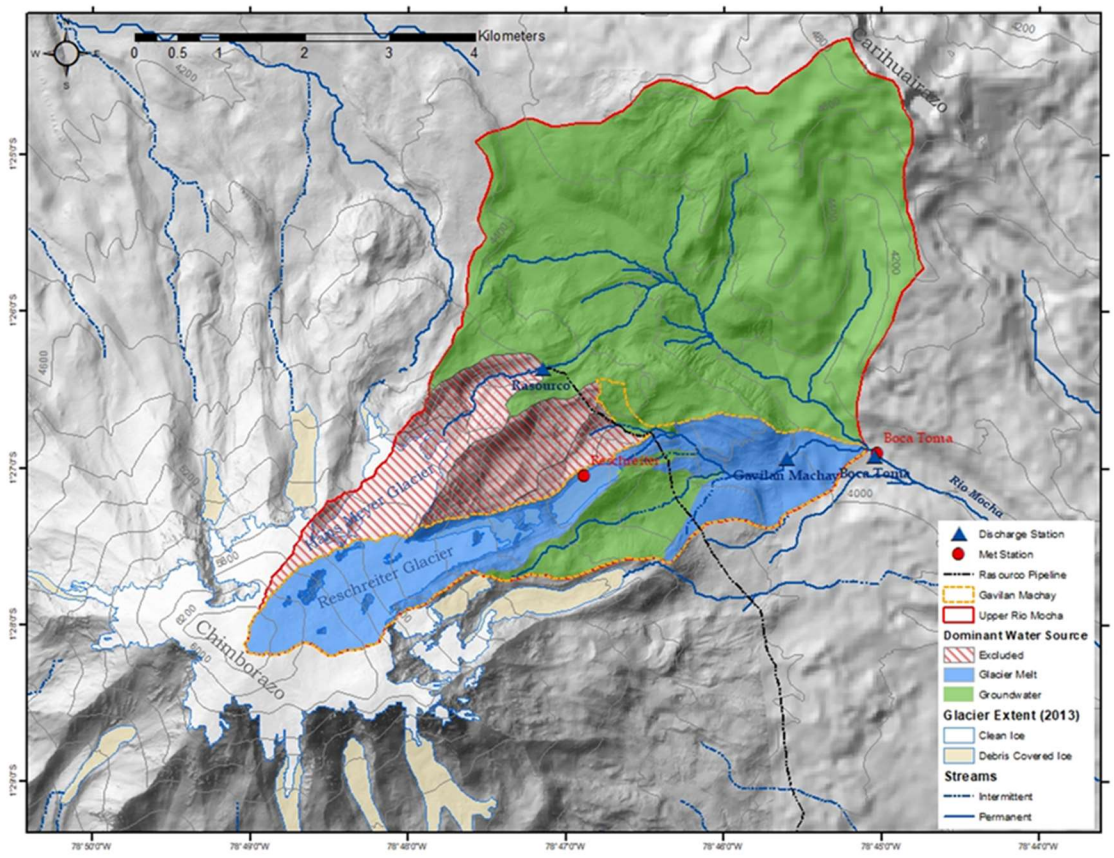

Figure 2.6 Upper Rio Mocha watershed and Gavilan Machay subcatchment. Watershed areas excluded from analysis (below Hans Meyer glacier) are indicated along with dominant source water for subcatchment areas. Map adapted from La Frenierre (2014).

hydrologically significant (La Frenierre 2014). Glacial features dominate the Upper Río Mocha geomorphology, with talus slopes and rock falls underlying large lateral moraines, and fluvial and lacustrine deposits infilling deep, U-shaped valleys (Figure 2.7). Additionally, abraded bedrock surfaces, rôche moutonnée, and valley steps are scattered around the Mocha valley. Layered volcanics outcrop in the valley steps and as large cliffs on the sides of the Río Mocha channel and its glacial tributaries (Clapperton & McEwan 1985; Field observations) (Figure 2.7). The watershed is predominately covered by páramo grasses and bofedales, though small groupings of *Polyepsis* trees are found close to streams

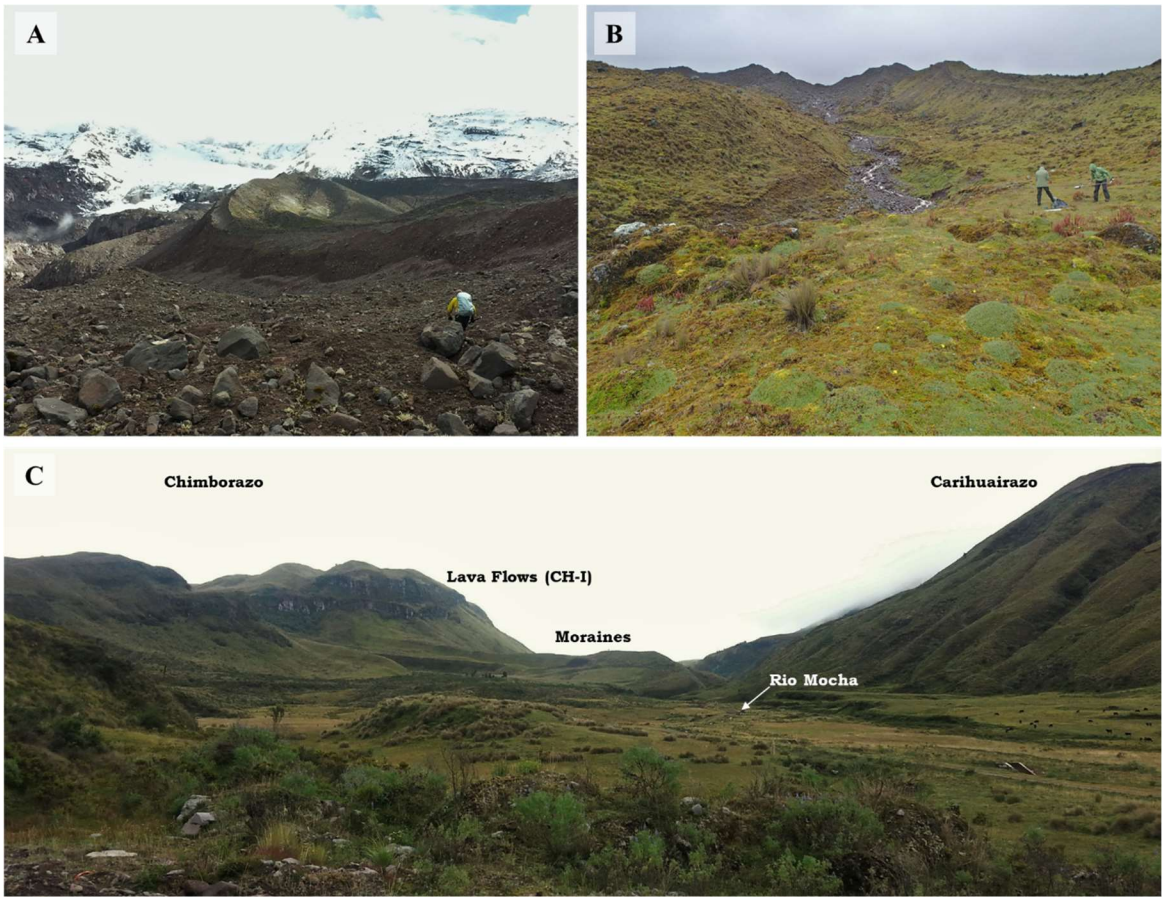

Figure 2.7 Geology and Geomorphology of Upper Rio Mocha Watershed. A) Looking up valley towards Reschreiter Glacier (left). Till in foreground acts as debris cover over the detached glacier tongue. A large lateral moraine starts in the middle of the frame and extends to the right. B) Looking up the Gavilan Machay valley from near Reschreiter camp. Glacial deposits from image A are visible upstream in the back. C) Looking northwest up the Upper Rio Mocha valley. Volcanic flows from Chimborazo's basal edifice outcrop as cliffs on the left side of the valley. Below the cliffs (image center) moraines from the Late Glacial period extend out from the Gavilan Machay Subcatchment.

and spring discharge points (Figure 2.4B). Above 4600 m asl little vegetation is found, with snow, rock, and ice dominating.

The Hans Meyer glacier generates little surface meltwater, almost all of which, along with a portion of runoff from the non-glacierized part of the Gavilan Machay subcatchment, is diverted into the Rasourco irrigation system. In total, 2.0 km^2 of the Gavilan Machay subcatchment and an additional 2.5 km^2 of the Upper Río Mocha

watershed below the Hans Meyer glacier drain to the Rasourco irrigation system and do not contribute to surficial discharge in the Río Mocha watershed (Figure 2.6) (La Frenierre 2014). Herein, these areas are excluded from all hydrologic analyses, and surficial melt contributions to runoff are considered limited to the Gavilan Machay subcatchment (Figure 2.6) that contains the Reschreiter glacier. All water discharging from the main Río Mocha channel, above the confluence with the Gavilan Machay stream, is assumed to be groundwater. The 7.5 km^2 Gavilan Machay subcatchment is 34% glacierized and discharges into the main Mocha channel just above Boca Toma. The ecology and geology of this subcatchment do not differ from that of the watershed as a whole.

2.2 Geologic Characterization: Digitization of Geologic Map & Generation Geologic Cross-Sections

2.2.1 Introduction

In order to evaluate the hydrogeology within the Upper Río Mocha watershed and Gavilan Machay subcatchment, I generated a series of geologic cross sections (Figures 2.8-2.11**)**. These cross-sections were constructed using the geologic map by Barba (2006), which was manually digitized and geospatially referenced in separate GIS layer files for each major unit (Figure 2.9), based on inferred buried contacts. Further stratigraphic relationships and unit thicknesses in the cross-sections were interpreted from recent studies on the structure and volcanic history of Chimborazo (summarized below).

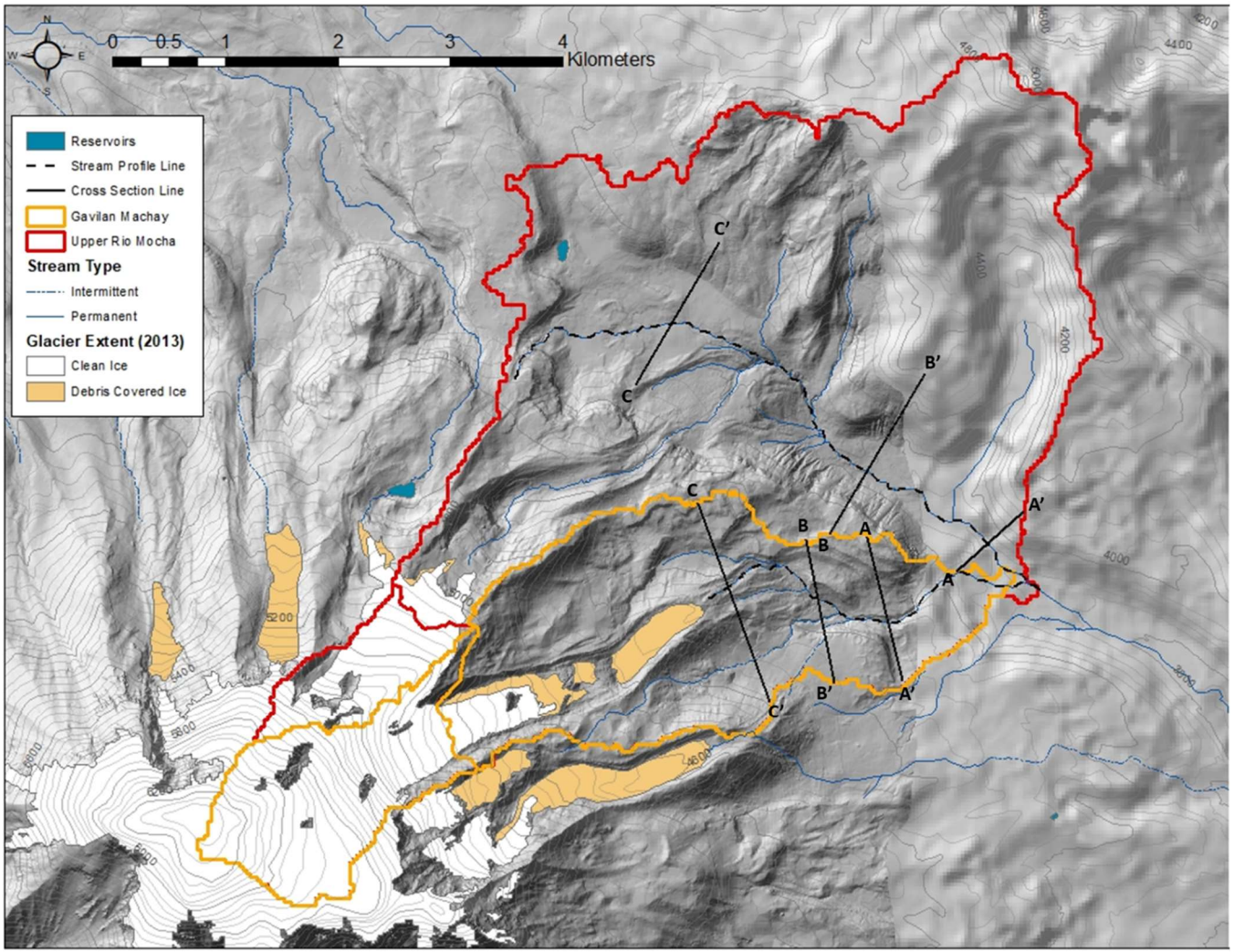

Figure 2.8 Location of cross-section and stream profile lines.

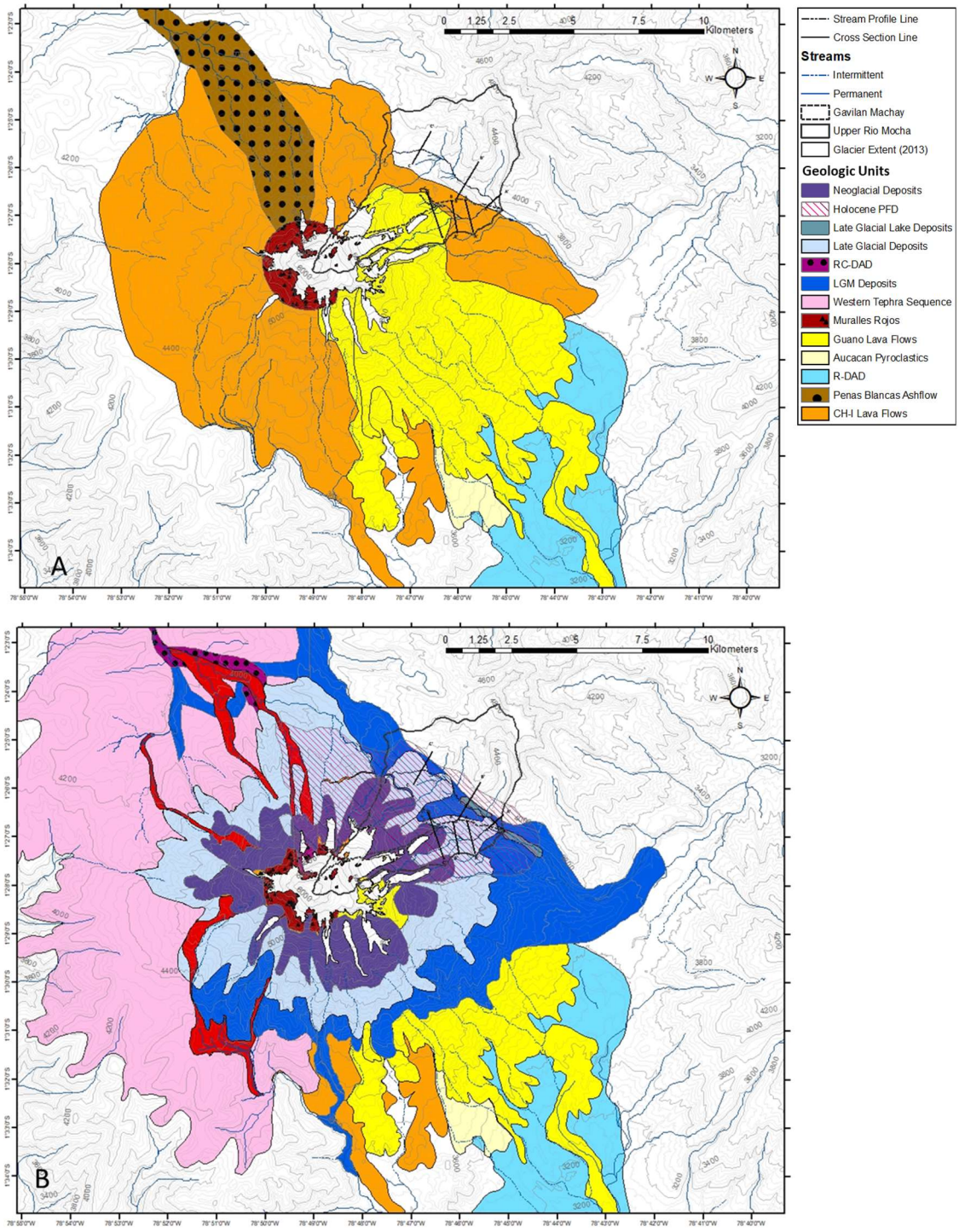

Figure 2.9 Geologic Maps. A) Pre-glaciation volcanic bedrock. B) Post-glaciation volcanic & glacial deposits. Acronyms- DAD: debris avalanche deposit, R: Riobamba, RC: Rio Colorado, PFD: pyroclastic flow deposit, and LGM: last glacial maximum.

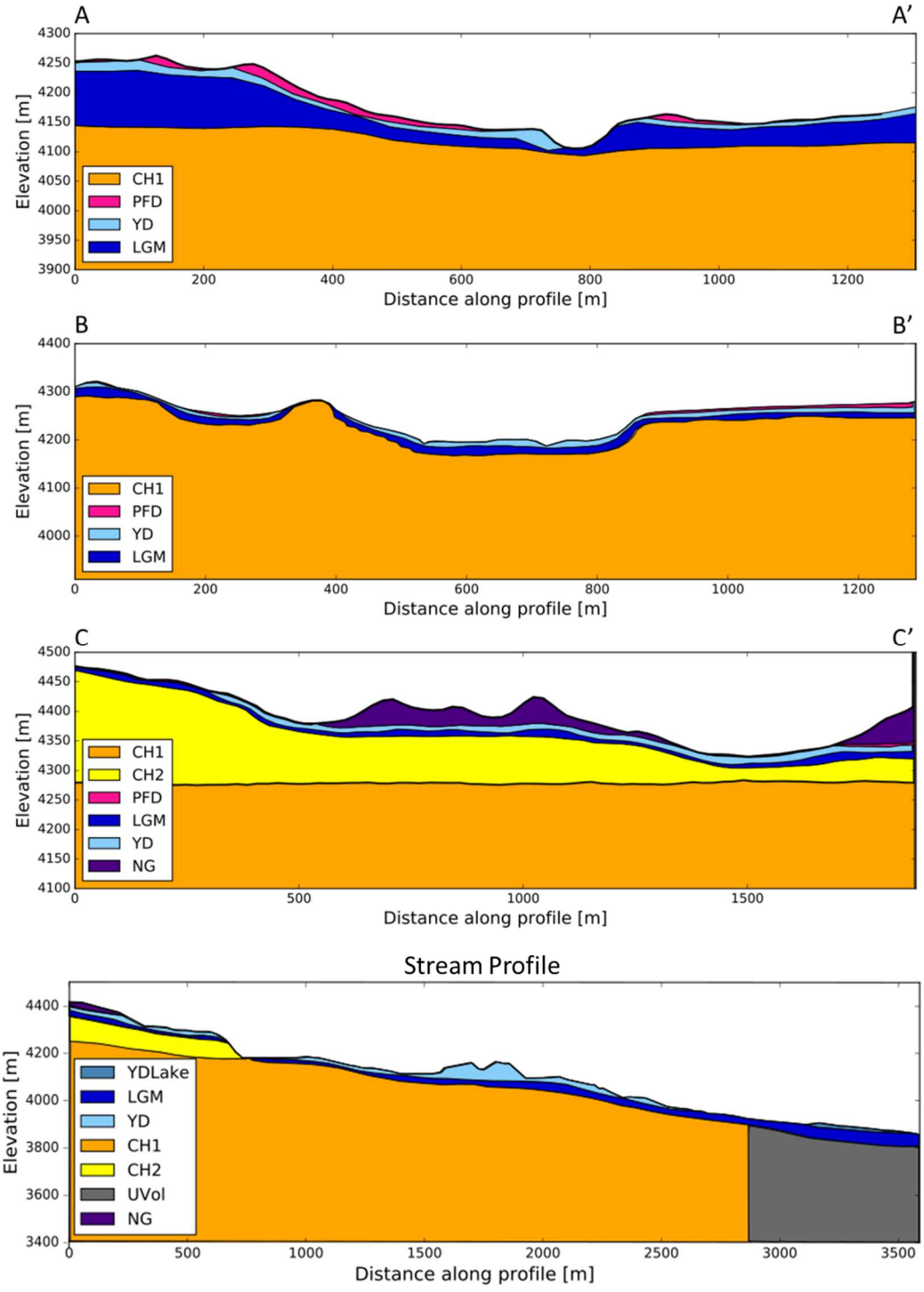

Figure 2.10 Cross sections from the Gavilan Machay subcatchment

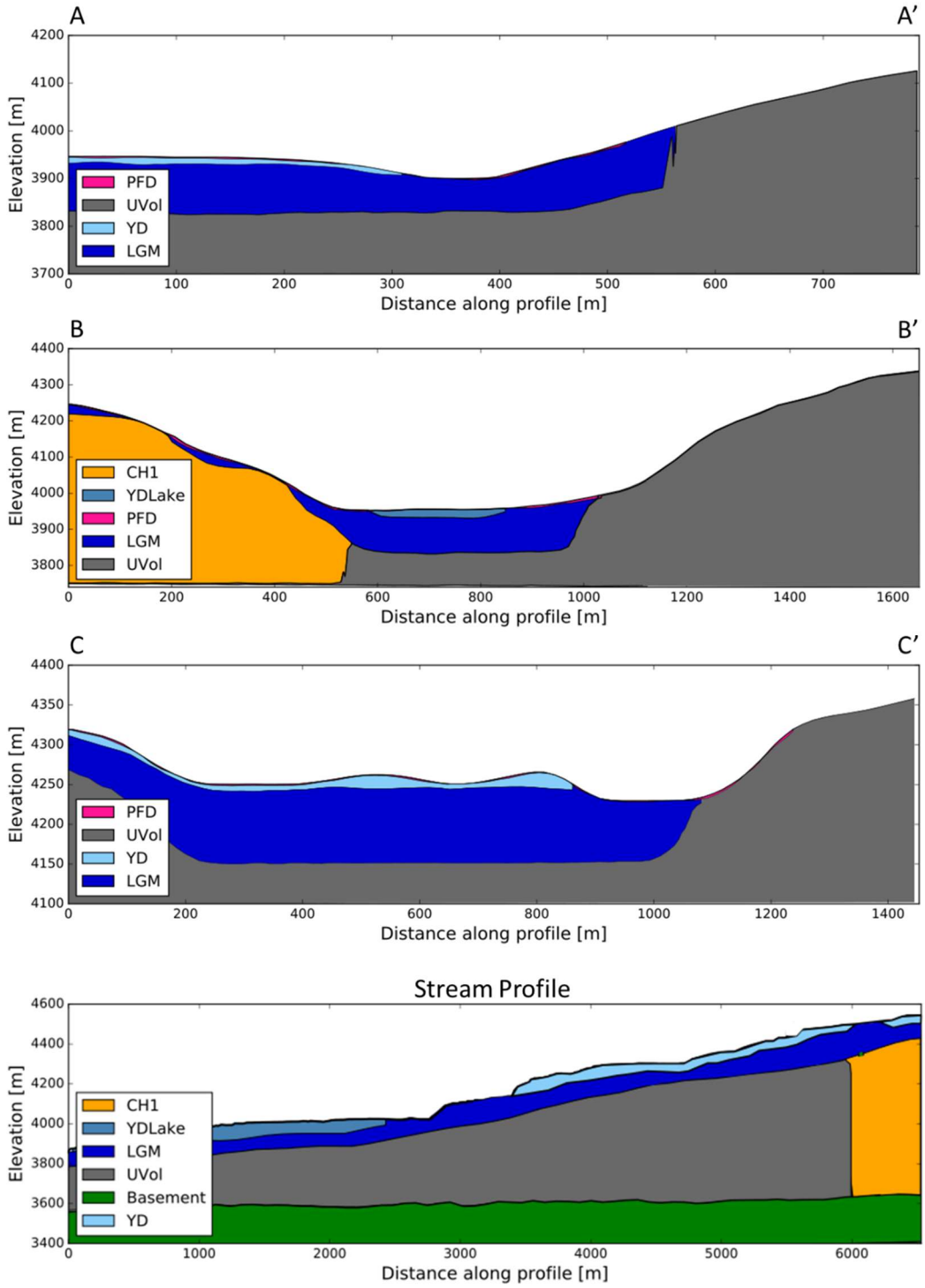

Figure 2.11 Cross sections from the Upper Rio Mocha valley

Cross Section Unit Abbreviation Key

CH1 – Abraspungo and El Castillo lava flows associated with the first cone building stage, and basal edifice, on Chimborazo.

CH2 – Guano lava flows & other volcanic deposits associated with the second cone building stage, and intermediary edifice, on Chimborazo.

LGM – Morainic material & associated deposits from the Last Glacial Maximum.

YD – Morainic material & associated deposits from the Late Glacial (Younger Dryas) period.

YDLake – Glaciofluvial and lacustrine deposits associated with lake from the Younger Dryas/Pleistocene time period.

NG – Morainic material from Neoglacial period.

PFD – Large pyroclastic flow deposits associated with eruptive activity during the Holocene, as argued by Barba et al. 2008.

UVol – Unknown Volcanics; possibly from Carihuairazo or from Chimborazo but not enough information available in literature to discern.

Basement – Possibly Mid-Pliocene volcanics or Cretaceous-Paleogene volcanics and sediments of the Western Cordillera basement.

2.2.2 Geologic History and Stratigraphy

Volcán Chimborazo sits atop the Western Cordillera basement, which is composed of Cretaceous oceanic plateau basalts and Cenozoic volcanic-sedimentary sequences overlain by Miocene-Pliocene volcanic arc sequences (Hughes & Pilatasig 2002; Samaniego et al. 2012). The earliest descriptions of Chimborazo's geology date back to Humboldt (1837-1838) and Whymper (1892), while modern studies aimed at characterizing its volcanic stratigraphy, structure, and petrology were conducted by Killian (1987), Beate and Hall (1989), and Killian et al. (1995). Clapperton and McEwan (1985) and Clapperton (1990) studied the glacial geomorphology of the Chimborazo-Carihuairazo Massif and delineated glacial events. More recently, an exhaustive study of Volcán Chimborazo was carried out using field observations along with geochronology and petrologic analysis to map its geology and reconstruct its volcanic history (Barba 2006; Barba et al. 2005; Barba et al. 2008; Bernard et al. 2008; Samaniego et al. 2012); these studies resulted in a new geologic map for Chimborazo and the identification of three successive edifices: a basal edifice (CH-I), an intermediary edifice (CH-II), and a young cone (CH-III).

Stratigraphy analyzed through various studies (Barba 2006; Barba et al. 2005; Barba et al. 2008; Bernard et al. 2008) and compiled in Samaniego et al (2012) indicates that Chimborazo's basal edifice (CH-I) represents the earliest cone building, which occurred between ~120 to 60 ka and reached a summit of 6200 m asl. It is characterized by two major lava flow sequences (Abrasprungo and El Castillo stages), two pyroclastic flow deposits, and the Riobamba debris avalanche deposit (R-DAD). The Abraspungo lavas are

sub-horizontal (slopes <10˚) and 300-400 meters thick, while El Castillo lavas, which constitute the majority of CH-I, have slopes between 15˚-25˚ and are 800m thick. These flows outcrop on slopes from the southwest to the northeast. In the Río Colorado and Río Condor Palta valleys, the Peñas Blancas ashflow and Condor Palta pyroclastic flow deposit (>200 m thick) outcrop, respectively. The end of CH-I growth is marked by a massive sector collapse on the southeast side that created the R-DAD, which fills the Riobamba basin out to 35 km from the mountain with an average thickness of 40 m (Bernard et al. 2008). Compositionally, the basal edifice is mainly andesitic with some dacitic portions (Samaniego et al. 2012).

Between ~60 and ~35 ka, the intermediary edifice (CH-II) was constructed in the eastern part of the avalanche depression left by R-DAD. It possesses two main stages, the effusive Guano stage and the cone building Politécnica stage, which produced the Politécnica and Martínez peaks. The Guano stage includes the Aucacán pyroclastic sequence (~10 m thick) and the Guano lava flows (75-100 m thick), which cover the southeast side of the mountain. Following the Guano flows, the Politécnica stage gave rise to thick lava piles of the Politécnica (~700 m thick) and Martínez (>400 m thick) peaks. Explosive activity towards the end of CH-II resulted in ashflows that outcrop in the Río Blanco valley to the north (~8 m minimum thickness) and tephra fallout deposits (5-6 m thick) on the southeast flank. Compared to the basal edifice, CH-II is compositionally more basic and rich in magnesium. Glacial activity during the LGM strongly affected this edifice and many of the units are overlain by morainic material from this period.

The young edifice (CH-III) was the final growth stage on Chimborazo and produced its highest summit, Whymper. CH-III is defined by one major cone building stage, Muralles Rojos, which is accompanied by explosive activity contemporaneous with the LGM period, and followed by a flank sector collapse. The Muralles Rojos stage comprises scoria-flow deposits and interlayered lava flows that are distributed radially around the cone and stretch from the R-DAD avalanche scar to the glacier limits (5400-6000 m asl) on the western and northern sides. The western slopes and plateau are covered by a 15-30 m thick sequence of tephra fallout deposits, that contain erosional unconformities interpreted by Barba (2006) to be glacial advances dating to the LGM period (~ *ca* 33-14 ka). The northern flank of this young cone experienced a small-volume sector collapse, which is visible along the Río Colorado valley terraces as a reddish debris avalanche deposit. The Río Colorado debris avalanche deposit (RC-DAD) is estimated to be 4-5 m thick on average (Samaniego et al. 2012) and is overlain by moraines from the Younger Dryas period (Clapperton 1990). The lower part of the amphitheater left by this collapse is filled by Neoglacial material and the current glacier. Deposits from CH-III range from basaltic-andesite to dacite-rhyolite compositions (Samaniego et al. 2012).

Chimborazo's young cone remained active into the Holocene with small magnitude eruptions that produced pyroclastic flow deposits (PFD). From the eastern to northern side of the mountain, stratified ash and fallout layers interbedded with paleosols lie atop moraines associated with the Younger Dryas (or Late Glacial) period and below Neoglacial deposits. The fullest exposed section is ~4-5 m thick, but in many places the ash has been reworked and manifests as thinner layers. Also connected with this eruptive activity are

red lahar deposits (1-2 m thick) in the north, west, and southwest catchments. These, too, overlie Late Glacial till and are covered by Neoglacial material.

Pleistocene glaciations have strongly affected the geomorphology of Chimborazo, and morainic and glaciofluvial deposits can be found on all sides of the mountain (Clapperton & McEwan 1985; Clapperton 1990; Heine 1993). On the north, east, and south flanks, older moraine complexes, dated to the LGM (~33- 14 ka), consist of 5-10 m high inner moraines and 100-200 m high outer moraines. Several meters of paleosols and reworked ash cover these moraines (Clapperton & McEwan 1985). Radially distributed around the mountain are terminal and lateral moraine deposits corresponding to the Late Glacial period (~13-15 ka)(Clapperton & McEwan 1985; Heine 1993). In the Río Mocha valley, the lateral moraines from this period range from 3-8 m in height (Clapperton 1990)and are associated with a sequence of interbedded glaciofluvial, till, and lacustrine deposits on the floor of the Río Mocha valley. A younger group of massive moraines and glacial deposits, found near the current glaciers all around the mountain, are ascribed to multiple small advances during the Neoglacial period (since ~5 ka). The true thickness of these deposits is unknown, but on the eastern side they rise 80-120 m above the ice and valley floors.

2.2.3 Geologic Cross-Sections

Within the Gavilan Machay subcatchment and the Upper Río Mocha main valley, three cross sections traversing the stream channel and one cross section running along the stream channel were constructed (Figure 2.8). Cross section line locations were chosen to obtain a representation of subsurface geology spaced according to elevation. Upper profile

lines follow surface and lithologic contacts were manually constructed based on interpretations from the geologic map and unit thicknesses in the literature. Overall, the near surface geology in the study watershed is dominated by glacial deposits with volcanic flows from the CH-I and CH-II stages outcropping on steep slopes. Owing to the extensive amount of poorly constrained colluvium deposits overlying older geology, cross-sections and unit thicknesses in the Upper Río Mocha main valley are more uncertain. Geomorphology and limited outcrops have been used to identify glacial moraines whose geomorphic heights, rather than true unit thicknesses, have been noted (Clapperton & McEwan 1985; Clapperton 1990; Heine 1993). Moreover, one 22 m sequence of glaciofluvial and glacial lacustrine sediments, resulting from moraine dams during the Late Glacial period, has been identified, but there may be other similar deposits associated with activity during the Last Glacial Maximum. The extent and origin of (Chimborazo vs. Carihauirazo) volcanic flows under the valley deposits is also unknown, as is depth to basement rocks.

2.2.4 Hydrogeologic Interpretation

The stratigraphy, now mapped through cross-sections, serves as a basis for inferring aquifers on Chimborazo. Certain types of geologic units may correlate with specific hydraulic properties, such as porosity and permeability, which can be used to infer major aquifers and subsurface flow. Various studies have identified recharge locations and aquifers according to geologic features in glaciated mountain catchments. In both the Cordillera Blanca of Peru (Baraer et al. 2015) and Frontal Range in Colorado (Clow et al. 2003), valley side deposits and talus slopes were identified as major recharge areas and

aquifers. Moraines, too, have been found to convey and store groundwater flow in the Ecuadorian Andes (Favier et al. 2008) as well as the Canadian Rockies (Langston et al. 2011). Additionally, poorly sorted moraine aquifers may have low but non negligible hydraulic conductivities that buffer hydrologic systems through slow flows and protracted discharge periods (Clow et al. 2003). Meltwater infiltration has been identified at the glacier base on Volcán Antizana, and has been hypothesized to flow through deep groundwater pathways before discharging at much lower elevations (Favier et al. 2008). On Chimborazo, such flow systems could occur in the relatively young volcanic bedrock that forms the base of the mountain. In the Cascade Range in Oregon, young fractured volcanic bedrock serves as an important reservoir (Tague et al. 2008). Chimborazo's location on the Pallatanga fault zone and history of sector collapse (Samaniego et al. 2012) would suggest its volcanic units are fractured as well. Although, geologic stratigraphy cannot be assumed to directly correspond to hydrostratigraphy, the mapped features presented here can be used, together with hydrologic observations, as a structural basis for quantifying the hydrogeologic properties of different units.

2.3 An Updated Land Cover Map of Volcán Chimborazo Using Object Based Image Analysis (OBIA)

2.3.1 Introduction

Through evapotranspiration, vegetation plays an important role in the water budget of a watershed, and thus mapping vegetation type and extent in the upper Río Mocha watershed on Volcán Chimborazo is critical for evaluating its hydrologic response to climate change. Before our work, the only available land cover and vegetation data comes

from a 1983 Ecuadorian Department of Geography (Departamento de Geografía) map that is based off of land surveys conducted between 1976-1978, Landsat images from that time, and topographic data from the Instituto Geográfico Militare del Ecuador (IGM). This map is unlikely to be an accurate representation of current urban, agricultural, and native plant cover. In the last three decades, the province containing Chimborazo has seen an approximately 50% population increase from 304,300 to 458,281, triggering urban and agricultural expansion in the region (INEC 2010). Moreover, recent studies have shown that warming trends and the exposure of new ground due to glacier shrinkage have contributed to upslope shifts in vegetation limits on Chimborazo (Morueta-holme et al. 2015) and other glaciated mountains (Schmidt et al. 2008). Such changes necessitate an updated land cover map, which can be created by utilizing remotely sensed imagery.

Until recently, pixel based approaches dominated analysis of remotely sensed data. For moderate resolution sensors, such as Landsat, SPOT, and ASTER, an object on the ground is generally smaller than a pixel size, and classification is carried out by analyzing the spectral signatures of each pixel individually. However, the ever-increasing availability of finer resolution imagery has led to algorithms that examine a group of pixels that together make up an object in an image. This object based image analysis (OBIA) allows for classification based on characteristics such as shape, area, elevation, and texture in addition to pixel spectra, and in this way, imitates the manner in which a person would classify features in an image. These advantages make object based image analysis one of the most comprehensive methods for analyzing data (Blaschke 2010; Blaschke et al. 2014).

Here, object based image analysis is conducted utilizing Landsat 8 imagery, high resolution (30 cm) RGB orthophotos, vector data, and a digital elevation model (DEM) in order to delineate new land cover class boundaries and create a revised land cover map of Chimborazo, focusing on our intensive study watershed in the upper Río Mocha. The ability of OBIA to accurately classify land cover in other mountainous regions has been well-documented (Dorren et al. 2003). Additionally, researchers have shown that because object based approaches can incorporate object characteristics such as geometry, placement, and size, in addition to spectral information, accurate classifications can be achieved on high resolution, RGB images alone (Hu et al. 2013; Kressler et al. 2005).

2.3.2 Methods

2.3.2a Data Retrieval and Pre-*eCognition* Processing

Central to the OBIA procedure here is the high 30-cm resolution RGB (red-green-blue) imagery of Volcán Chimborazo, which is available from aerial photo surveys conducted by the Sistema Nacional de Informacion de Tierras Rurales e Infrastructura Tecnológica (SIGTIERRAS; http://www.sigtierras.gob.ec/descargas/) initiative of the Ecuadorian Ministry of Agriculture, Livestock, Aquaculture and Fisheries. Images over the Chimborazo area were collected during March-October 2011. A mosaic of two of the SIGTIERRAS images was needed to span the entire upper Río Mocha watershed. The white border surrounding each image was removed by tracing the edge of the image and creating a subset in *ERDAS Imagine;* the resulting images were then merged with the Mosaic Pro feature (Figure 2.12).

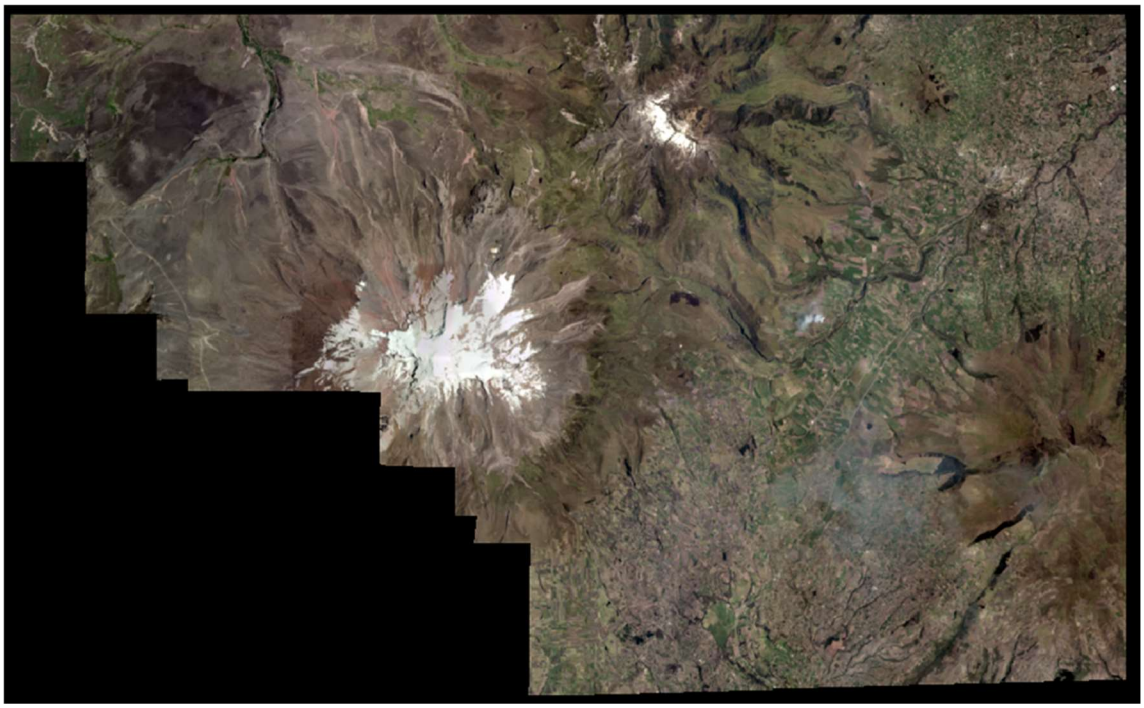

Figure 2.12. Mosaic of two RGB orthophotos from the SIGTIERRAS initiative. Spatial resolution is 30 cm. A third photo comprising the Southwest corner of the image was available, but processing time constraints necessitated limiting the mosaic for rule set development to only two images. The two shown above were selected because they included the main study watershed—the Upper Rio Mocha.

A Landsat 8 L1T (terrain corrected) satellite image from September 15th 2015 of the Chimborazo region (obtained using USGS Earth Explorer) is composed of 11 bands, 8 of which were utilized in this analysis: Coastal Aerosol, Blue, Green, Red, NIR, SWIR 1 & 2, and Panchromatic. Landsat 8 L1T satellite data delivers multispectral data at a spatial resolution of 30 meters and panchromatic data at 15-meter resolution. An HPF (High Pass Filter) resolution merge was applied using the ERDAS Imagine software to pansharpen the 30-meter multispectral bands using the higher resolution 15-meter panchromatic band.

ERDAS Imagine model builder was then used to create a cloud mask binary layer, in which a value of one indicates non-cloud cover. All pixels in the pansharpened image with brightness level above a certain value were assumed to represent cloud cover and were

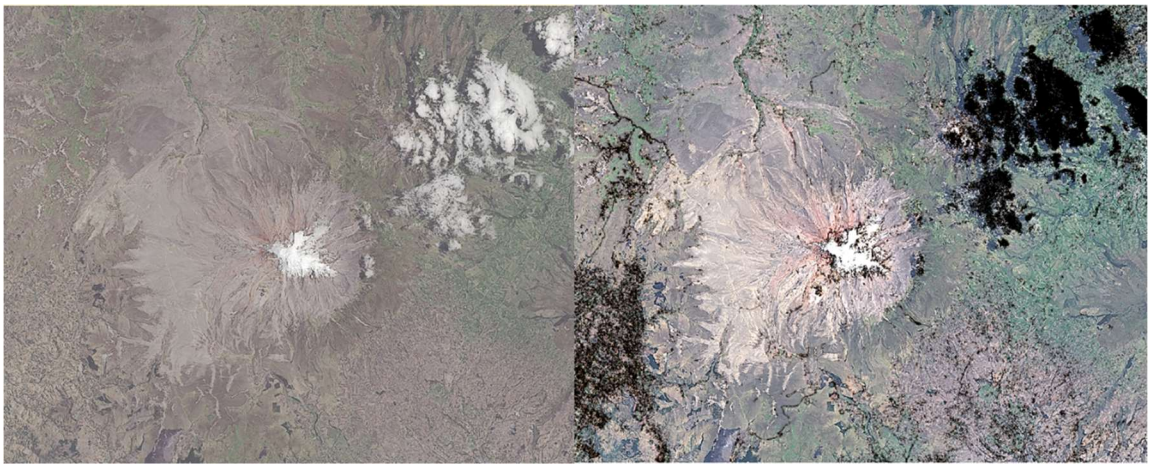

Figure 2.13: Comparison of pansharpened Landsat 8 image (right) with cloud masked image created in ERDAS Imagine (left). Black areas in the top right quadrant are clouded. A standard deviation stretch is applied to both images—the left image appears different because the range of digital number (DN) values changed post masking.

assigned values of zero. This binary layer was then applied to the original pansharpened image to produce an image in which the clouded pixels are masked out (Figure 2.13).

Two additional layers were used for OBIA: a 30-meter digital elevation model (DEM) from ASTER global DEM version 2 (https://asterweb.jpl.nasa.gov/gdem.asp), which is a product of NASA and METI and a vector layer delineating the 2013 extent of clean and debris-covered glacier ice (La Frenierre & Mark 2017).

All four layers-- DEM, RGB orthophoto, Landsat 8 scene, and glacier vector layer—were projected using *ArcMap* into Transverse Mercator, NAD 1983, UTM Zone 17S and then imported into the eCognition software program for OBIA. eCognition is a software that can import multiple forms of geospatial data – elevation rasters, spectral data, lidar, vector files – and utilize them together in the generation and classification of image objects in order to produce a single classified image.

2.3.2b Development of *eCognition* Rule Set

OBIA in eCognition is based on an iterative process of segmentation, classification, and examination. In segmentation, eCognition uses the spectral similarities of neighboring pixels to group them and define image objects. There are different types of segmentation algorithms with parameters, such as spectral band weight, that can be adjusted to define the factors (i.e. shape, color, compactness) by which image objects are segmented. Vector layers (thematic layers) can also be used during this step to create an image objects. During classification, eCognition uses the unique characteristics (features), or sets of characteristics, of image objects to classify them. Hundreds of features can be used for classification including geometry (roundness, area, sinuosity, etc.), layer value (spectral band value, brightness, etc.), texture, and location context (i.e. proximity to water, elevation, etc.). Additionally, basic layer values can be used to calculate new values, such as the normalized difference vegetation index (NDVI) or the mean value of a spectral band, upon which to classify. The simplest classification method involves setting thresholds (i.e. mean blue > 170) to define classes. Multiple feature thresholds can be used simultaneously to define a single class (i.e. elevation > 3000 & red < 40), and classification can be done step-wise such that classified objects are excluded from subsequently executed algorithms. The set of segmentation and classification algorithms used to produce a classified image is referred to as a rule set. After both segmentation and classification, the user should examine the rule set results. If it has not produced a physically plausible result, parameters should be adjusted and the process executed again.

Level	Stage	Process	Specifications & Conditions
1	Segmentation	Multi-resolution	Weighted based on RGB mosaic R- 2, G- 3 , B-1
			Utilized Thematic layers to isolate glaciers and agricultural area
			Scale: 40, Shape: 0.1, Compactness: 0.2
	Classification	Assign Class by Thematic Layer	Assigned Glacier area by Glacier vector layer using attribute = "Glacier_type" (i.e. Debris Covered vs. Clean Ice)
			Assigned Agricultural area using Agriculture vector layer, attribute = "ID"
2	Segmentation	Spectral Difference	Max spectral difference: 10
			Weights: DEM-1, G- 3, R- 2
			Yes to weighting thematic layers
			Segment on "unclassified" areas
	Classification	Assign Class (all processes act on "unclassified" unless otherwise stated)	SNOW - At image object level based on mean Blue from mosaic> 160 & mean DEM value>4780
			ROCK/DIRT/GRAVEL - Image object level based on LS_NDVI<0.11
			LAKES/PONDS- Image Object Level, acts on unclassified and agricutlure areas, based on mosaic R+G+B <220, Roundness< 1.05, Area>=759 pixels
			DARK TREES/SHRUBS - img object level, based on mosaic R+G+B <200
			BUILDINGS- Image Object Level, acts on unclassified and agriculture image objects, based on mean Blue from mosaic > 170 & compactness <2.2
			NATIVE GRASSLAND/GROUNDCOVER- Image object level, unclassified area, no conditions.

Table 2.1. Final *eCognition* rule set. All weightings and conditions used by the software to differentiate between land cover classes are shown for each process. Segmentation and classification processes are shown in sequence; designations of unclassified refer to image objects that have not been classified by any previous process. The mosaic label signifies that data from the orthophoto mosaic was utilized in the process.

Long rule set processing times for the high resolution orthophotos (>26 hours to test one rule set) made it impractical to use the automated program to separate agricultural areas from bare earth and native vegetation. Instead, a visual assessment of the agricultural area was used to generate a vector layer in ArcMap, which was then imported into ECognition and used to classify agriculture. Once agricultural area was established, different combinations of rules to classify the rest of the image were tested in eCognition, resulting in a final rule set involving two levels of segmentation and classification (Table 2.1) for identifying 9 land cover types (agriculture, clean ice, debris-covered ice, bright buildings, lakes/ponds, rock/dirt/gravel, snow, dark trees/shrubs, native grassland and ground cover).

In the first level, a multi-resolution segmentation was executed on the RGB orthophoto to generate image objects. Within this segmentation, weightings were assigned to the red, green, and blue bands on the orthophoto, with green most heavily weighted. This was found to produce the best visual alignment between image objects and vegetation borders. The vector layers described above were used to define the glacier extent and agricultural area as image objects as well as directly classify them. This was done to distinguish debris covered glacier area from other rock/dirt/gravel, and agricultural area from native grassland or rock/dirt/gravel, since these may otherwise be confused in the second level processing. Since classes at this level were only assigned according to these vector layers, a scale factor of 40 was used. The scale factor controls the amount of spectral variation allowed within a signal image object; here 40 allows moderate variation in objects' spectral signatures. Compactness and shape parameters were left at their default values, which proved to provide an adequate segmentation. Compactness is a weighting for the closeness of pixels within an image objects (i.e. do they cluster in a circle, or is their spread more sinuous), while shape is a weighting for how heavily the shape, as opposed to the color, of an object influences segmentation. Higher values of each correspond to a stronger effect on pixel groupings.

In the second level, a spectral difference segmentation grouped the smaller segments that were not yet classified ("unclassified": non-glacier, non-agriculture) into larger regions to avoid overly fragmented land-cover mapping. The spectral difference algorithm merges neighboring objects when the difference in the spectral band means are less than a given threshold (here: 10). Weightings were again assigned, but this time to the

DEM as well as the orthophoto green and red bands. A second round of classification then identified the remaining land cover types—snow, rock/dirt/gravel, buildings, ponds/lakes, dark trees/shrubs— using the specific conditions and rules shown in the Table 2.1. NDVI, in which vegetated areas appear brighter and bare earth darker, was calculated using the Landsat red and near infrared bands and utilized to threshold areas of rock, dirt, and gravel. DEM information was used to threshold the elevation of snow and calculations of RGB band information (sum, mean, etc.) were used in thresholding other classes. No classification parameters were used for the native grassland and groundcover class, as it was assumed that by this step any unclassified land must belong to the class. The resulting output was a classified raster file at 30 cm resolution.

2.3.3 Results and Discussion

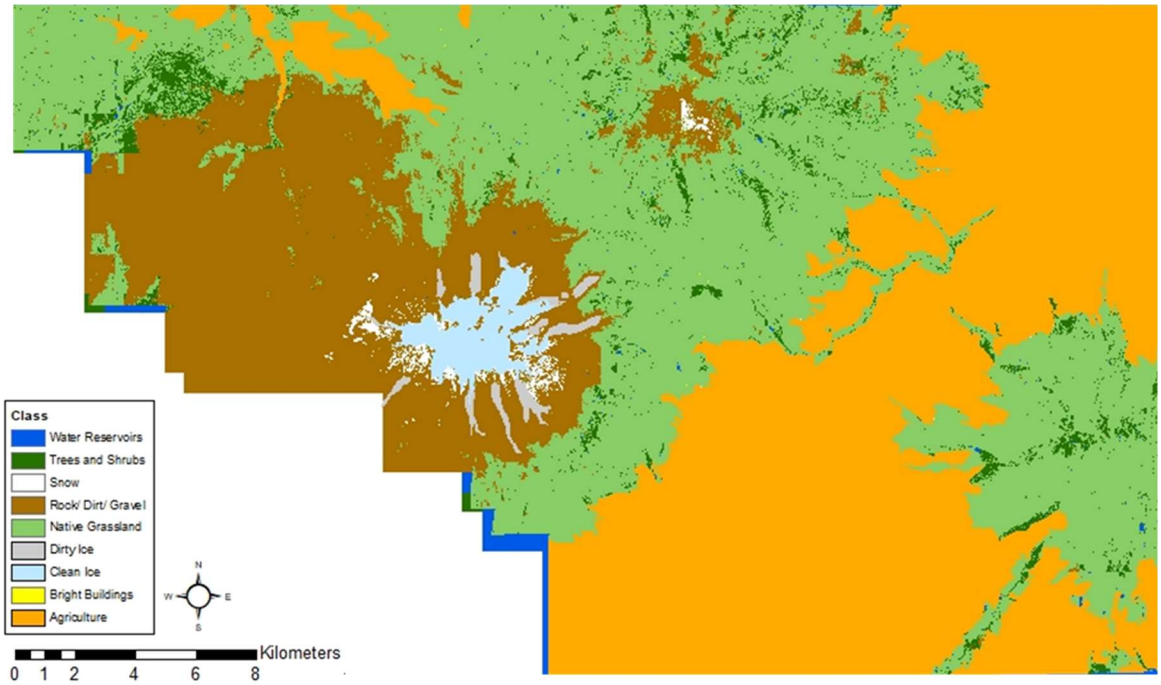

Figure 2.14 Final Landcover Classification Using OBIA Approach. Only 8 of 9 classes are visible, as bright buildings are too small to discern at this viewing scale. Blue edges along the lower left margin are misclassified due to no data pixels.

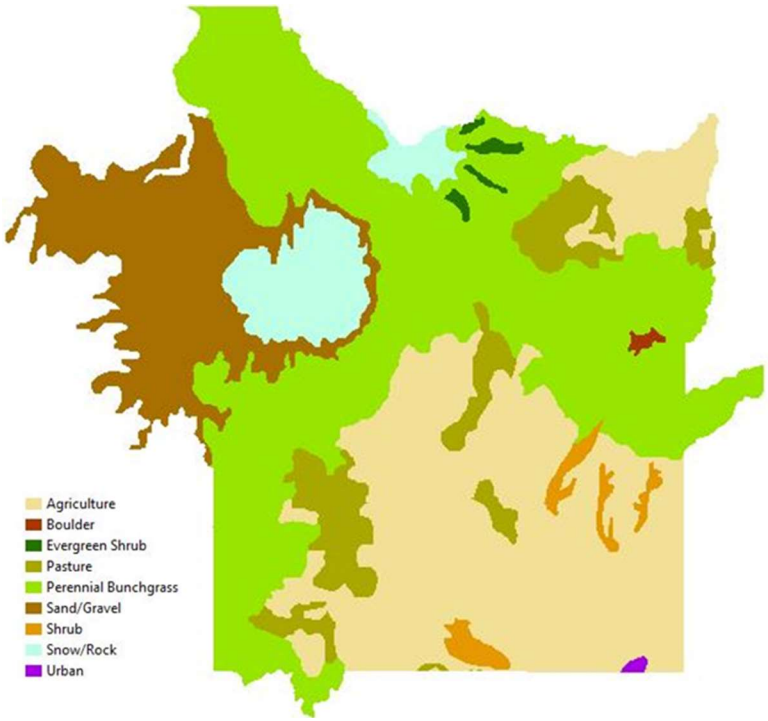

Figure 2.15. 1978 Land cover classification for the area surrounding Chimborazo. This classification came from a 1983 Ecuadorian Department of Geography Map that is based off of land surveys conducted between 1976-1978, and was digitized by Jeff La Frenierre (2014).

Figure 2.14 shows the final land cover classification map containing nine different classes (note that "bright buildings" are not easily discernable at the figure scale). The rock/dirt/gravel class represents glacial and volcanic geologic material that cap the top and western side of the mountain; its extensive area in the west reflects the rain shadow effect that produces semi-arid conditions. The aim is to cl assify semi-permanent land-cover types, yet it should be noted that lake and pond extents and snow cover can be highly dynamic.

A digitized version of the 1978 land cover map for this region is shown in Figure 2.15. Though this map has slightly different classes than those used in the updated map, it is still possible to qualitatively evaluate major land cover changes between 1978 and 2011.

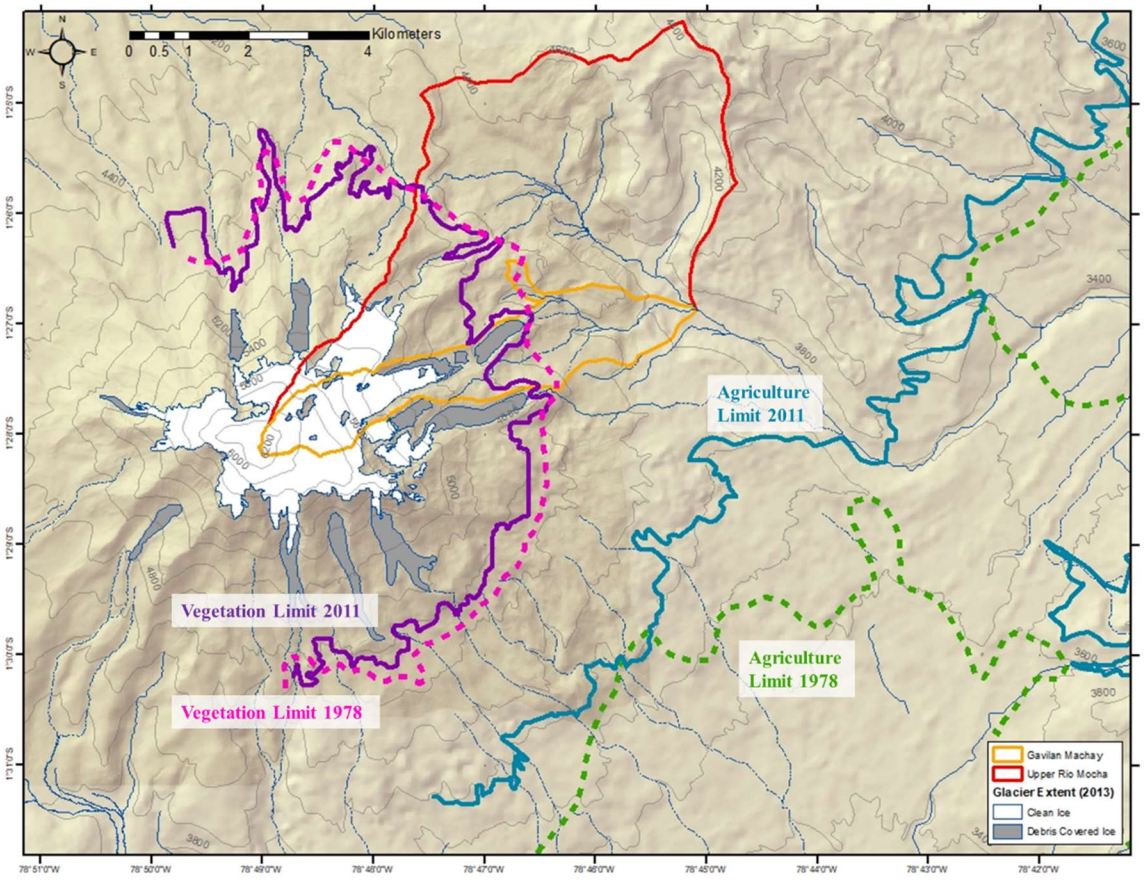

Figure 2.16 Comparison of 1978 (dashed) and 2011 (solid) boundaries of vegetation limit on Chimborazo and agricultural area in the Riobamba valley. On the mountain slopes (left) the upper limit of vegetation migrated upslope from between 20 to 150 m during the 1978 (pink) to 2011 (purple) period. In the Riobamba Valley (right), from 1978 (green) to 2011 (blue), pasture land and agriculture have expanded appreciably both uphill on Chimborazo and further North in the valley.

The upper elevation limit migration of vegetation and the expansion of agriculture and pasture land are particularly noteworthy (Figure 2.16). The limit of vegetation appears to have moved upslope by approximately 20 m to 150 m, depending on the location. This shift in elevation appears most pronounced on the east to southeast side of the mountain. Such changes are consistent with Morueta-Holme *et al.* (2015), which found an upslope shift in vegetation on Chimborazo of over 500 m since 1802 using field surveys. Similarly,

from 1978 to 2011, the boundaries of agriculture and pasture land appear to have shifted upslope by as much as 250 m and entirely filled the southeast valley that was previously perennial bunchgrass (Figure 2.15). The conversion of native grasslands (called "páramo") to agricultural fields with population growth has been documented across the Andes (Van der Hammen et al. 2002; Buytaert et al. 2006; Kintz et al. 2006), further motivating the need for assessing changing ecohydrologic regimes that impact water resources.

The map produced here is an improvement on the previous 1978 land cover classification in a number of ways. For instance, the 1978 map assigns the entire mountain top to the general class of "snow/rock", but resolving the delineations between glacier, rock, and snow in the new map is valuable for future glacier change analysis. Additionally, this new map has a finer spatial resolution, while still covering a large area, which allows for analyses to be conducted at a range of scales from sub-watershed to regional.

The map presented here demonstrates a successful OBIA rule set for land-cover mapping for the main study watershed (upper Río Mocha) and can be expanded in future work to incorporate a third orthophoto covering the southwest slopes of Chimborazo. A significant east-west precipitation gradient on Chimborazo results in distinct ecosystems on the different slopes, and land-cover shifts on the west side could differ from that found on the east side. Additionally, ground surveys, field observations, and new data from SIGTIERRAS (if available) could be synthesized to refine classifications within agricultural categories (e.g. crop type, pasture) and native vegetation groupings. Lastly, a preliminary visual accuracy check was carried out in isolated portions of the map, but a

more thorough comparison against the original RGB image is needed to detect mis-classifications.

2.4 Conclusions

Mapping surface and subsurface geologic features and vegetation is critical for understanding the roles of groundwater and transpiration in the water balance and discharge within a watershed. Ultimately, hydrologic properties inferred from the geologic cross-sections and the updated vegetation map will be used in an integrated watershed model to quantify the hydrologic response of Chimborazo's watersheds to climate change. Accurate mapping of hydrologic parameters, glacier extent, bare ground, and vegetation types will be essential for simulating infiltration, groundwater flow, and evapotranspiration – key processes in determining watershed discharge.

Chapter 3: Using Hydrochemical Tracing to Partition Glacial Melt Between Surface and Groundwater Sources

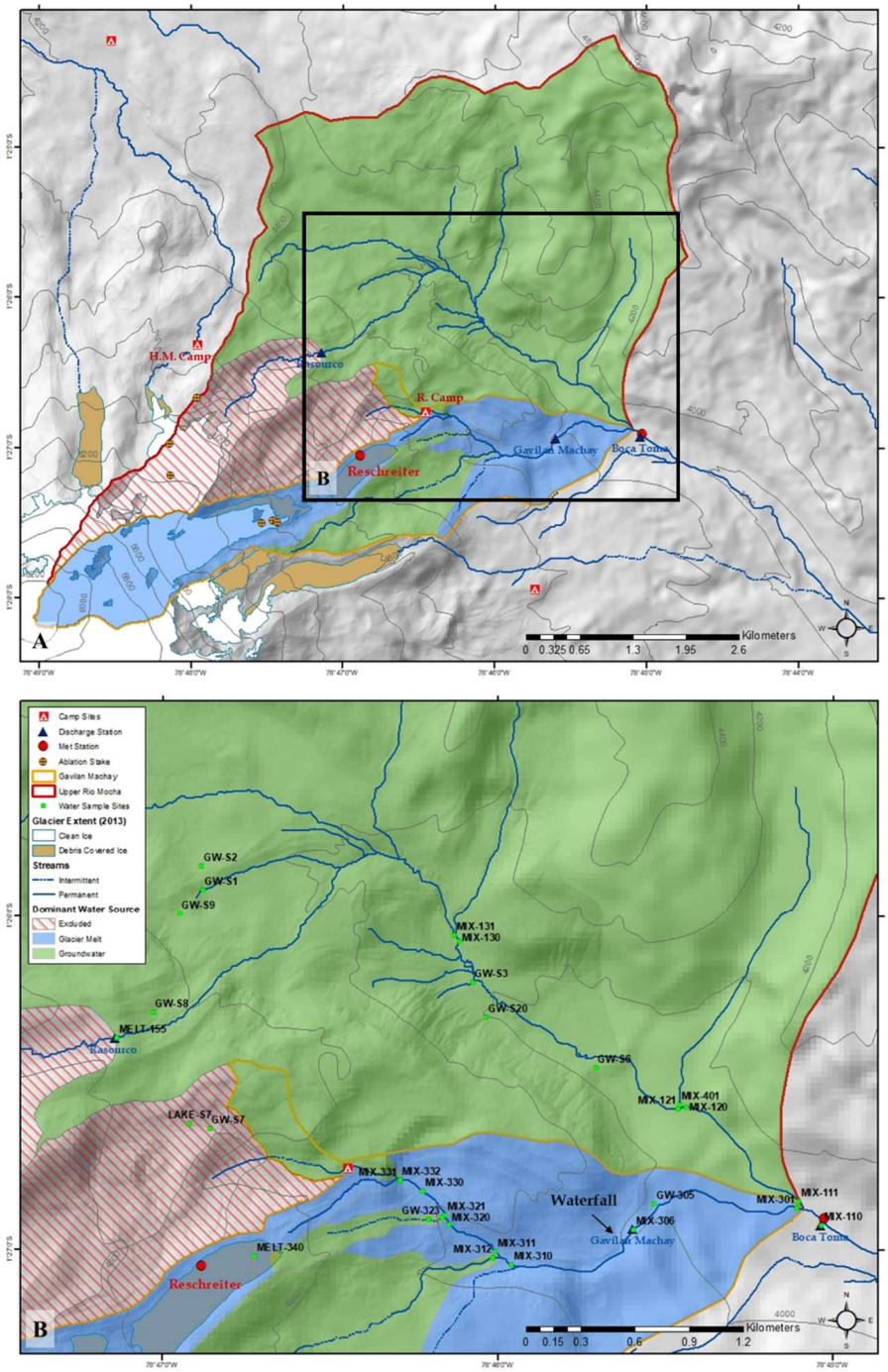

Figure 3.1 Monitoring network (A) and water sampling sites (B) in the Upper Rio Mocha watershed.

3.1 Methods

3.1.1 Water Sample Collection and Laboratory Analysis

Water samples were collected using a synoptic sampling approach in June 2015 and June 2016 during the long dry season (June to September) and in February 2017 just following the short dry season (December to January). Water samples from June 2015 were collected by Jeff La Frenierre and Helen Thompson (Gustavus Adolphus College). In synoptic sampling, all samples are taken over a sufficiently short period of time that they mainly capture the spatial variability in hydrological conditions and not temporal variability (Mark & Mckenzie 2007). In 2015, samples were collected between June 12th and 15th, in 2016 between June 25th and July 7th, and in 2017 on February 4th and 7th. Though logistical difficulties extended the sampling period in 2016, efforts were made in the 2017 season to ensure that all samples from each subcatchment (i.e. Gavilan Machay and the main valley of the Upper Río Mocha) were collected over short time periods on single days (Figure 3.1).

In addition to avoiding long multi-day time periods over which water chemistry may evolve, it is necessary to ensure that diurnal hydrochemical variability due to variable melting is not significant. To check this, in 2017 in the Gavilan Machay subcatchment, I used an Atlas Scientific EZO^{TM} conductivity probe and attached thermistor to measure conductivity (µS/cm) and temperature (˚C) changes in the stream at the tongue of Reschreiter glacier over a 24-hour period. The probe was deployed using the ALog Arduino Datalogger (Wickert 2014) to collect data at 1-minute intervals over the 24-hour

period during which water samples were taken. The conductivity data were temperature-corrected using the formula:

$$SC = AC/ (1 + R*(T-25)),$$

where SC is Specific Conductance (μS/cm), AC is Actual Conductivity (μS/cm), T is temperature of sample in degrees C, and R is a temperature correction coefficient for the sample (0.0191) (American Public Health Association, 1999). A calibration curve generated in the lab using a YSI Pro Plus was also applied to correct an additional offset detected in the Atlas EZO probe measurements. After calibration and temperature correction, the fine time resolution data confirmed that the diurnal variability in stream was negligible when compared to the spatial variability in specific conductivity across the Gavilan Machay subcatchment (Appendix A).

In 2015, 16 samples were collected in the Upper Río Mocha catchment: 1 glacial melt, 4 groundwater (taken from springs), and 11 stream. In 2016 a total of 37 water samples were collected: 6 ice (melted after collection), 1 glacial melt, 3 precipitation, 11 groundwater, 1 surficial pond, and 15 stream. Finally, in 2017, 34 samples were collected: 1 glacial melt, 1 overland flow (representing precipitation), 12 groundwater, 23 stream. More stream samples were collected in 2017 owing to a duplication of samples at the Gavilan Machay-Boca Toma confluence and the addition of four sampling points in the Gavilan subcatchment that had been omitted during the 2015 and 2016 campaigns. From both the main Río Mocha channel and Gavilan Machay stream, samples were collected in sets of three at each confluence, with one sample taken from each tributary immediately upstream of the junction point, and then one sample in the main channel at least 50 m

downstream of the junction point in order to obtain mixing of the two tributaries. Glacial melt samples were collected from the water running out from the glacier tongue and groundwater samples were taken from natural springs. Springs ranged from developed concrete capture boxes to small seeps coming out from valley walls.

Precipitation samples in 2016 were collected using evaporation-proof totalizing rain gauges constructed of a series of nested funnels feeding into 30 ml nalgene sample bottles, with a ping pong ball inside the funnels to prevent evaporation. Gauges were installed at the Boca Toma weather station (3899 masl), the Reschreiter base camp (4471 masl), and the Hans Meyer base camp (4780 masl) (Figure 3.1) and left for 3-6 days. Surficial pond water was collected from a large pond in a *bofedal* above Reschreiter base camp (Lake-S7). In 2017, an overland flow sample was taken during a precipitation event at a normally dry location at Reschreiter base camp to capture any chemical signature in overland flow that is distinct from precipitation.

Ice samples were obtained during the installation of ablation stakes (described below) on both Reschreiter and Hans Meyer glaciers. A drill-powered ice-auger was used for installing the stakes, and ice samples were taken from the chips coming up the bore hole. Average drill depth was ~2.5 m and bulk samples were taken from three depth intervals generally categorized as top, middle, and bottom. To avoid contamination by either snow or refrozen surface ice, snow was cleared from the glacier surface prior to drilling, and chips from the first ~30 cm of augering were discarded.

For each non-ice sampling site, 30mL of water was collected, filtered in the field using either 0.45 μm (2016) or 0.2 μm (2017) filter, and stored in Nalgene bottles. Ice

samples were collected in 1 L Nalgene bottles and allowed to melt and homogenize before being transferred into 30 mL bottles. All bottles were capped and sealed with electrical tape to prevent leakage of water or vapor, and then stored near 4˚C as soon as possible. In both years, temperature (˚C), pH, electrical conductivity (µS), and specific conductance (µS/cm) were measured in situ using a YSI Professional Plus Multi Probe System. Major ions were measured at the Environmental Chemistry Lab at Gustavus Adolphus College. Cations (Na^+, K^+, Mg^{2+}, Ca^{2+}) were measured using an Agilent 7700X Inductively Coupled Plasma-Mass Spectrometer (ICP-MS) and Anions (F^-, Cl^-, SO_4^{2-}) were measured using a Dionex ICS1000 Ion Chromatographer (IC). The bicarbonate (HCO_3^-) concentration was assumed to be the charge balance residual, calculated as the difference between the sum of cation charge equivalence and the sum of other anion charge equivalence. The stable isotopes of water ($\delta^{18}O$ and δ^2H) were measured by the Biometeorology Group in the University of Minnesota Department of Soil, Water, and Climate using an LGR DLT-100 Liquid Water Analyzer (a laser spectroscopy system). Reported isotope ratios are relative to the Vienna Standard Mean Ocean Water (VSMOW) and typical precisions are +/-1.0 ‰ for deuterium/hydrogen values and +/-0.25 ‰ for $^{18}O/^{16}O$ values.

3.1.2 Field Instrumentation

Stream depth measurements were collected at two locations in the Upper Río Mocha Watershed: in the Gavilan Machay stream 1.1 km above its confluence with the Río Mocha, and in the Río Mocha at the Boca Toma diversion structure (Figure 3.1). Depth measurements were made using Solinst Leveloggger Junior pressure transducers. Atmospheric pressure corrections were made on data from both Leveloggers using

synchronous measurements collected by a Solinst Barologger Gold sensor installed at Boca Toma. Depth measurements were converted to discharge volumes with rating curves developed by La Frenierre (2014) according to standard USGS techniques (https://pubs.usgs.gov/twri/twri3a8/).

Meteorological stations installed at 4515 m asl on the debris-covered portion of the Reschreiter Glacier and at 3895 m asl at Boca Toma measured precipitation using Hobo tipping bucket rain gauges. At the Reschreiter Station, the rain gauge was deployed with an Onset Hobo Micro Station Data Logger, while the Boca Toma station rain gauge possessed a Hobo Pendant® Event Data Logger.

In addition to hydrological and meteorological sensors, in June 2016 six ablations stakes (3 each) were installed on the Hans Meyer and Reschreiter glaciers (Figure 3.1). Each ablation stake contained temperature and relative humidity sensors, along with a look-down ultrasonic sensor for measuring changes in distance to the ice surface, which can be used to constrain an estimate of mass loss on the glacier. Ablation stakes were designed by Andrew Wickert and deployed using an open-source Arduino-based ALog data loggers (Wickert 2014). Stakes were positioned along an elevation transect from the toe of the Reschreiter glacier into the edge of the accumulation zone on Hans Meyer glacier. For installation, snow was first cleared from the ice surface and then a drill-powered ice auger was used to drill a hole to a depth of ~2.5 m. All sensors were mounted at the top of a 3 m long PVC tube, which was then sunk into hole. Though data from these stations is not presented here, in the future it will be used to quantify meltwater inputs to the Gavilan Machay stream and Upper Río Mocha catchment.

3.1.3 Hydrochemical Characterization and Mixing Model Method

It is well established that dissolved ions and stable isotopes of water ($\delta^{18}O$ and $\delta^{2}H$) can be utilized in catchment studies to track contributions of different source waters to watershed discharge and identify groundwater flow paths (Ryu et al. 2007; Crossman et al. 2011; Hooper & Shoemaker 1986; Clow et al. 2003; Kendall & Doctor 2003). As water moves through a porous medium, physical, chemical, and biological processes mediate the exchange of ions between the substrate and the water, allowing for unique hydrochemical signatures to develop. Stable isotope signatures, on the other hand, arise from Rayleigh fractionation effects during the hydrologic cycle and are unaltered by interaction with a substrate (Sidle 1998; Kendall & Doctor 2003). During the hydrologic cycle, stable isotope ratios can change due to the amount of precipitation, the amount of evaporation, and the elevation precipitation occurs at (Dansgaard 1964). In mountainous catchments that span wide elevation ranges, the elevation effect tends to be an important control on the spatial variability in precipitation isotopes (Tappa et al. 2016), as demonstrated in many Andean catchments (Mosquera et al. 2016; Baraer et al. 2015; Gonfiantini et al. 2001; Rozanski & Araguas 1995; Vimeux et al. 2005). Aqueous concentrations and stable water isotope observations can thus provide information about sources and pathways of water moving through a watershed. Together, stable isotopes and hydrochemistry have been used in the Andes, and other alpine watersheds, to study the role of glaciers in local and regional hydrology (La Frenierre 2014; Baraer et al. 2009; Mark & Mckenzie 2007; Mark & Seltzer 2003).

All water discharged at the Upper Río Mocha watershed outlet comes from either glacier melt, groundwater discharge, or runoff from precipitation. Here, the proportion of glacier melt in watershed discharge is quantified using the Hydrochemical Basin Characterization Model (HBCM) (Baraer et al. 2009), a multi-component hydrochemical mixing model that was developed for use in data-sparse, glacierized tropical watersheds. Given input and outflow chemistries at different mixing points throughout the watershed, HBCM solves an over-constrained set of mass balance equations to determine the relative contributions of each identified input component to surface flow at that point. By starting the HBCM analysis at a water source (i.e. melt, groundwater, precipitation), the results can be utilized to determine the successive dilution of that source water moving down a stream network to the outlet of the watershed. In this analysis, I assume precipitation is not a significant contributor to overall watershed discharge since sampling is conducted during the dry season, which leaves groundwater and glacier melt as the end members in our mixing model.

HBCM's calculation of relative source contributions depends on three fundamental assumptions. First, end member chemistry is unique and spatially homogeneous within the watershed. In these remote and data sparse catchments end members are typically represented by single samples, making this assumption necessary. Secondly, tracers must be conservative within the stream network, such that their concentrations are purely a result of mixing and not of chemical reactions during or after mixing. HBCM provides some flexibility in the definition of conservative tracers, as its approach of dividing a watershed into overlapping cells (discussed more below) requires that a tracer be conservative only

at the cell scale and not the entire watershed scale (Baraer et al. 2017). Lastly, HBCM assumes that water source mixing is instantaneous and complete (Baraer et al. 2009; Soulsby et al. 2003). The model is capable of analyzing multiple tracers simultaneously as long as they are conservative natural constituents, such as stable isotopes and major ions.

HBCM handles spatial information within a study watershed through the specification of nested interconnected sub-basins called cells. For each cell, HBCM takes the chemistries of contributing waters and solves for the relative contribution of each component to cell outflow using the following set of mass balance equations:

$$C_{tot_j} = \frac{\sum_{i=1}^{n}(C_i * Q_i) + \varepsilon_j}{Q_{tot}}$$

Where:

j : represents natural tracer

i : the input component to the cell

Ctot$_j$: concentration of tracer ***j*** at the cell outlet

Ci$_j$: concentration of tracer ***j*** in component ***i***

n : total number of possible input components to cell

Qtot : Total discharge at cell outlet

Q$_i$: Contribution to discharge from input component ***i***

ε_j : the accumulation of inaccuracies and uncertainties that occur during the sampling and analysis of tracer ***j***

HBCM solves for the unknown relative contributions of each component (Q_i/Q_{tot}) by minimizing the summation of the residual error:

$$\sum_{j=1}^{m} \varepsilon_j$$

where ***m*** represents the number of tracers. In order to over-constrain the problem, the model requires m =n tracers and, preferably, m>n tracers should be utilized in order to avoid the possibility of correlated tracers that do not independently constrain the problem. HBCM in its current form (HBCMQ) limits the maximum number of tracers to m = n + 4. HBCM checks that a tracer is conservative within each cell via three tests:

1. A tracer value in a cell outflow cannot be outside the range bracketed by the possible contributors.
2. The tracer value at the cell outflow, along with that of at least one input component, must be greater than the detection limit of the analytical methods (user confirmed).
3. There must be a minimum 5% difference between the extreme input component tracer values.

If any of these requirements is not met, HBCM will reject the tracer for use in the studied cell.

Cells can either consist of a stream confluence or a stream reach. Reach cells assume groundwater (in the absence of rainfall) to be the only possible addition along the channel, and thus water samples taken at the start of a reach and groundwater serve as input components to be compared with water samples taken at the end of the reach. HBCM is capable of analyzing multiple groundwater sources in a single stream reach and optimizing for the one that best explains observed changes in chemistry between the start and end samples. Confluence cells are where two or more streams join; HBCM considers these tributaries to be the only inputs, ignoring any groundwater contribution unless otherwise directed. Cells are inter-connected by having the outflow of one become inflow to the

subsequent downstream cell. In the Upper Río Mocha catchment, HBCM is applied beginning at the tongue of Reschreiter Glacier (where the stream is considered 100% glacier meltwater) and moving downstream in the Gavilan Machay subcatchment, through the confluence with the main Río Mocha, and to the outlet at Boca Toma. Conceptual schematics of Gavilan Machay for HBCM for 2015, 2016 and 2017are shown in Figure 3.2. The differences between the three years result from slight differences in the sample locations.

Prior to executing HBCM, potential conservative tracers were identified using bivariate (mixing) diagrams and tracer sets were confirmed to constitute unique end-member chemistries with hierarchical clustering analysis (HCA). Mixing diagrams using pairwise combinations of solute concentrations and isotopes were plotted with regression lines through the data to examine whether samples fell along a single mixing line. If the mixing line condition is met, end-members (melt and groundwater) will plot at opposite ends of the mixing line and all mixed samples (stream water) will fall along the line in between the end-members (Christophersen & Hooper 1992; Hooper 2003; James & Roulet 2006). When this occurs, the pair of solutes or isotopes can be considered suitable candidate tracers, because the end-members show distinct signatures, and they appear to conservatively mix in the stream system. Selected tracers are shown in Figures 3.3- 3.5 in the Results and Discussion section.

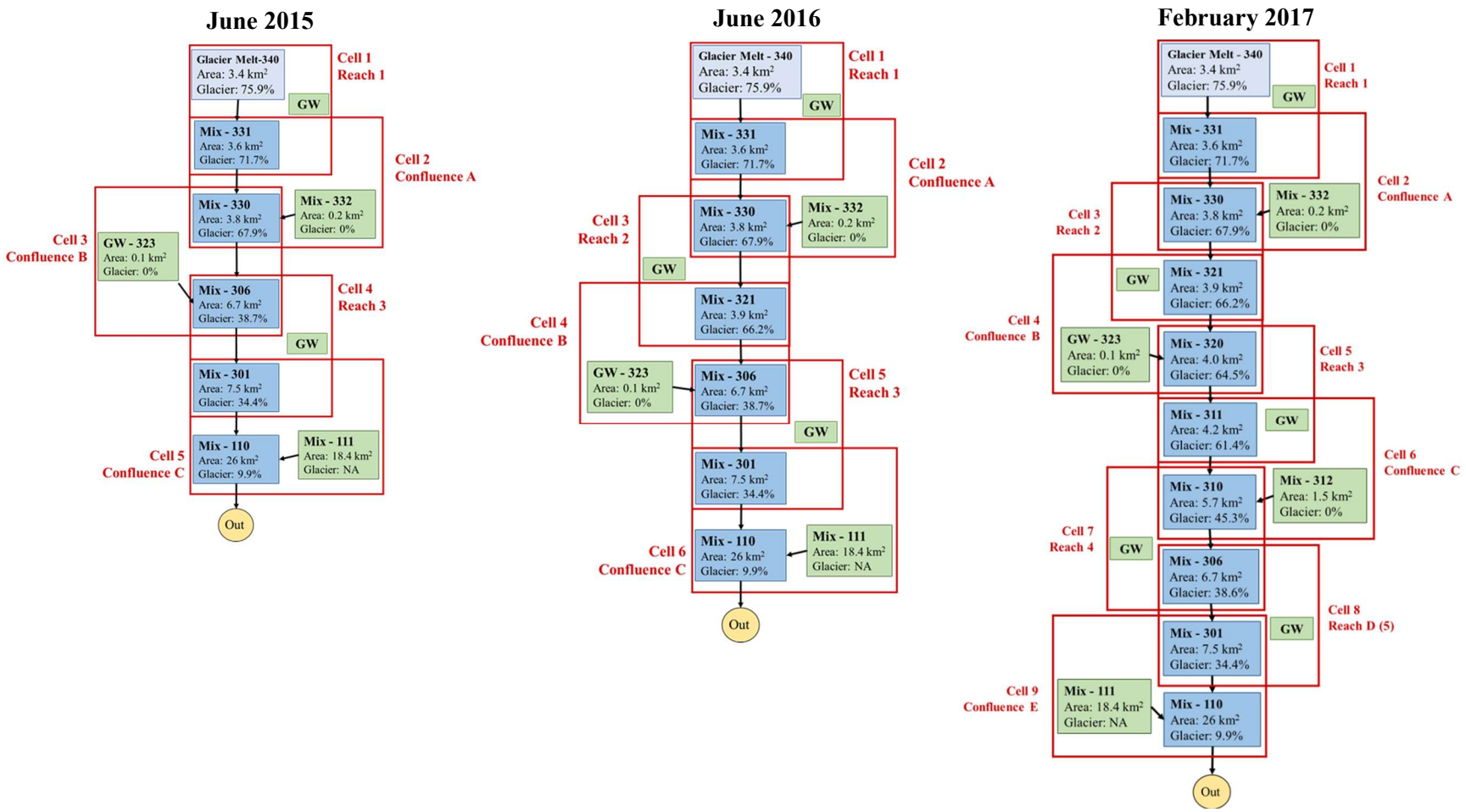

Figure 3.2 Schematic representation of the Upper Rio Mocha watershed for HBCM analysis for 2015-2017 sampling periods.

A hierarchical clustering analysis (HCA) was used to verify uniqueness of end member chemistries for each year based on the tracer combination selected with the bivariate diagrams. To mitigate the effect of subsurface residence time on potential tracer values, which typically increases absolute ion concentrations, relative ion concentrations (i.e. $SO_4^{2-}/\Sigma A^-$, where ΣA^- is the sum of all anion concentrations) were used in the HCA (Baraer et al. 2017). Additionally, water stable isotope values were left out of the HCA, as the inclusion of isotopic values has the potential to confuse the grouping because groundwater isotopic signatures depend on recharge source, which here could be glacial melt or precipitation. The advantage of HCA over the bivariate plots is the ability to simultaneously account for multiple solutes, which permits confirmation that the set of selected tracers is conservative between precipitation, groundwater, and meltwater end members. If the tracer set is conservative, like sources will group together and separately from one another. If they do not, chosen tracers should be re-evaluated.

Chosen tracer concentrations were utilized within each HBCM cell. Stable isotopes can only serve as tracers for confluence cells (Baraer et al. 2017). Isotopes cannot serve as tracers in reach cells for which groundwater serves as an end-member, because groundwater is unlikely to have a single characteristic isotopic signature throughout the watershed. This is because isotopes in precipitation are highly elevation dependent, and assuming groundwater receives recharge at different elevations as it moves through a steep watershed such as the Upper Río Mocha, its isotopic signature would correspondingly change. For each cell, all possible unique tracer combinations are tested in gradually

reducing numbers, such that if the maximum number of available tracers is 7, the first run will include 7 tracers, and the subsequent runs will test all combinations of 6, then all combinations of 5, and so on until the model reaches combinations of only 2 tracers. Output for each tested combination is given as percent contributions from each input component and the corresponding cumulative residual ($\sum_{j=1}^{m} \varepsilon_j$) of the solution (See example: Appendix B). From the output array of different results, those with cumulative residuals within 3x the minimum residual are selected to bracket the optimal range of solutions, and upper and lower bounds of possible input contributions are reported from these solutions (Baraer et al. 2012). Subsequently, the minimum and maximum glacial melt percent contribution at each sampling point is calculated by starting at the glacier tongue (where streamflow is assumed 100% melt) and then applying the input contribution solutions while moving downstream, and assuming that the meltwater is diluted by groundwater contributions.

3.1.4 Isotopic and Hydrochemical Analysis of Groundwater Provenance

The stable isotopes of water are largely unaffected by travel through the subsurface and thus shallow groundwater often mimics the isotopic signature of their source meteoric waters, assuming no fractionation occurs along the groundwater flow path (Clark & Fritz 1997). This has allowed stable isotopes to be used in the identification of origins and pathways of groundwater recharge (Baraer et al. 2015; Mark & Mckenzie 2007; Windhorst et al. 2013). Meteoric water becomes imprinted with signatures of isotopic fractionation during melting, condensation, and evaporation, and meteoric water (i.e. precipitation)

isotope ratios are affected by rainout via Rayleigh fractionation as moisture moves inland and to higher elevations. Studies in the tropical Andes have shown that seasonal isotopic trends in precipitation track closely with volumes of precipitation (Vuille et al. 2003; Vimeux et al. 2005), such that mean annual $\delta^{18}O$ and $\delta^{2}H$ values are dominated by the wetter months (Gonfiantini et al. 2001). Observed spatial variability in $\delta^{18}O$ and $\delta^{2}H$ values are largely dictated by the elevation effect (Rozanski & Araguas 1995; Windhorst et al. 2013). Generally, as water vapor rises and cools, it becomes depleted in heavier isotopes, resulting in decreasing $\delta^{18}O$ and $\delta^{2}H$ values with elevation. The rate of heavy isotope depletion, termed a "lapse rate", is generally linear and measured per 100 m rise in elevation (Dansgaard 1964; Kendall & Doctor 2003; Blasch & Bryson 2007). In Ecuador, $\delta^{18}O$ lapse rates have been measured to be between -0.17 to –0.5 per mil/100m (Garcia et al. 1998; Windhorst et al. 2013; Rozanski & Araguas 1995; Mosquera et al. 2016), while for $\delta^{2}H$ a lapse rate of -1.12 per mil/100m has been measured (Windhorst et al. 2013).

The relationship between elevation and the isotopic composition of precipitation is used to estimate the minimum elevation of precipitation recharging springs (groundwater) in the Upper Río Mocha watershed. The groundwater pathways following recharge is then inferred from total dissolved solids (TDS) calculated as the sum of ion concentrations (ppm). Assuming geochemical reactions whose rates are governed by kinetics gradually release ions from sediment into groundwater, TDS can serve as a proxy for residence time and flow path length.

3.2 Results and Discussion

3.2.1 Sources of Surface Discharge: Quantifying Melt Contribution to Streamflow

Hydrochemical results for the 2015-2017 sampling campaigns (Tables 1-3 in Appendix C) were used to generate bivariate, or mixing, diagrams to identify potential tracers for use in the HBCM mixing model. Because samples were collected in the dry season, when precipitation runoff is minimal, stream discharge samples should consist of varying mixes of groundwater and surficial meltwater only. Bivariate plots of ideal tracers for HBCM will exhibit groundwater (represented by springs) and melt samples as end-members plotting at opposite ends of a clear mixing line along which stream samples lie. For all years, stream samples from the Gavilan Machay stream do comprise an approximate mixing line for Mg^{2+}, Ca^{2+}, Na^{+} + K^{+}, SO_4^{2-}, Cl^{-}, HCO_3^{-}, and $\delta^{18}O$, and these were determined to be adequate tracers and selected for use in the mixing model (Figures 3.3-3.5). Some tracers, in particular sulfate and chloride, have low regression correlation coefficients (R^2) and similar concentrations across samples, which would imply they are weak tracers for mixing at the watershed scale. However, since HBCM tests and rejects non-conservative tracers for each cell, and only requires tracers to be conservative at the cell scale, the inclusion of a tracer that appears non-conservative at the watershed scale is not detrimental to the entire analysis.

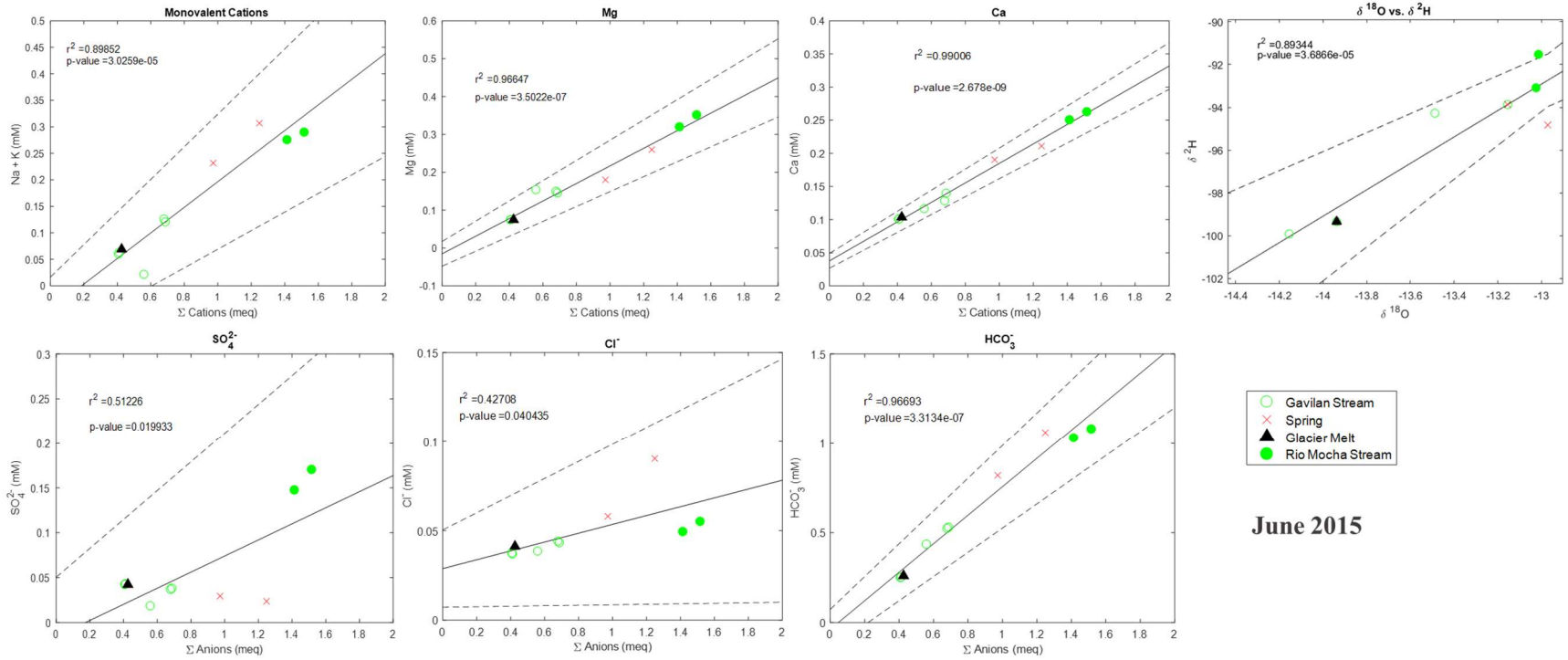

Figure 3.3. Bivariate diagrams of tracers selected for June 2015 HBCM analysis. The solid black lines represent linear regressions through all samples and dashed black lines indicated the regressions' 95% confidence intervals. Samples from the main Rio Mocha channel before and after the Gavilan stream joins it (filled green circles) consistently plot outside or away from the mixing line created between groundwater and meltwater. These samples are also responsible for the poor R^2 and p-values of sulfate and chloride.

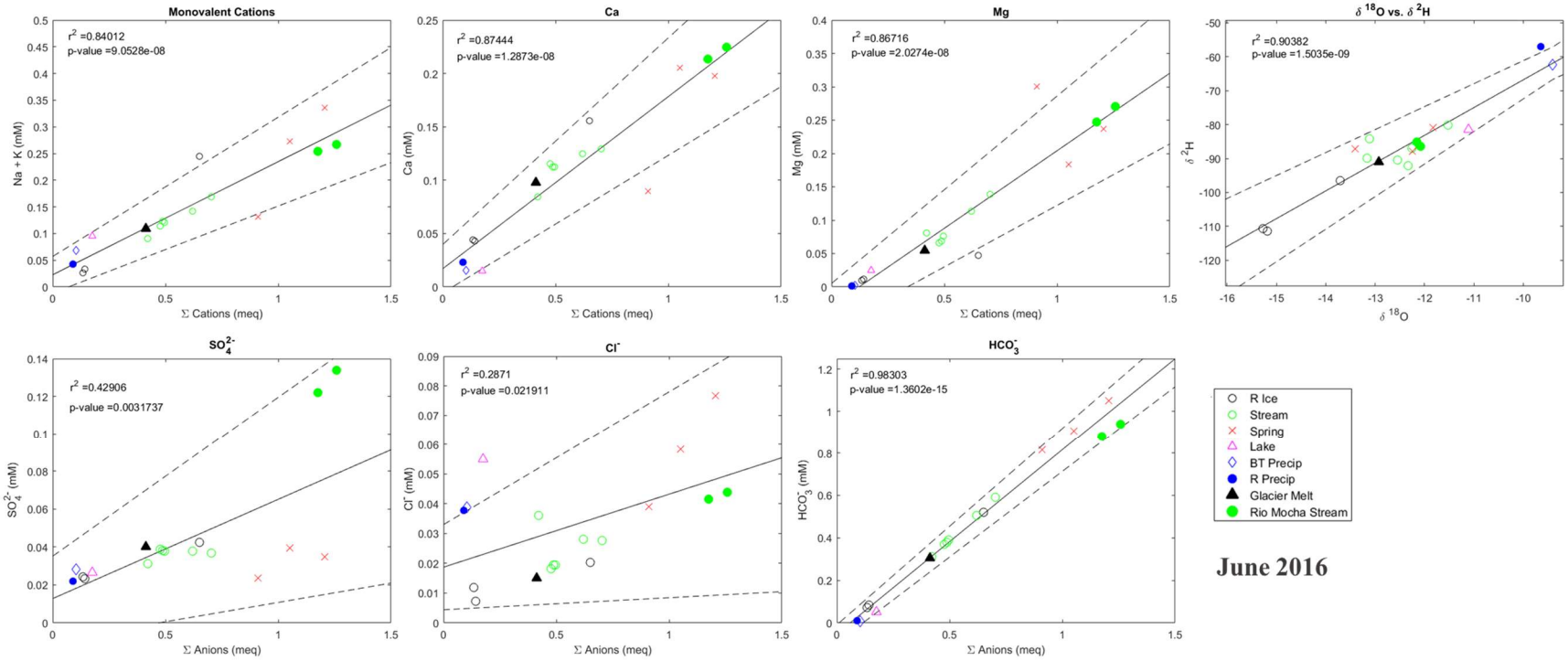

Figure 3.4. Bivariate diagrams of tracers selected for June 2016 HBCM analysis. The solid black lines represent linear regressions through all samples and dashed black lines indicated the regressions' 95% confidence intervals. Samples from the main Rio Mocha channel before and after the Gavilan stream joins it (filled green circles) plot largely outside or away from the mixing line created between groundwater and meltwater. Precipitation samples during this sampling were collected directly from rainfall.

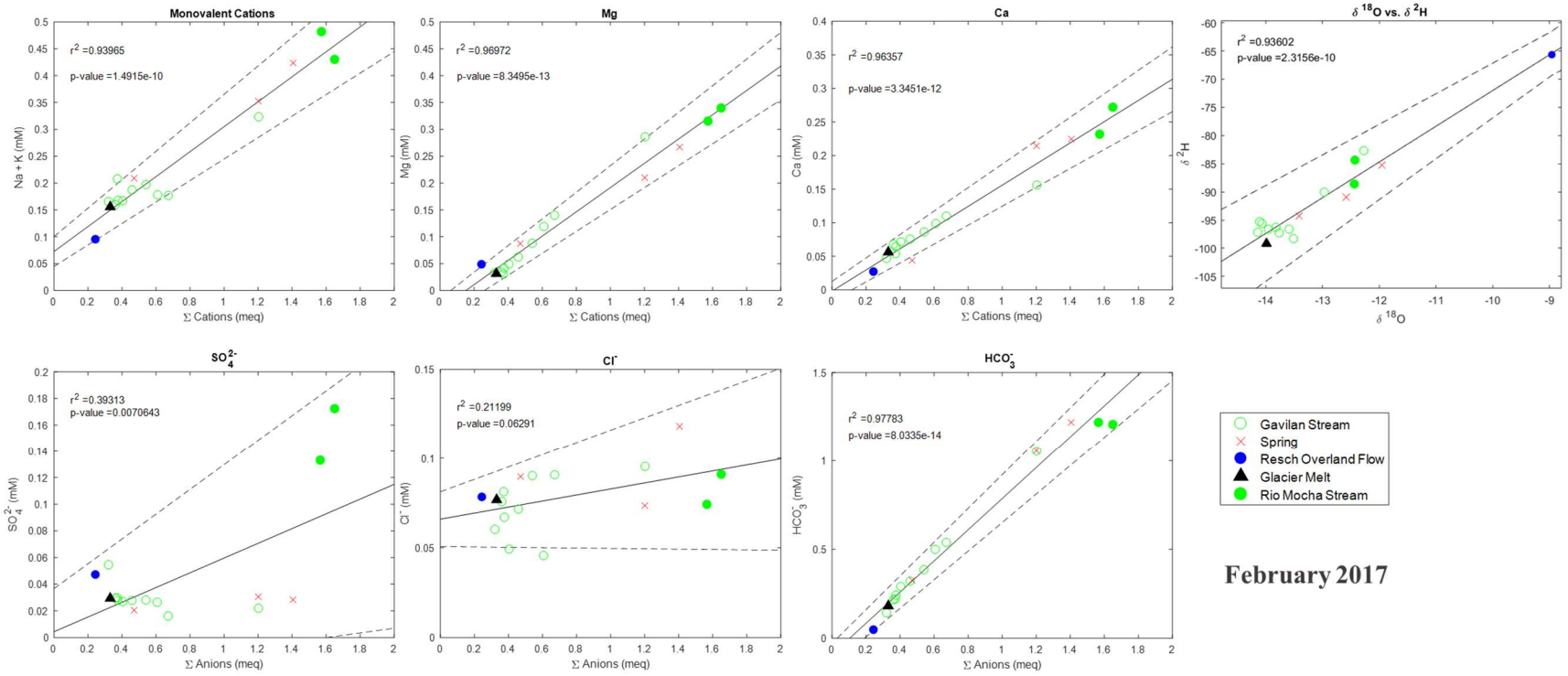

Figure 3.5. Bivariate Diagrams of tracers selected for February 2017 HBCM analysis. The solid black lines represent linear regressions through all samples and dashed black lines indicated the regressions' 95% confidence intervals. Samples from the main Rio Mocha channel before and after the Gavilan stream joins it (filled green circles) plot largely outside or away from the mixing line created between groundwater and meltwater. Reschreiter overland flow is a sample of precipitation collected from flow coming off a small sheer face during a rainfall event.

On the bivariate diagrams, stream samples taken from the main Río Mocha channel, just before and after its confluence with the Gavilan Machay stream, consistently plot away from or outside of the melt-groundwater mixing line. This indicates that the stream water feeding into the main channel is chemically distinct from the stream water coming from the Gavilan Machay subcatchment. The precipitation (rain) samples almost always fall outside the range of stream samples bracketed by groundwater and melt, confirming that precipitation was not a major contributor to streamflow during the dry season sampling periods. The one exception is a slight precipitation influence in the February 2017 sampling, when one stream sample plots outside the melt-groundwater range and towards precipitation. Additionally, one spring in both the 2016 and 2017 analyses plots away from the other spring samples and tends to have lower total cations and anions. This spring (GW-S7) may be a mixed source sample (both groundwater and recent rainfall) or originate from a unique geology, and thus is not considered an appropriate end member for the HBCM analysis for the entire Gavilan Machay subcatchment.

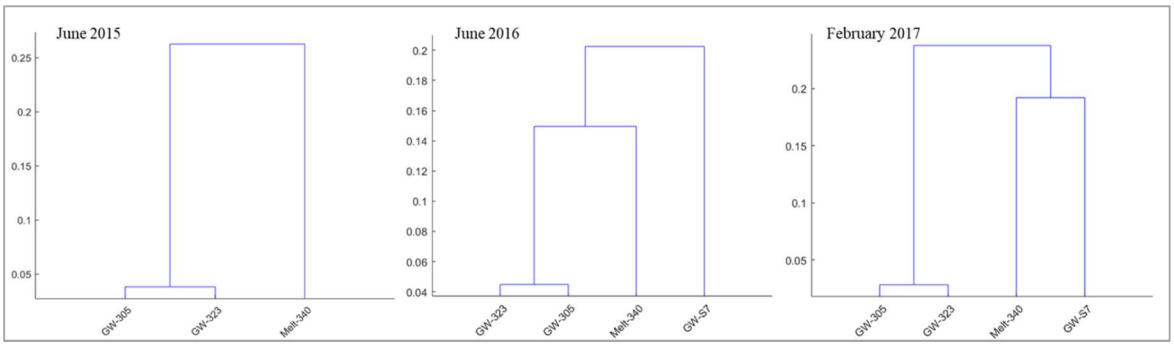

Figure 3.6. Hierarchical cluster analysis dendrograms for tracers used in HCBM. Sample grouping verifies effectiveness of selected tracers in distinguishing between source waters, as groundwater samples (GW) cluster separately from melt water (Melt) samples. GW-7 is considered an outlier, and is suspected to be a mixed source sample or to originate from a unique geology.

To confirm that the above selected tracer set comprise distinct end member chemistries, hierarchical clustering analysis (HCA) was performed using the relative concentrations (i.e. $SO_4^{2-}/\Sigma A^-$, where ΣA^- is the sum of all anion concentrations) of the tracers, with the exception of $\delta^{18}O$. The inclusion of isotopic values has the potential to confuse grouping in the HCA because groundwater isotopic signatures depend on recharge source, which could be glacial melt or precipitation, while ionic signatures of groundwater depend on water passing through the subsurface and will be unique to those samples. Results are shown in Figure 3.6 in the form of dendrograms, where samples considered to be the most similar are connected by low vertical bars, and those that are the least similar by high vertical bars. Groundwater samples group together and separately from melt samples, confirming that the selected tracers provide a clear differentiation between the end members. Here, again, GW-S7 can be identified as distinct from other springs, grouping loosely with melt in 2017 and completely apart in 2016.

Results for 2015, 2016, and 2017 HBCM analyses, along with the 2012 results obtained by La Frenierre, 2014, are shown in Tables 3.1-3.5. Combined with La Frenierre's 2012 results, new HBCM results support the importance of groundwater in total stream discharge, showing that it contributes 38-72% of dry season flow in the Gavilan Machay subcatchment (Figure 3.7), but with significant variability among sampling periods (January 2012 to January 2017) for both the short (December-January) and long (June-September) dry seasons. As compared to 38.9% in July 2012, in June 2015 and 2016 melt accounted for 57.8% and 51.5% of stream discharge, respectively. In February 2017, the melt proportion rose again to comprise 62.2% of flow,

					February 2017		
Stream	Location	HBCM Cell	Area (km^2)	Glacier Area %	Min Melt %	Max Melt %	Mean Melt %
Gavilán Machay	Glacier Tongue	1	3.4	74.9	100	100	100
Gavilán Machay	Confluence A - In	1	3.6	71.7	95.6	100.0	97.8
Gavilán Machay	Confluence A - Out	2	3.8	67.6	91.8	96.0	93.9
Gavilán Machay	Confluence B - In	3	3.9	65.3	89.9	94.1	92.0
Gavilán Machay	Confluence B - Out	4	4.0	63.3	80.2	83.9	82.1
Gavilán Machay	Confluence C - In	5	4.2	61.0	76.5	80.0	78.2
Gavilán Machay	Confluence C - Out	6	5.7	44.7	71.9	76.8	74.3
Gavilán Machay	Reach D - In	7	6.7	38.1	66.7	71.2	69.0
Gavilán Machay	Reach D - Out/ Con. E - In	8	7.5	33.9	57.6	66.8	62.2
Rio Mocha	Confluence E - Out	9	26.0	9.8	9.8	11.4	10.6

					June 2016		
Stream	Location	HBCM Cell	Area (km^2)	Glacier Area %	Min Melt %	Max Melt %	Mean Melt %
Gavilán Machay	Glacier Tongue	1	3.4	74.9	100	100	100
Gavilán Machay	Confluence A - In	1	3.6	71.7	87.0	95.0	91.0
Gavilán Machay	Confluence A - Out	2	3.8	67.6	79.9	89.3	84.6
Gavilán Machay	Confluence B - In	3	3.9	65.3	77.5	86.6	82.0
Gavilán Machay	Confluence B - Out	4	6.7	38.1	58.1	65.8	62.0
Gavilán Machay	Confluence C - In	5	7.5	33.9	46.5	56.6	51.5
Rio Mocha	Confluence C - Out	6	26.0	9.8	5.7	7.5	6.6

					June 2015		
Stream	Location	HBCM Cell	Area (km^2)	Glacier Area %	Min Melt %	Max Melt %	Mean Melt %
Gavilán Machay	Glacier Tongue	1	3.4	74.9	100	100	100
Gavilán Machay	Confluence A - In	1	3.6	71.7	100	100	100
Gavilán Machay	Confluence A - Out/B-in	2	3.8	67.6	92.0	92.0	92.0
Gavilán Machay	Confluence B - Out	3	6.7	38.1	59.6	59.6	59.6
Gavilán Machay	Confluence C - In	4	7.5	33.9	57.8	57.8	57.8
Rio Mocha	Confluence C - Out	5	26.0	9.8	5.2	5.2	5.2

La Frenierre (2014)					July 2012		
Stream	Location	HBCM Cell	Area (km^2)	Glacier Area %	Min Melt %	Max Melt %	Mean Melt %
Gavilán Machay	Glacier Tongue	1	3.4	74.9	100	100	100
Gavilán Machay	Confluence A - In	1	3.6	71.7	99.1	99.1	99.1
Gavilán Machay	Confluence A - Out	2	3.8	67.6	98.3	98.3	98.3
Gavilán Machay	Confluence B - In	3	3.9	65.3	96.5	96.5	96.5
Gavilán Machay	Confluence B - Out	4	4.0	63.4	94.7	94.7	94.7
Gavilán Machay	Confluence C - In	5	4.2	61.0	91.6	91.6	91.6
Gavilán Machay	Confluence C - Out	6	5.7	44.7	88.6	89.2	88.9
Gavilán Machay	Confluence D - In	7	7.5	33.9	35.5	42.4	38.9
Rio Mocha	Confluence D - Out	8	26.0	9.8	3.0	5.7	4.3

La Frenierre (2014)					January 2012		
Stream	Location	HBCM Cell	Area (km^2)	Glacier Area %	Min Melt %	Max Melt %	Mean Melt %
Gavilán Machay	Glacier Tongue	1	3.4	74.9	100	100	100
Gavilán Machay	Confluence A - In	1	3.6	71.7	95.5	100.0	97.7
Gavilán Machay	Confluence A - Out	2	3.8	67.6	83.4	95.2	89.3
Gavilán Machay	Confluence B - In	3	3.9	65.3	79.5	92.9	86.2
Gavilán Machay	Confluence B - Out	4	4.0	63.4	76.6	89.6	83.1
Gavilán Machay	Confluence C - In	5	4.2	61.0	72.9	87.1	80.0
Gavilán Machay	Confluence C - Out	6	5.7	44.7	70.7	84.8	77.8
Gavilán Machay	Confluence D - In	7	7.5	33.9	23.1	32.4	27.8
Rio Mocha	Confluence D - Out	8	26.0	9.8	2.8	4.9	3.8

Tables 3.1 – 3.5. Estimated proportional contributions of surficial glacier meltwater to total watershed discharge for 2012 -2017 sampling periods. Calculated estimates of minimum and maximum melt contribution is shown for each sampling point between the Reschreiter glacier and the outlet at Boca Toma.

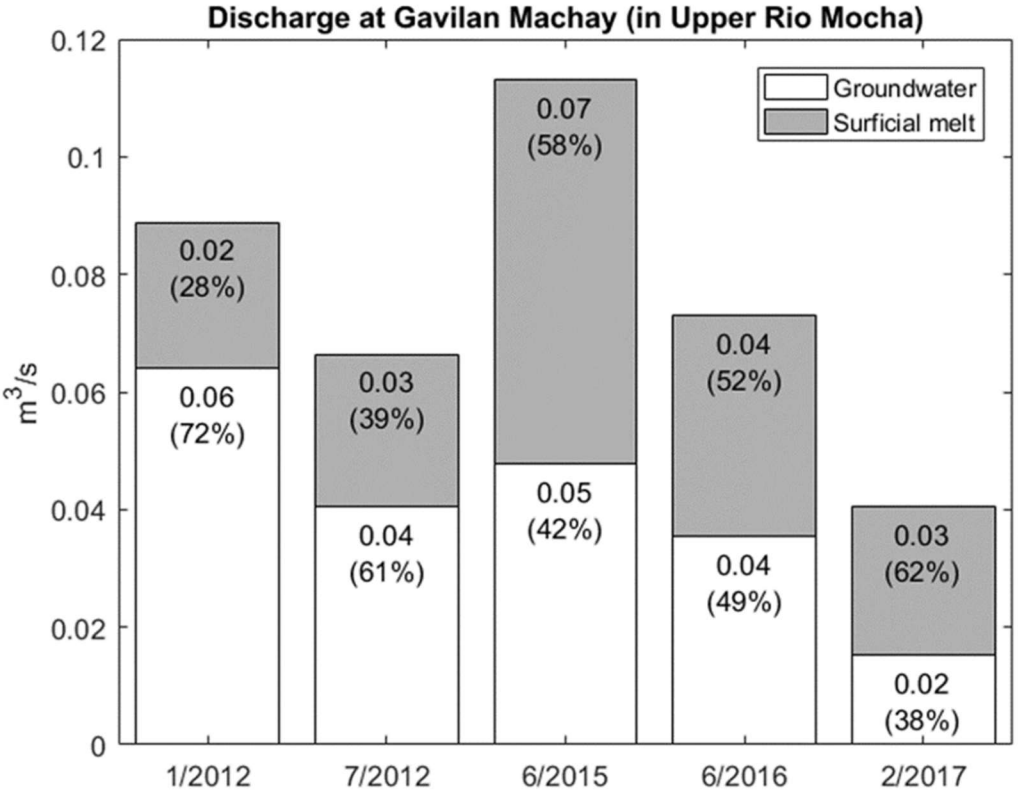

Figure 3.7. Absolute and proportional contributions of groundwater and surficial melt to discharge in the Gavilan Machay subcatchment. Percent contributions (in parentheses), calculated using hydrochemical tracers and the HBCM mixing model, show an increasing percent of surficial melt over time. When these percentages are applied to measured discharge (top text in bars), the calculated absolute groundwater and melt discharges reveal that the change over time is due largely to decreasing groundwater inputs.

as compared to 27.8% in January 2012. Taken in isolation, these results would appear to imply that surficial melt discharge was significantly higher in 2015-2017 compared to 2012, which could reflect the accelerated melt rates observed on Chimborazo (La Frenierre & Mark 2017). However, it is important to consider absolute changes in groundwater discharge alongside the proportional changes in meltwater contribution. Applying HBCM's relative proportions to our observed discharge measurements reveals different groundwater and meltwater trends, as shown in Figure 3.7. For example, although the

proportional surficial meltwater contribution in February 2017 is more than three times higher than in January 2012, absolute discharge is only about 50% higher; the dramatic change in proportional surficial meltwater contribution occurs because of the much lower groundwater discharge in February 2017. Clearly, to properly interpret changes in meltwater and groundwater discharge amounts the proportional contributions provided by the HBCM mixing model should be paired with absolute discharge measurements.

Furthermore, caution should be taken in interpreting a long-term temporal trend from the five sampling periods in Figure 3.7. Figure 3.8 shows weekly averages for the entire Gavilan Machay discharge time series (2012-2017) along with data from the Boca Toma (2015-2017) and Reschreiter (2012-2013) rainfall gauges with periods water sampling periods marked. The Reschreiter gauge (4515 m asl) receives less rainfall than the Boca Toma gauge (3899 m asl), and therefore its precipitation has been amplified for comparability by a factor of 5.6 on the plot— the average difference in rainfall magnitude between the two stations. There is high uncertainty in this magnitude difference, as the windier conditions and greater chance of freezing temperatures at Reschreiter likely lead to an underestimation of precipitation amounts. As seen in Figure 3.7, variability in melt and groundwater discharge between sampling periods depends on total discharge, which is normally correlated with precipitation and incoming solar radiation. Indeed, in Figure 3.8, it can be seen that temporal discharge patterns tend to mirror those of precipitation. For example, greater discharge in June 2015 corresponds to higher precipitation amounts in the week prior to that sampling than were measured before the 2016 and 2017 sampling

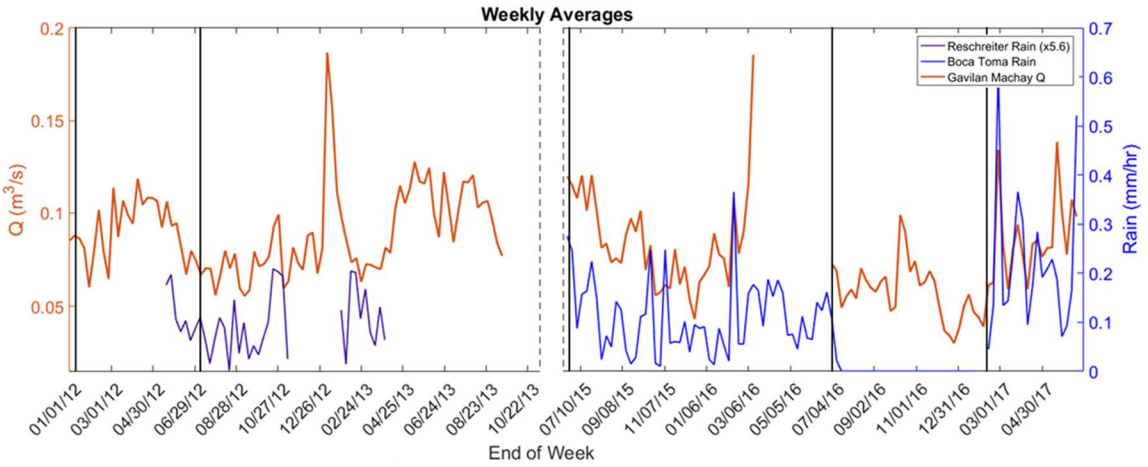

Figure 3.8 Comparison of average weekly discharge (m^3/s) at Gavilan Machay (2012-2017) and rainfall (mm/hr) at Boca Toma (2015-2017) and Reschreiter (2012-2013) weather stations. Vertical black, solid lines indicate weeks where sampling occurred, and vertical dashed lines indicate a temporal gap in data collection. Reschreiter rainfall has been multiplied by the average difference in magnitude between it and Boca Toma: 5.6. Despite gaps in data, it can be seen that precipitation was higher in the time surrounding the 2015 sampling campaign than in the times surrounding the other campaigns.

periods. The relationship is not perfect however owing to melt contributions, which likely increase during warm, sunny periods with little rain.

Though precipitation is not considered an end member in my HBCM analyses, it is apparent that precipitation patterns directly preceding water sampling do influence stream discharge. This relationship may mean our sampling times do not sufficiently cover the range of normal interannual discharge variability. The El Nino Southern Oscillation (ENSO) significantly impacts interdecadal precipitation and temperature trends, with El Nino (La Nina) years bringing drier, hotter (wetter, cooler) conditions (Vuille et al. 2000; Vuille & Keimig 2004). Consequently, ENSO strongly influences glacier mass balance and stream discharge in glaciated Andean catchments (Veettil et al. 2014; Francou 2004; Wagnon et al. 2001). Here I capture a weak La Nina year (2011-2012) and a strong El Nino year (2015-2016), but nothing in between, which limits our perspective on the watershed

hydrologic response to longer term climatic cycles. In addition, Figure 3.8 shows that precipitation dramatically increased in the period directly following the February 2017 sampling campaign. Had samples been collected in June 2017 they may have shown an increase in both the relative and absolute contributions of groundwater and meltwater.

Figure 3.9 shows for all years (2012-2017) HBCM's calculated melt contribution at each sampling point moving downstream from the tongue of the Reschreiter glacier to the outlets at Gavilan Machay and Boca Toma. In general, the surficial melt percent decreases as the drainage area increases. At the outlets, the trend of increasing melt percent over time is apparent; however, upstream, mean HBCM estimates of melt contribution are variable from year to year. For instance, July 2012 maintains higher melt percentages than all other years, at almost all sampling points, but drops off steeply between the penultimate sampling point (Area = 22%) and the Gavilan Machay outlet (Area = 28%). June 2016 and February 2017, on the other hand, have lower melt contributions high in the catchment, and exhibit a much subtler drop between its penultimate sampling (Area = 26%) point and the Gavilan Machay outlet. As noted above, it is important to consider absolute groundwater discharge and not just relative melt percentage.

Figure 3.10 reveals that the decrease in melt contribution closer to the Gavilan Machay outlet (Drainage Area > 22%) is due to a sudden increase in groundwater discharge. Up to the point where the stream drains 22-26% of the Upper Rio Mocha watershed, groundwater discharge into the stream appears to increase linearly, which corresponds with the expected stream discharge-watershed area relationship described by Dunne & Leopold (1978). However, near the Gavilan Machay outlet (Area > 22%) there

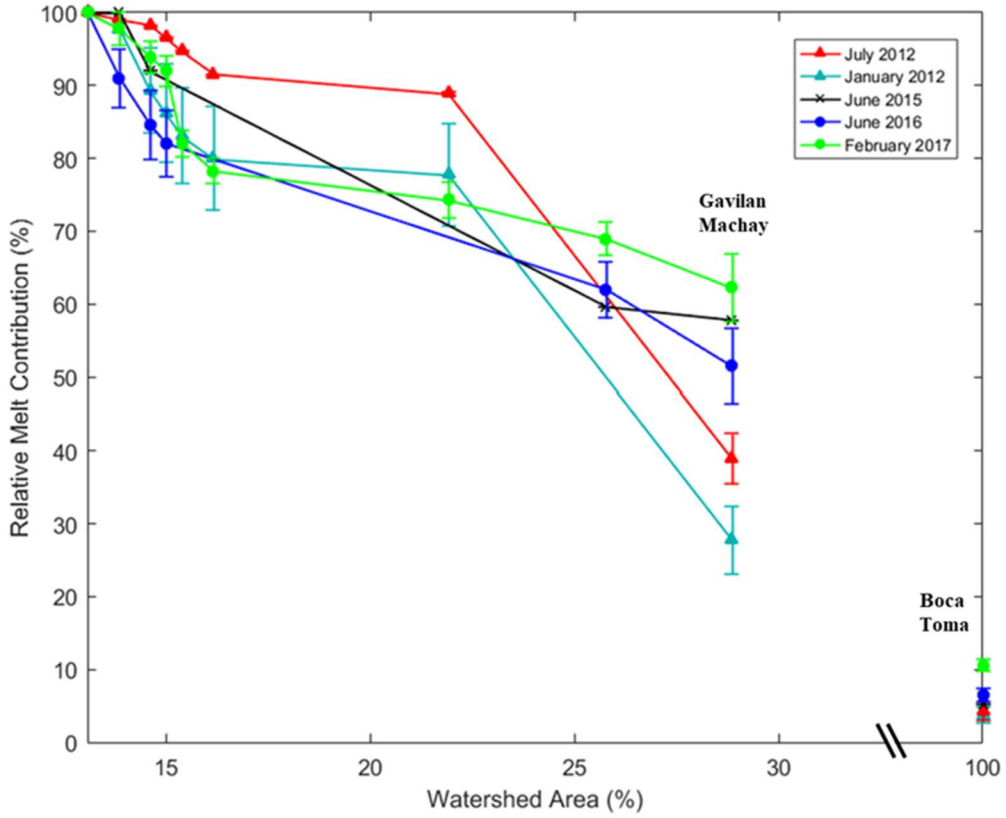

Figure 3.9 Percentage of stream discharge from surficial glacier meltwater versus percentage of total watershed area drained. HBCM was used to determine the relative contribution of surficial glacier melt to watershed discharge at sampling points between the Reschreiter glacier tongue and the Upper Rio Mocha watershed outlet at Boca Toma. Data points for January and July 2012 are taken from La Frenierre, 2014, while data for 2015-2017 were obtained by this study. Outlets of the Gavilan Machay subcatchment and Upper Rio Mocha watershed are indicated. The uncertainty in HBCM melt estimates are shown by vertical error bars.

is a sudden, non-linear increase in groundwater contributions, which may be due to how the topography intersects the underlying geology near these sampling points. These results imply that while there is variability among the sampling periods, the groundwater contribution generally increases at the lowest reaches of the Gavilan Machay stream (Area $\geq$ 22%). Higher in the catchment (Area < 22%), there is more overlap in the HBCM estimates of melt contribution, with relatively constant proportional surficial meltwater contributions in the mid-slopes of the catchment (17-22% Area).

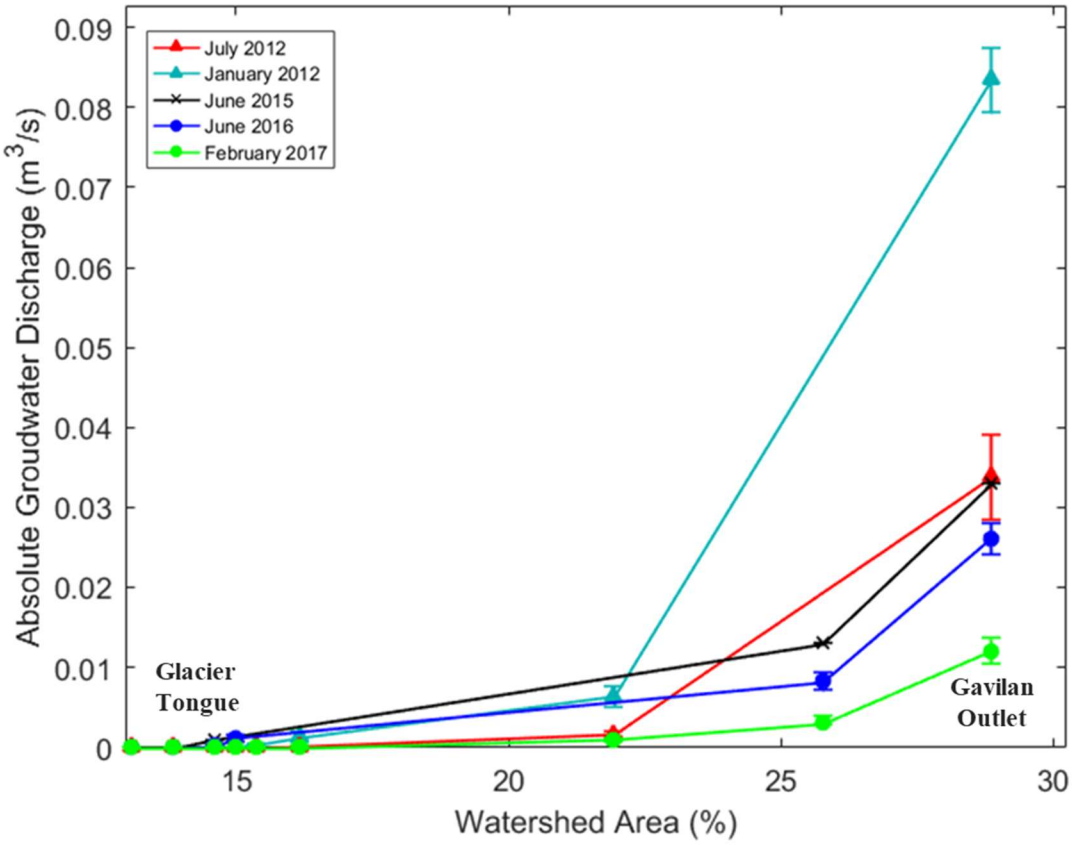

Figure 3.10. Calculated absolute groundwater discharge verses percentage of total watershed area drained for Gavilan Machay subcatchment. Measurements of discharge at Boca Toma and relative source proportions calculated by HBCM for each sampling point were used to calculate absolute groundwater discharge at each sampling location between the Reschreiter Glacier and Boca Toma outlet. Uncertainties in calculated groundwater discharge are shown as vertical error bars. The Boca Toma outlet is not pictured, only those points within the Gavilan Machay subcatchment are shown in order to highlight the non-linear trend in groundwater discharge with increasing watershed area drained.

Overall, the spatiotemporal patterns in the estimated melt and groundwater contributions suggest the influence of precipitation dynamics (as noted above) and geologic controls over the Gavilan Machay watershed. Major groundwater influx occurs each year near the same sampling points (Area≥ 22%). These points are located near a large break in slope (Figure 3.1), where there is an exposed sheer face and waterfall feature in the stream

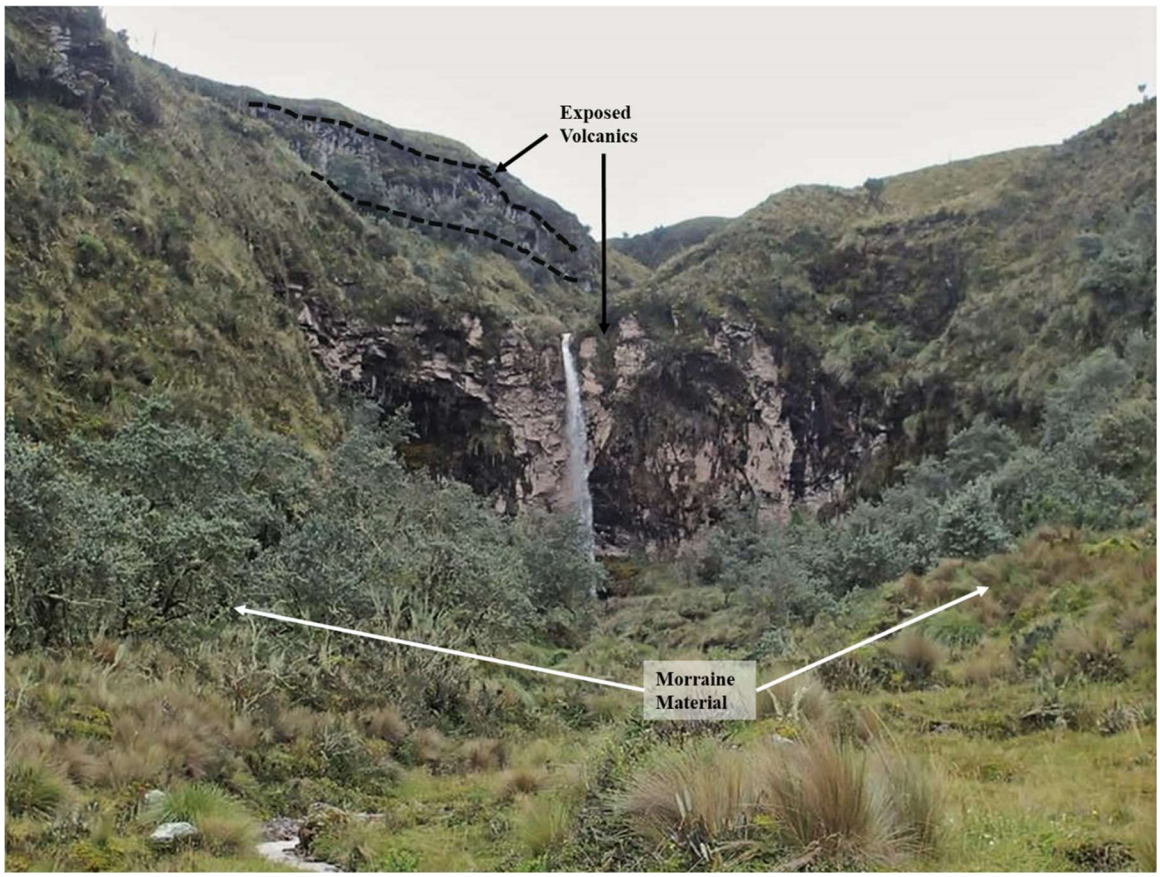

Figure 3.11 Gavilan Machay waterfall. Exposed volcanic flows are visible on the wall behind the waterfall as well as on the cliff face above (indicated by dashed lines). The valley walls on either side of the waterfall are likely thin layers of glacial moraine material lying over volcanic bedrock.

valley (Figure 3.11), followed by a gentler slope down to the outlet. The valley walls on either side of the sheer face are largely morainic material, while the face itself is exposed volcanics, likely lava flows from Chimborazo's early cone building stage (Samaniego et al. 2012). Above the waterfall, there are layered flows that outcrop (Samaniego et al. 2012) on the southern valley wall and in-field observations suggest the presence of fractures. The samples immediately before the Gavilan Machay outlet in 2012 (Area = 22%) were collected just above the waterfall slope break, and in 2015-2017 (Area = 28%) they were collected just below it. Given these features, it is probable that groundwater flowing in the

morainic and glaciofluvial deposits of the shallow subsurface (Geologic Cross-sections, Ch. 2.2) is forced to discharge at and after this slope break. Groundwater flowing through the volcanic deposits, too, and may be discharging here.

Regardless of discharge point, the high proportional groundwater contribution in the Gavilan Machay subcatchment is anomalous for a glacierized watershed. In the Cordillera Blanca in Peru, Baraer et al. (2015) found there to be an exponential relationship between glacierized fraction of a watershed and groundwater contributions, where small increases in the glacierized fraction sharply decrease groundwater contributions. In fact, it is not until glacierized area is less than 8% of the watershed that this model predicts groundwater contribution to exceed 50% of discharge. By this model, at Boca Toma (glacierized area ~9.8%) the groundwater contribution should be between 45-75% of discharge, when in reality it is ~90-95%. Similarly, at Gavilan Machay (glacierized area ~33.9%) this model would predict groundwater to be between 10-40% of discharge, but according to our results, it is much larger at ~37-72%. Previous studies, in addition, have shown that specific discharge increases with glacierized area (Baraer et al. 2009; Mark & Seltzer 2003), which would imply that the Gavilan Machay subcatchment should have greater specific discharge than the non-glaciated area of the Upper Río Mocha watershed. However, this is not the case: for all five sampling periods Gavilan Machay's specific discharge is less than 60% of the non-glaciated area's specific discharge. The unusually high groundwater contributions combined with the anomalously low specific discharge, may suggest that rather than discharging through surface networks, meltwater is infiltrating

higher in the catchment and traveling through groundwater systems that may or may not discharge to the Gavilan Machay stream and/or the Río Mocha.

3.2.2 Sources of Groundwater: Examining Isotopic Signatures of Melt and Groundwater

To investigate this possible recharge pathway, the stable isotopes of water ($^{1}H/^{2}H$ & $^{16}O/^{18}O$) were utilized to estimate the elevation of the precipitation source recharging the springs in the Upper Río Mocha watershed. Assuming that little fractionation occurs while water infiltrates through the land surface and unsaturated zone, stable isotopes in groundwater will reflect the elevation of the precipitation that recharges it (Clark & Fritz 1997; Kendall & Doctor 2003; Blasch & Bryson 2007).

Thus, to use the stable isotope values of water as indicators of precipitation source elevation, first I confirmed that, from infiltration to discharge, there was negligible fractionation of isotopes in the spring samples. This is done by comparing the $\delta^{2}H$/ $\delta^{18}O$ value of each sample to a Local Meteoric Water Line (LMWL). No published meteoric water line exists for Chimborazo; instead a LMWL derived from an ice core on Volcán Antizana (Williams et al. 2002) and another generated from precipitation in the Zhurucay Ecohydrological Observatory near Cuenca (Mosquera et al. 2016), are used as to represent the range of possible meteoric water lines (Figure 3.12). Together these lines cover the range of climatic conditions across the Ecuadorian Andes as well as the range of elevations present on Chimborazo, with the Antizana measurements coming from 5752 m asl on the eastern cordillera and the Zhurucay measurements spanning 3297-3779 m asl on the western cordillera. One of the most common causes of fractionation is evaporation, which

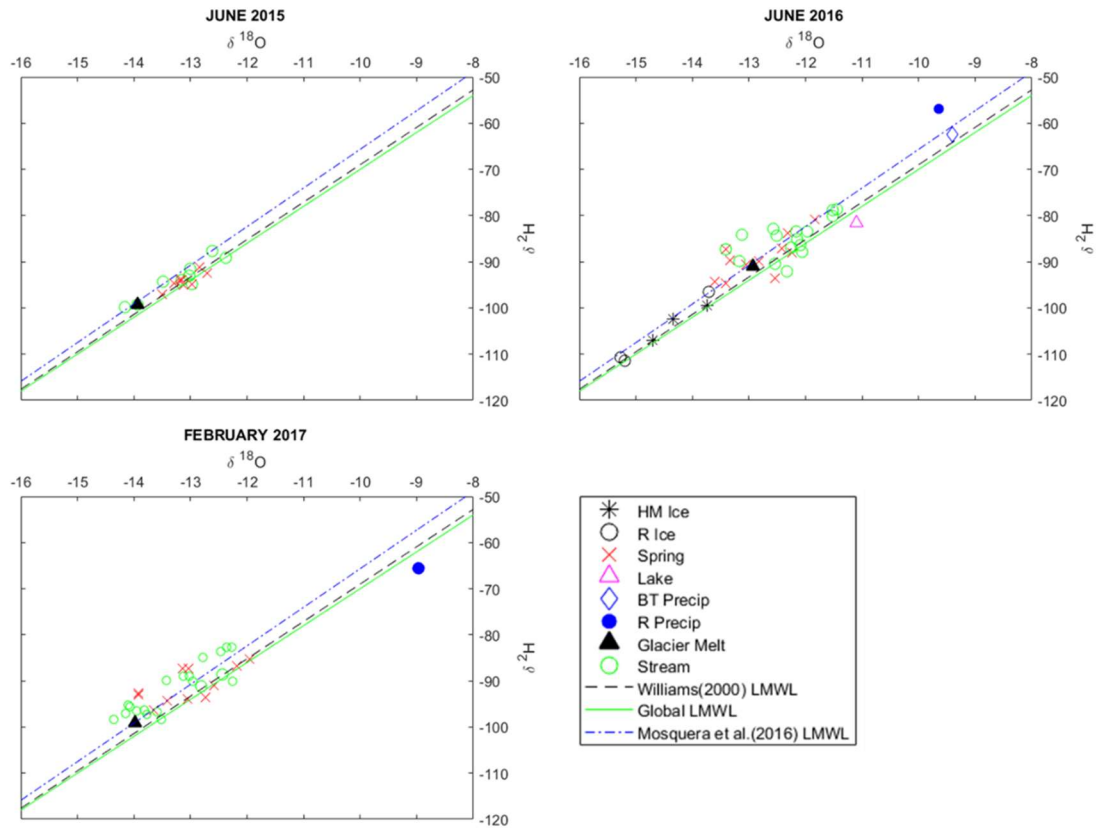

Figure 3.12 Comparison of sample isotopic signatures to global and local meteoric water lines. Two LMWLs from Ecuador are shown: Williams et al. 2002 (black, dashed) is from Volcán Antizana and Mosquera et al. 2016 (Blue, dot-dash) from the Zhurucay Ecohydrological Observatory near Cuenca. The global meteoric water line (green, solid) is shown for comparison. Ice samples from the Hans Meyer (HM) and Reschreiter (R) glaciers were collected during only the 2016 field campaign. Precipitation samples were collected in 2016 and 2017, near the tongue of the Reschreiter glacier (R) and at the Boca Toma (BT) meteorological station. Alignment of sample isotopic values to meteoric water lines indicate little to no post-precipitation fractionation occurring prior to collection. Analytical uncertainty is +/- <1.0 ‰ for $^{2}H/^{1}H$ and <0.25 ‰ for $^{18}O/^{16}O$.

in groundwater is likely to happen prior to recharge in the unsaturated zone and then near the discharge point, as the flow path becomes shallower. If fractionation due to evaporation occurs along their flow paths, the Upper Río Mocha samples would fall below the meteoric water line, towards a heavier $\delta^{18}O$ isotopic signal as lighter isotopes of oxygen preferentially evaporate faster than those of hydrogen. Samples shown in Figure 3.12

largely match the meteoric water lines, with no preferential scatter towards heavier isotopic values. This confirms that isotope fractionation is negligible in the samples and agrees with other studies in high Andean wet meadow settings, which have shown that evaporation in páramos and pampas is low and has little effect on the isotopic values of groundwater (Buytaert et al. 2006; Baraer et al. 2015).

Groundwater is recharged by precipitation (rain or snow) and, in glacierized catchments, by glacial meltwater. Given the results above, the elevation of source precipitation responsible for recharging spring water in the Upper Río Mocha catchment can be approximated using the relationship between elevation and isotope values. On a plot of elevation vs. δ18O, applying the lapse rate to isotopic values from precipitation samples collected in situ generates a line representing the minimum precipitation source elevation. Many studies have calculated isotope lapse rates for Ecuador, from the scale of a single catchment (Windhorst et al. 2013; Mosquera et al. 2016) to across the entire country (Garcia et al. 1998) and the equatorial latitudinal band (Rozanski & Araguas 1995) (Table 3.6).

Author	$\delta^{18}O$ (‰ $100m^{-1}$)	$\delta^{2}H$ (‰ $100m^{-1}$)	Elevation Range (m asl)		Sampling Period	Location
Mosquera *et al.* (2016)	**-0.31**		3297	3900	May 2011- May 2013	Ecuador: Zhurucay Ecohydrological Observatory, Cordillera Occidental, Cuenca side.
Windhorst *et al.* (2013)	-0.22	**-1.12**	1800	2800	September - December 2010	Ecuador: San Francisco Catchment Cordillera Oriental, Amazonian side.
Garcia *et al.* (1998)	-0.17		400	3870	January-December 1997	Ecuador: Average over east-west transects across the northern and southern Ecuadorian Andes.
Rozanski & Araguas, (1995)	-0.20			<3000	NA	IAEA/WMO database for stations thorughout South America. Shown lapse rate is for the equatorial region.
	-0.50			>3000		

Table 3.6 Isotopic lapse rates for Ecuador.

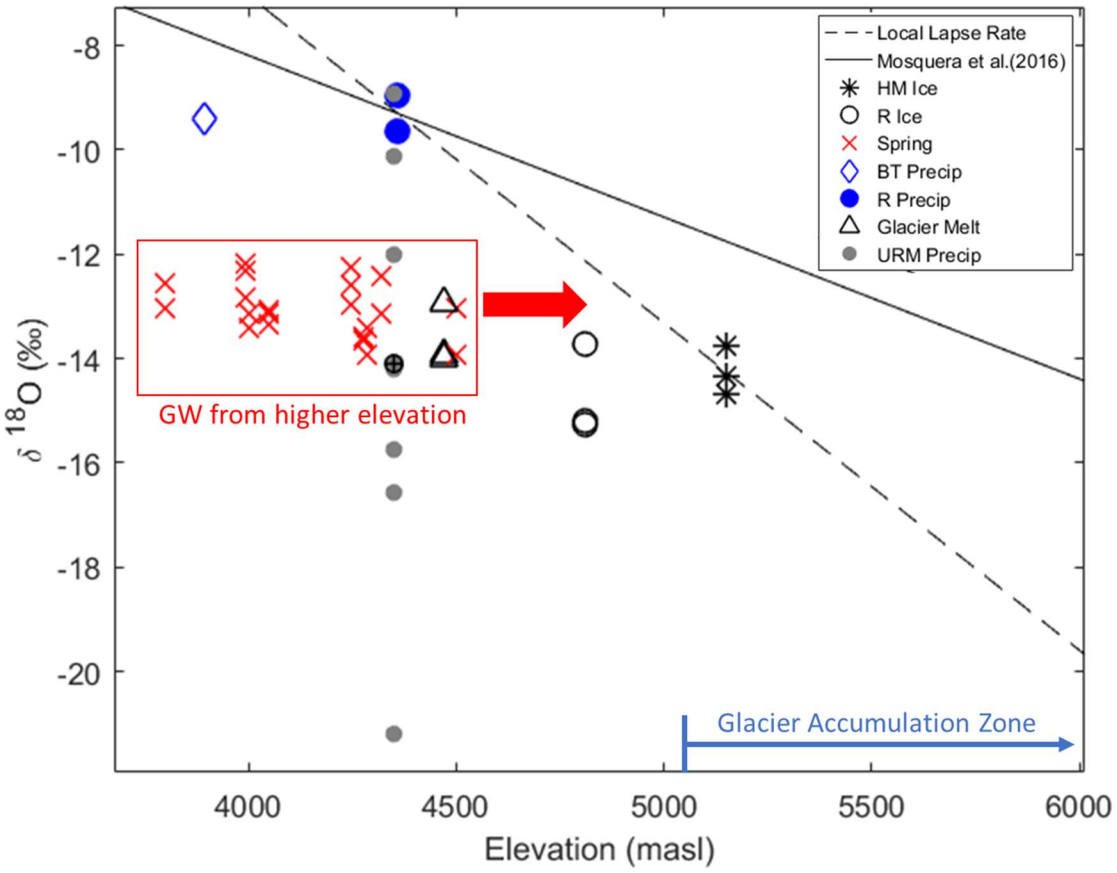

Figure 3.13 $\delta^{18}O$ (‰VSMOW) versus sample elevation. Samples of groundwater, glacial melt water, ice from Reschreiter (R) and Hans Meyer (HM) glaciers, and precipitation from Boca Toma (BT) and the Reschreiter glacier tongue are shown. Ice samples were collected only during the 2016 sampling campaign. The solid black line is a line of minimum recharge elevation based on a regional lapse rate of -0.31 ‰ $100m^{-1}$ taken from Mosquera et al., 2016. The dashed line is a line of minimum recharge elevation based a local lapse rate of -0.63 ‰$100m^{-1}$ calculated from a regression through greatest concentration of precipitation samples and highest collected ice samples. All groundwater samples fall below both lines of minimum recharge elevation, indicating that most groundwater is sourced from higher elevations, corresponding to areas where ice and melt dominate. URM precip samples represent 9 months of rainfall isotope data from 2012, and the circle with a cross is the mean weighted by the amount of rainfall each month. The ELA on Chimborazo is ~5050 m asl (La Frenierre 2014). All ice on the mountain originates in the accumulation zone above the ELA (indicated in lower right corner) and may come from a range of elevations.

Figure 3.13 shows two possible lines of minimum precipitation source elevation. One utilizes the mean precipitation value at the Reschreiter weather station (location shown in Figure 3.1) and a lapse rate (-0.31 ‰ $100m^{-1}$) calculated by Mosquera et al., 2016. This

is the lowest published lapse rate (specific to Ecuador), and therefore produces the most conservatively low estimate of precipitation source elevation. In addition, the study area is geographically similar to the Upper Río Mocha Watershed as it lies on the Cordillera Occidental at high elevation (>3000 m asl). The other line of minimum precipitation source elevation is a linear regression through the mean values of the highest collected ice samples and of precipitation from the Reschreiter weather station, which produces a local lapse rate equal to -0.63 ‰ $100m^{-1}$. Ice was selected because it more closely represents an in-situ precipitation sample than melt, which is a homogenization of ice from a range of elevations. Ice, however, is not truly in situ either as it accumulates above the ELA and flows downslope into the ablation zone. Reschreiter rain samples were utilized instead of the lower elevation rain sample (BT Precip) owing to the larger number of data points for the former. Isotopic values of precipitation can vary significantly between storm events (Kendall & Doctor 2003; Tappa et al. 2016). Reschreiter samples exhibit consistency across the events measured and with other samples (URM Precip) collected at similar elevations on the northeast slopes of Chimborazo (personal communication, Jeff La Frenierre, 9/20/16). In contrast, the single sample collected at Boca Toma is not sufficient to establish an isotope-elevation relationship there.

Noticeably, the local isotope lapse rate is much steeper than that of Mosquera et al. (2016) in the Zhucuray watershed. These two lines likely bracket the range of possible lapse rates and uncertainties in minimum recharge source elevations on Chimborazo. The Mosquera et al. line is limited in its application to this catchment as the elevational range of the Zhurucay watershed is much lower than that in the Upper Río Mocha watershed.

Both Gonfiantini et al., 2001 and Rozanski and Araguas, 1995, observed in tropics that the δ-altitude relationship deviates from linearity at high elevations, where temperatures become low and condensation rates increase. Rozanski and Araguas (1995) further concluded that above 3000 m asl in the equatorial Andes, the average lapse rate increases from -0.2 to -0.5 ‰ $100m^{-1}$, which is much closer to our local lapse rate estimate of -0.63 ‰ $100m^{-1}$. Consequently, the Mosquera line may be an underestimation of the lapse rate on Chimborazo. Our local lapse rate may be overly steep though, owing to the fact that it comes from only dry-season precipitation values and ice that has flowed downslope. In addition to changing with elevation, isotopic values of precipitation will also change seasonally, with the wet season bringing more depleted (more negative) values than the dry season. Wetter periods tend to heavily influence the annual average isotopic value of groundwater at a given elevation (Kendall & Doctor 2003; Baraer et al. 2015) and, if used here, such values would likely decrease the local lapse rate. Moreover, as mentioned above, the glacier ice would have formed at higher elevations above the ELA, which on Chimborazo is approximately 5050 m asl (Jeff La Frenierre, personal communication, 3/20/16), and then moved downslope into the ablation zone where it was collected. Though the Hans Meyer ice samples were collected above the ELA, they may still represent ice flowing down from higher elevations. Depending on how much higher the ice source precipitation occurred, the local lapse rate could be significantly lower and closer to the Mosquera et al. lapse rate. Nevertheless, these two lines still provide conservative estimations of the possible extremes in the local lapse rate.

Despite the range of spring collection elevations, in Figure 3.13 springwater (representing groundwater) $\delta^{18}O$ values clearly cluster near melt values as opposed to near values for precipitation at the spring elevation. Both melt and springwater values fall well below either precipitation source line, suggesting that groundwater is recharged by precipitation falling at higher elevations that correspond to areas where ice and snow melt may dominate the hydrologic system.

Isotope seasonal variability can be large (Kendall & Doctor 2003; Baraer et al. 2015), and to adequately develop a relationship between precipitation δ values and elevation it is necessary to sample precipitation isotopes, at varying elevations, over a long enough period of time to capture this range. Ideally, annual mean isotopic values of precipitation at multiple elevations would be used to generate an average lapse rate (Tappa et al. 2016) and line of the minimum precipitation source elevation. A mean annual isotopic value for precipitation in the Upper Río Mocha watershed has not been determined, as there is no complete 12-month precipitation isotope series.

A 9-month series (Nov 2011 - Jul 2012) of mean monthly isotope values for precipitation collected at a single elevation does exist, and exhibits $\delta^{18}O$ values that span the range of spring water values in this study (Figure 3.13). Typically, homogenization during recharge and dispersion is considered to result in groundwater representing a mix of seasonal precipitation isotope values that is heavily influenced by high rainfall periods (Kendall & Doctor 2003; Baraer et al. 2015). In Figure 3.13, the mean of the 9-month series, weighted by precipitation amount, falls below the sampled spring values and approximately matches the mean ice value. If a line were to be drawn through this weighted

average precipitation point and the ice samples, the slope (lapse rate) would be close to zero. This line is not considered to represent a plausible lapse rate, because it would suggest that precipitation throughout the catchment would (on average) have the same isotopic signal, which contradicts the many studies confirming an altitude effect in the tropical Andes (Garcia et al. 1998; Rozanski & Araguas 1995; Gonfiantini et al. 2001; Windhorst et al. 2013; Mosquera et al. 2016). Additionally, such a line would fall below the majority of groundwater points, problematically implying that groundwater was sourced from precipitation at lower elevations. Overall, these inconsistencies imply that groundwater does not reflect the weighted mean isotopic value of precipitation and is therefore unlikely to be a homogenization of annual precipitation. Instead, groundwater may have shorter than one-year residence times, and inferring precipitation source elevations using lapse rates applied to relatively recent precipitation isotopic values (as in Figure 3.13) may be reasonable.

Groundwater residence times and corresponding path lengths, gleaned qualitatively from isotopic and hydrochemical observations, also provide evidence of higher elevation precipitation sources for spring samples in Figure 3.14. Mineral phase dissolution and desorption reactions are often kinetic and thus gradually release ions from sediments into groundwater (Stumm & Morgan 2013). Assuming kinetic reactions are the dominant geochemical process, I use calculated total dissolved solids (TDS) as a proxy for residence time and flow path length (Cushman & Tartakovsky 2016; Lal & Stewart 2012). Combined with isotopic values serving as an indicator of precipitation source elevation, our water samples can be placed along a two-dimensional grid corresponding to lower elevation

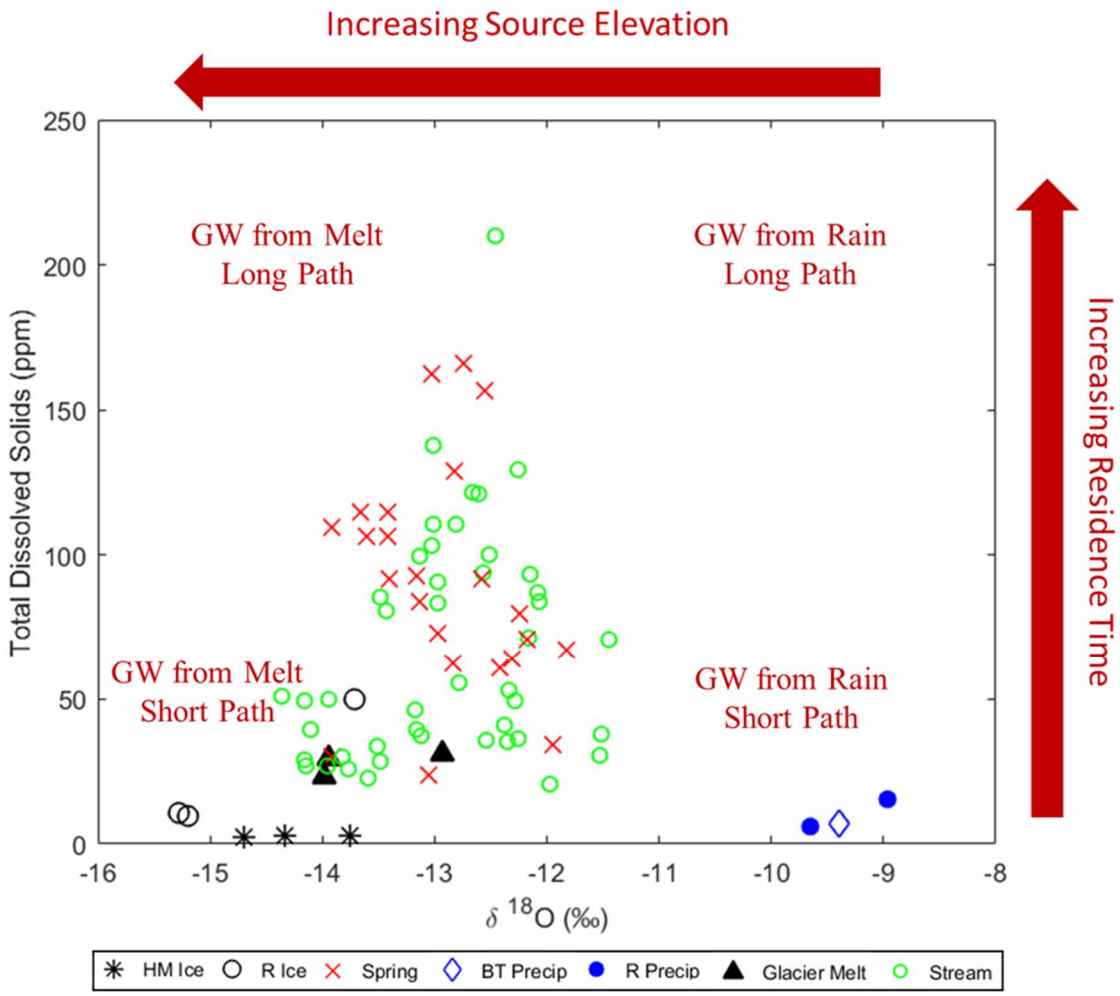

Figure 3.14 $\delta^{18}O$ (‰VSMOW) versus TDS (ppm). Here, sample TDS (total dissolved solids) and δ18O values are used to infer groundwater residence time and source, respectively. The arrows and overlain text shows the interpretation of these values, where, for example, a higher δ18O value and lower TDS value would fall in the lower right and indicate rain sourced groundwater that spent comparatively little time in the ground. The majority of groundwater samples have mid-length residence times, with TDS values between 50-150, and exhibit isotopic signatures more similar to melt and ice.

rainfall to higher elevation meltwater, and with travel over a shorter to longer flow path in Figure 3.14. Ice, melt, and rain samples have the lowest TDS values, as expected. One Reschreiter ice sample does have unusually high TDS, but this likely is due to contamination from the ice drill passing through an ash layer deposited by explosive

activity from nearby Tungurahua. Spring samples exhibit a range of TDS concentrations, indicating variable flow path lengths and residence times. Stream samples have also been added to this plot as well and generally cluster near spring samples, supporting the conclusion that the Gavilan Machay stream is groundwater-dominated, though the stream samples collected nearer to glacier tongue do fall near melt and ice as expected. The closer clustering of groundwater and spring water isotopic values to meltwater (compared to precipitation samples), and the scatter of groundwater and spring water TDS at high

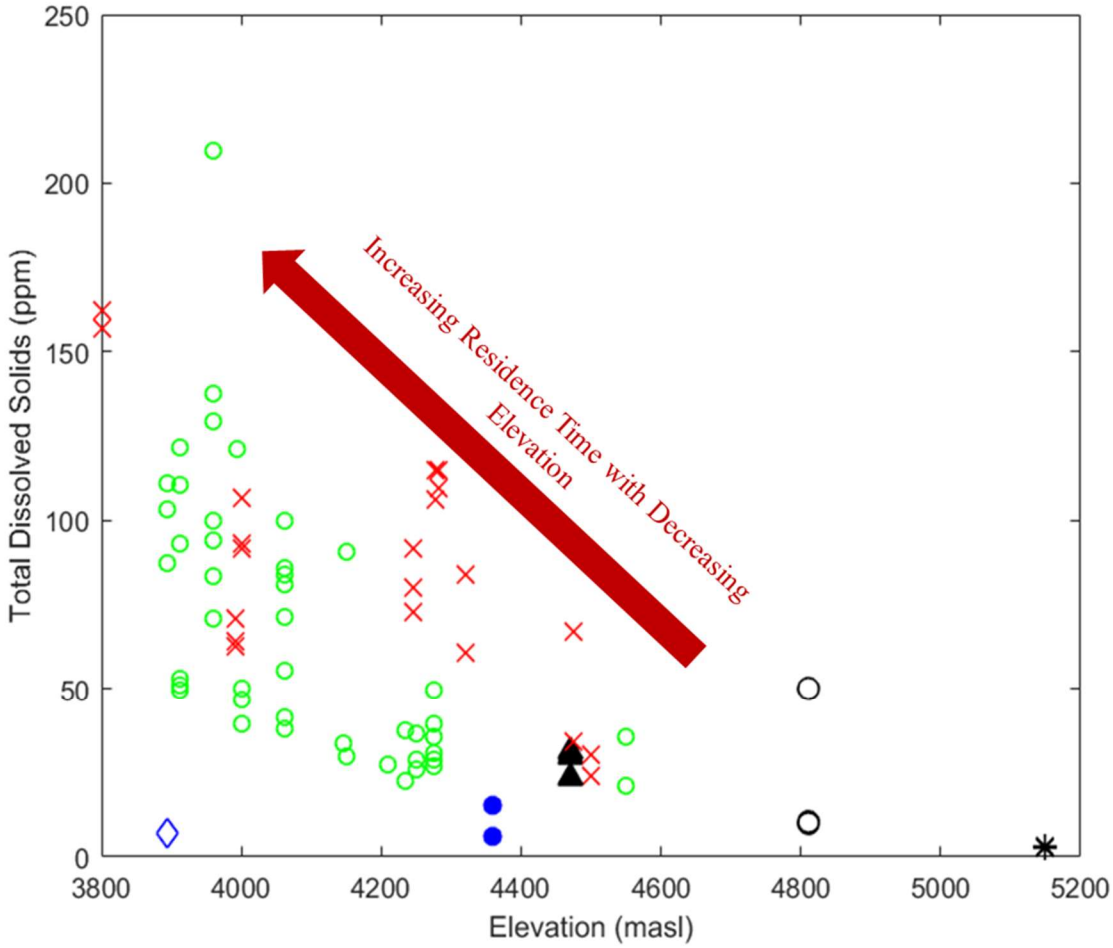

Figure 3.15. TDS (ppm) vs collection elevation (m asl). There is an apparent trend in groundwater that as discharge elevation decreases, TDS increases, indicating an increase in residence time.

concentrations (compared to meltwater and precipitation), supports the conceptual model that meltwater contributes notably to groundwater and then is transported to various distances throughout the watershed. Figure 3.15 provides further evidence of high elevation meltwater traveling downslope. The inverse relationship between elevation and TDS is consistent with a shared high elevation, low TDS meltwater source having progressively greater TDS before discharging at various lower elevations.

Chapter 4: Conclusions and Future Work

4.1 Summary of Key Findings

The rapid recession of tropical glaciers is generating unease about future water availability in Ecuador and other tropical Andean nations. The remote nature of glaciated watersheds has resulted in sparse data sets, making it difficult to predict hydrologic change in response to glacier retreat. Additionally, the heterogeneity in climatic conditions both latitudinally, between the inner and outer tropics, and longitudinally, across the Andean Cordillera, constrains the degree to which study results in one region can be applied in another. Here I examined a glaciated watershed on an inner tropical, western cordillera peak: Volcán Chimborazo. Hydrochemical and stable isotope signatures were used to investigate the hydrologic connections between groundwater, meltwater, and streamflow in the catchment. Additionally, recent geologic studies were utilized to evaluate the hydrogeology of the study watershed and a geospatial analysis of remotely sensed imagery was conducted to assess land cover change on Volcán Chimborazo since 1976. The results provide insight into important hydrologic processes and site characteristics that must be taken into consideration when evaluating the hydrologic response to climate change. Key findings in response to the main questions posed by this thesis as well as directions for future work are summarized here.

1. *Have the proportions of meltwater runoff and groundwater discharge in streamflow changed over 2012-2017?*

Absolute contributions of groundwater and meltwater, calculated using discharge measurements and the relative contributions given by the HBCM mixing model, would

suggest that groundwater discharge in the Gavilan Machay subcatchment has decreased over the five sampling periods spanning 2012-2017. However, total discharge during sampling periods appears to reflect recent weekly antecedent precipitation conditions, suggesting precipitation dynamics can influence groundwater discharge on relatively short time scales. Considering the documented influence of the multi-year ENSO cycle on precipitation in the tropical Andes, along with the limited temporal range of our data, a long-term trend in groundwater discharge remains uncertain. However, it is clear that short time-scale processes, on the order of weeks to months, create high variability in discharge and should be accounted for when assessing changes in the hydrologic regime of glaciated, alpine catchments.

Examinations of spatiotemporal trends in melt and groundwater contributions to streamflow reveal that groundwater discharge is not only temporally dynamic but also spatially variable, with the largest proportional groundwater discharge occurring in the lower Gavilan Machay reaches near a major slope break and bedrock outcropping. This implies linked geologic and topographic controls on groundwater-surface water processes in the Gavilan Machay catchment.

2. *How is glacial meltwater partitioned between surface water and groundwater sources within a glacierized catchment on Volcán Chimborazo?*

Stable isotope signatures of springwater resemble those of melt and ice, and suggest recharge from a precipitation source falling at high elevations where ice and snow melt are the dominant hydrologic inputs. Solute concentrations in conjunction with isotopic signatures further support the conceptual model of meltwater recharging at high elevation

and traveling downslope through an inverse relationship found between discharge elevation and solute concentration. Though some uncertainty remains, as the seasonal variability in precipitation isotopes is unknown, the presence of short time scale groundwater discharge response (as noted above) implies shorter residence times such that groundwater would only represent an average of only a few preceding months of precipitation, rather than an annual average.

3. *What are the climatic, hydrogeologic, and vegetation factors that affect the hydrologic response to glacial melt?*

As noted above, it appears meteorological conditions can control the temporal variability of melt and groundwater contributions on a weekly to monthly time scale. Continued measurements will confirm this response, which is likely mediated by both the hydrogeology and the vegetation within the watershed. Cross sections of the Upper Río Mocha and Gavilan Machay subcatchment show that near-surface geology is dominated by glacial till and glaciofluvial deposits and underlain by volcanic lava flows from Chimborazo's first two cone building stages. Research in the Andes, Cascades, and Canadian Rockies suggest that glacial moraines may act as recharge areas and aquifers for shallow groundwater flow systems, while fractured volcanic units could host deeper groundwater circulations.

A new land cover map for Chimborazo was created using object based image analysis and demonstrates an upslope shift in the upper limit of vegetation around the mountain. The map additionally reveals that agriculture and pasture land have expanded further up Chimborazo's slopes as well as filled the valley to the southeast of the mountain.

Both these changes are likely to affect the hydrologic regime in the catchment as they alter evapotranspiration rates and water demand for irrigation.

4.2 Future Research Directions

Additional research in several areas is needed to further support and extend the conclusions reached here and to understand how the hydrologic regime in the Upper Río Mocha will respond to climate change in the future. Isotopic and hydrochemical signatures here suggest a melt-groundwater path, but lack of intra-annual precipitation isotope data makes this uncertain. Analyzing isotopic signatures of monthly precipitation samples can help determine whether groundwater truly exhibits a meltwater signature, or if it more closely resembles the mean annual precipitation value. Further, meltwater input to the watershed could be quantified through mass loss and energy balance calculations using ablation stations measuring temperature, relative humidity, ice melt, and incoming solar radiation. Compared against discharge measurements taken near the tongue of the glacier, the results would provide insight into the amount of melt infiltrating to the water table.

Geologic cross sections presented here provide a first approximation of subsurface geology in the Upper Río Mocha watershed, and can be further refined through field surveys and/or geospatial analysis of remotely sensed imagery. Better constraints on unit thicknesses and outcrop locations could be used, along with the already digitized GIS unit layers, to create a 3D model of subsurface geology. Such a model could be incorporated into a hydrological model and each geology unit assigned properties, such as hydraulic conductivity, to investigate detailed subsurface flow mechanisms and explain spatial variability in groundwater discharge.

Lastly, the land cover map awaits an in-depth accuracy assessment. Different groupings within the agricultural (e.g. crop type, pasture) and native vegetation (e.g. bunch grass, cushion plants) classes could be resolved with ground surveys and new geospatial data from the SIGTIERRAS initiative. Once that is completed, the map can also be utilized in a watershed model with an ecohydrological component to better simulate infiltration and losses to evapotranspiration. With new and extended data on vegetation, geology, and hydrology, an integrated watershed model can be used to further resolve the spatiotemporal melt and groundwater dynamics of this catchment under climate change and confirm the results from our hydrochemical and stable isotope analyses.

References

Andermann, C. et al., 2012. Impact of transient groundwater storage on the discharge of Himalayan rivers. *Nature Geoscience*, 5(2), pp.127–132. Available at: http://dx.doi.org/10.1038/ngeo1356.

Baraer, M. et al., 2009. Characterizing contributions of glacier melt and groundwater during the dry season in a poorly gauged catchment of the Cordillera Blanca (Peru). *Advances in Geosciences*, 22, pp.41–49.

Baraer, M. et al., 2015. Contribution of groundwater to the outflow from ungauged glacierized catchments: A multi-site study in the tropical Cordillera Blanca, Peru. *Hydrological Processes*, 29(11), pp.2561–2581.

Baraer, M. et al., 2012. Glacier recession and water resources in Peru's Cordillera Blanca. *Journal of Glaciology*, 58(207), pp.134–150.

Baraer, M., McKenzie, J. & Mark, B.G., 2017. Applied Geochemical Methods for Mountain Hydrology Workshop. , p.Jan 9th-11th, 2017.

Barba, D., 2006. *Estudio Vulcanologico del Complejo Volcanico Chimborazo- Ecuador*. Escuela Politecnica Nacional.

Barba, D. et al., 2005. Geology and structure of the late Pleistocene to Holocene Chimborazo stratovolcano (Ecuador). In *6th International Symposium on Andean Geodynamics*. Barcelona, Spain: ISAG, pp. 90–93.

Barba, D. et al., 2008. Holocene recurrent explosive activity at Chimborazo volcano (Ecuador). *Journal of Volcanology and Geothermal Research*, 176(1), pp.27–35.

Barnett, T.P., Adam, J.C. & Lettenmaier, D.P., 2005. Potential impacts of a warming climate on water availability in snow-dominated regions. *Nature*, 438(7066), pp.303–309. Available at: http://www.ncbi.nlm.nih.gov/pubmed/16292301.

Beate, B. & Hall, M.L., 1989. *Informe final de Volcanología: Tungurahua, Cotopaxi, Chimborazo*, San Francisco, CA.

Bernard, B. et al., 2008. The Chimborazo sector collapse and debris avalanche: Deposit characteristics as evidence of emplacement mechanisms. *Journal of Volcanology and Geothermal Research*, 176(1), pp.36–43.

Bigo, A., 2013. *Estudio hidrogeológico de la subcuenca del rió Chambo: Perspectivas para un uso sostenible del recurso hídrico*, Riobamba, Ecuador.

Blasch, K.W. & Bryson, J.R., 2007. Distinguishing Sources of Ground Water Recharge by Using d 2 H and d 18 O. , 45(3), pp.294–308.

Blaschke, T. et al., 2014. Geographic Object-Based Image Analysis – Towards a new paradigm. *ISPRS Journal of Photogrammetry and Remote Sensing*, 87, pp.180–191. Available at: http://dx.doi.org/10.1016/j.isprsjprs.2013.09.014.

Blaschke, T., 2010. Object based image analysis for remote sensing. *ISPRS Journal of Photogrammetry and Remote Sensing*, 65, pp.2–16. Available at: http://dx.doi.org/10.1016/j.isprsjprs.2009.06.004.

Bradley, R.S., 2006. CLIMATE CHANGE: Threats to Water Supplies in the Tropical Andes. *Science*, 312(5781), pp.1755–1756. Available at: http://www.sciencemag.org/cgi/doi/10.1126/science.1128087.

Bradley, R.S. et al., 2003. Low latitude ice cores record Pacific sea surface temperatures. *Geophysical Research Letters*, 30(4), pp.2–5. Available at: http://doi.wiley.com/10.1029/2002GL016546.

Braun, L.N., Weber, M. & Schulz, M., 2000. Consequences of climate change for runoff from Alpine regions. *Annals of Glaciology*, 31, pp.19–25.

Bustamante, M., Albán, M. & Argüello, M.A. eds., 2011. *Los páramos de chimborazo. Un estudio socioambiental para la toma de decisiones*, Quito, Ecuador: Gobierno autónomo descentralizado de Chimborazo/EcoCiencia/CONDESAN/Programa BioAndes/Proyecto Páramo Andino.

Buytaert, W. et al., 2006. Human impact on the hydrology of the Andean páramos. *Earth-Science Reviews*, 79, pp.53–72.

Buytaert, W. et al., 2004. The use of the linear reservoir concept to quantify the impact of changes in land use on the hydrology of catchments in the Andes. *Hydrology and Earth System Sciences*, 8, pp.108–114.

Buytaert, W. et al., 2010. Uncertainties in climate change projections and regional downscaling in the tropical Andes: Implications for water resources management. *Hydrology and Earth System Sciences*, 14, pp.1247–1258.

Buytaert, W., Célleri, R. & Timbe, L., 2009. Predicting climate change impacts on water resources in the tropical Andes: Effects of GCM uncertainty. *Geophysical Research Letters*, 36, pp.1–5.

Buytaert, W., Cuesta-Camacho, F. & Tobón, C., 2011. Potential impacts of climate change on the environmental services of humid tropical alpine regions. *Global Ecology and Biogeography*, 20(1), pp.19–33. Available at: http://doi.wiley.com/10.1111/j.1466-8238.2010.00585.x.

Caceres, B. et al., 2006. El glaciar 15 del Antisana investigaciones glaciológicas y su relación con el recurso hídrico. *Climate Variability and Change—Hydrological Impacts. Proceedings Fifth FRIEND World Conference*, (November), pp.1–4.

Cáceres, B., 2010. *Actualización del inventario de tres casquetes glaciares del Ecuador*. Nice, France: Université Nice, France.

Carey, M. et al., 2017. Impacts of Glacier Recession and Declining Meltwater on Mountain Societies. *Annals of the American Association of Geographers*, 107(2), pp.350–359. Available at: https://www.tandfonline.com/doi/full/10.1080/24694452.2016.1243039.

Carey, M. et al., 2014. Toward hydro-social modeling: Merging human variables and the social sciences with climate-glacier runoff models (Santa River, Peru). *Journal of Hydrology*, 518(PA), pp.60–70. Available at: http://dx.doi.org/10.1016/j.jhydrol.2013.11.006.

Cauvy-Fraunié, S. et al., 2013. Technical Note: Glacial influence in tropical mountain hydrosystems evidenced by the diurnal cycle in water levels. *Hydrology and Earth System Sciences*, 17(12), pp.4803–4816. Available at: http://www.hydrol-earth-syst-sci.net/17/4803/2013/.

Chevallier, P. et al., 2011. Climate change threats to environment in the tropical Andes: Glaciers and water resources. *Regional Environmental Change*, 11(SUPPL. 1), pp.179–187.

Christophersen, N. & Hooper, R.P., 1992. Multivariate analysis of stream water chemical data: the use of principal compenents analysis for the end-member mixing problem. *Water Resources Research*, 28(1), pp.99–107.

Clapperton, C. & McEwan, C., 1985. Late Quaternary moraines in the Chimborazo area, Ecuador. *Arctic and Alpine Research*, 17(2), pp.135–142. Available at: http://www.jstor.org/stable/10.2307/1550843.

Clapperton, C.M., 1990. Glacial and volcanic geomorphology of the Chimborazo-Carhuairazo Massif, Ecuadorian Andes. *Transactions of the Royal Society of Edinburgh: Earth Sciences*, (81), pp.91–116.

Clark, I.D. & Fritz, P., 1997. *Environmental Isotopes in Hydrogeology*, New York: Lewis Publishers.

Clow, D.W. et al., 2003. Ground water occurrence and contributions to stream ow in an alpine catchment. *Colorado Front Range. Ground Water*, 41(7), pp.937–950.

Clow, D.W. et al., 2003. Ground Water Occurrence and Contributions to Streamflow in an Alpine Catchment, Colorado Front Range. *Ground Water*, 41(7), pp.937–950. Available at: http://doi.wiley.com/10.1111/j.1745-6584.2003.tb02436.x.

Collins, D.N., 2008. Climatic warming , glacier recession and runoff from Alpine basins after the little ice age maximum. *Annals of Glaciology*, 48, pp.119–124.

Cordova, M. et al., 2015. Evaluation of the Penman-Monteith (FAO 56 PM) Method for Calculating Reference Evapotranspiration Using Limited Data Application to the Wet Paramo of Southern Ecuador. *Mountain Research and Development*, 35(3), pp.230–239. Available at: http://dx.doi.org/10.1659/MRD-JOURNAL-D-14-0024.1.

Crossman, J. et al., 2011. Water Flow Dynamics of Groundwater-Fed Streams and Their Ecological Significance in a Glacierized Catchment. *Arctic, Antarctic, and Alpine Research*, 43(3), pp.364–379. Available at: http://www.bioone.org/doi/abs/10.1657/1938-4246-43.3.364.

Cushman, J.. & Tartakovsky, D.M. eds., 2016. *The Handbook of Groundwater Engineering* Third Edit., CRC Press.

Dansgaard, W., 1964. Stable isotopes in precipitation. *Tellus XVI*, 16(4), pp.436–468.

Dorren, L.K.A., Maier, B. & Seijmonsbergen, A.C., 2003. Improved Landsat-based forest mapping in steep mountainous terrain using object-based classification. *Forest Ecology and Management*, 183(1–3), pp.31–46. Available at: http://linkinghub.elsevier.com/retrieve/pii/S0378112703001130.

Favier, V. et al., 2008. Evidence of groundwater flow on Antizana ice-covered volcano, Ecuador / Mise en évidence d'écoulements souterrains sur le volcan englacé Antizana, Equateur. *Hydrological Sciences Journal*, 53(1), pp.278–291. Available at: http://www.tandfonline.com/doi/abs/10.1623/hysj.53.1.278.

Favier, V., 2004a. Glaciers of the outer and inner tropics: A different behaviour but a common response to climatic forcing. *Geophysical Research Letters*, 31(16), p.L16403. Available at: http://doi.wiley.com/10.1029/2004GL020654.

Favier, V., 2004b. One-year measurements of surface heat budget on the ablation zone of Antizana Glacier 15, Ecuadorian Andes. *Journal of Geophysical Research*, 109(D18), p.D18105. Available at: http://doi.wiley.com/10.1029/2003JD004359.

Francou, B., 2004. New evidence for an ENSO impact on low-latitude glaciers: Antizana 15, Andes of Ecuador, 0°28′S. *Journal of Geophysical Research*, 109(D18), p.D18106. Available at: http://doi.wiley.com/10.1029/2003JD004484.

Francou, B., 2003. Tropical climate change recorded by a glacier in the central Andes during the last decades of the twentieth century: Chacaltaya, Bolivia, 16°S. *Journal of Geophysical Research*, 108(D5), p.4154. Available at: http://doi.wiley.com/10.1029/2002JD002959.

La Frenierre, J. & Mark, B.G., 2014. A Review of methods for estimating the contribution of glacial meltwater to total watershed discharge. *Progress in Physical Geography*, 38(2), pp.173–200.

La Frenierre, J. & Mark, B.G., 2017. Detecting patterns of climate change at volcan chimborazo, ecuador, by integrating instrumental data, public observations, and glacier change analysis. *Annals of the American Association of Geographers*, 0(0), pp.1–19.

La Frenierre, J.D., 2014. *Assesing the Hydrologic Implication sof Glacier Recession and the Potential for Water Resources Vulnerability at Volcán Chimborazo, Ecuador*. Ohio State University.

Garcia, M. et al., 2004. Dynamics of reference evapotranspiration in the Bolivian highlands (Altiplano). *Agricultural and Forest Meteorology*, 125(1–2), pp.67–82. Available at: http://linkinghub.elsevier.com/retrieve/pii/S0168192304000681.

Garcia, M. et al., 1998. The role of atmospheric circulation patterns in controlling the regional distribution of the stable isotope contents in precipitation: Preliminary results from two transects in the Ecuadorian Andes. In *Isotope Techniques in the Study of Environmental Change*. Vienna, Austria: International Atomic Energy

Agency, pp. 127–140.

Gerten, D. et al., 2004. Terrestrial vegetation and water balance - Hydrological evaluation of a dynamic global vegetation model. *Journal of Hydrology*, 286(1–4), pp.249–270.

Ginot, P. et al., 2010. Influence of the Tungurahua eruption on the ice core records of Chimborazo , Ecuador To cite this version : The Cryosphere Influence of the Tungurahua eruption on the ice core records of Chimborazo , Ecuador. *The Cryosphere*, 4(4), pp.561–568.

Godsey, S.E., Kirchner, J.W. & Tague, C.L., 2014. Effects of changes in winter snowpacks on summer low flows: case studies in the Sierra Nevada, California, USA. *Hydrological Processes*, 28(19), pp.5048–5064. Available at: http://doi.wiley.com/10.1002/hyp.9943.

Gonfiantini, R. et al., 2001. The altitude effect on the isotopic composition. *Chemical Geology*, (181), pp.147–167.

Van der Hammen, T. et al., 2002. El cambio global y los ecosistemas de alta montaña de Colombia. In C. Castaño, ed. *Páramos y ecosistemas alto andinos de Colombia en condición hotspot y global climatic tensor*. Bogotá, Colombia: IDEAM, pp. 163–209.

Hastenrath, S., 1994. Recession of Tropical Glaciers. *Science*, 265(5180), pp.1790–1791.

Hastenrath, S., 1981. *The Glaciation of the Ecuadorian Andes*, Rotterdam, Germany: A.A. Balkema.

Heine, J.T., 1993. A Reevaluation of the Evidence for a Younger Dryas Climatic Reversal in the Tropical Andes. *Quaternary Science Reviews*, 12(11), pp.769–779.

Hood, J.L., Roy, J.W. & Hayashi, M., 2006. Importance of groundwater in the water balance of an alpine headwater lake. *Geophysical Research Letters*, 33(13), pp.1–5.

Hooper, R.P., 2003. Diagnostic tools for mixing models of stream water chemistry. *Water Resources Research*, 39(3), pp.1–13. Available at: http://doi.wiley.com/10.1029/2002WR001528.

Hooper, R.P. & Shoemaker, C.A., 1986. A Comparison of Chemical and Isotopic Hydrograph Separation. *Water Resources Research*, 22(10), pp.1444–1454.

Hu, Q. et al., 2013. Exploring the Use of Google Earth Imagery and Object-Based Methods in Land Use/Cover Mapping. *Remote Sensing*, 5(11), pp.6026–6042.

Hughes, R.A. & Pilatasig, L.F., 2002. Cretaceous and tertiary terrane accretion in the Cordillera Occidental of the Andes of Ecuador. *Tectonophysics*, 345(1–4), pp.29–48.

Humboldt, A., Geognostische und physikalische Beobachtungen über die Vulkane des Hochlandes von Quito. *Annals of Physical Chemistry*, 40 & 44, pp.161–193 & 193–219.

Huss, M. et al., 2008. Modelling runoff from highly glacierized alpine drainage basins in a changing climate. *Hydrological Processes*, 22(19), pp.3888–3902. Available at:

http://doi.wiley.com/10.1002/hyp.7055.

INEC, 2010. *Cencos de Poblacion y Vivienda 2010*, Quito, Ecuador.

IPCC, 2014. *Climate Change 2014 - Impacts, Adaptatiom, and Vulnerability: Regional Aspects*, Cambridge University Press.

James, A.L. & Roulet, N.T., 2006. Investigating the applicability of end-member mixing analysis (EMMA) across scale: A study of eight small, nested catchments in a temperate forested watershed. *Water Resources Research*, 42(8), pp.1–17.

Juen, I., Kaser, G. & Georges, C., 2007. Modelling observed and future runoff from a glacierized tropical catchment (Cordillera Blanca, Perú). *Global and Planetary Change*, 59(1–4), pp.37–48. Available at: http://linkinghub.elsevier.com/retrieve/pii/S0921818106002967.

Kaser, G., 1999. A review of the modern fluctuations of tropical glaciers. *Global and Planetary Change*, 22(1–4), pp.93–103.

Kaser, G., 2001. Glacier-climate interaction at low latitudes. *Journal of Glaciology*, 47(157), pp.195–204.

Kaser, G., Großhauser, M. & Marzeion, B., 2010. Contribution potential of glaciers to water availability in different climate regimes. , 2010.

Kaser, G. & Ostmaston, H., 2002. *Tropical Glaciers. International Hydrology Series* 207th ed., Cambridge: Cambridge University Press.

Kendall, C. & Doctor, D.H., 2003. Stable Isotope Applications in Hydrologic Studies. In *Treatise on Geochemistry*. Elsevier, pp. 319–364. Available at: http://dx.doi.org/10.1016/B978-0-08-095975-7.00510-6.

Kilian, R. et al., 1995. Magma evolution within the accretionary mafic basement of Quaternary Chimborazo and associated volcanos (Western Ecuador). *Revista Geológica de Chile*, 22(2), pp.203–218.

Kilian, R., 1987. *The development of the Chimborazo (6310 m), Carihuairazo (5106 m) and other volcanoes of Ecuador*, Stuttgart.

Kintz, D.B., Young, K.R. & Crews-Meyer, K.A., 2006. Implications of land use/land cover change in the buffer zone of a National Park in the tropical Andes. *Environmental Management*, 38(2), pp.238–252.

Kressler, F.P., Franzen, M. & Steinnocher, K., 2005. Segmentation based classification of aerial images and its potential to support the update of existing land use data bases. *Commission VI, WG VI/4*.

Lal, R. & Stewart, B.A., 2012. *Soil Water and Agronomic Productivity (Advances in Soil Science)*, Hoboken, NJ: Taylor and Francis.

Langston, G. et al., 2011. Internal structure and hydrological functions of an alpine proglacial moraine. *Hydrological Processes*, 25(19), pp.2967–2982. Available at: http://doi.wiley.com/10.1002/hyp.8144.

Lemke, P. et al., 2007. Observations: Changes in Snow, Ice and Frozen Ground. In M. T. and H. L. M. Solomon, S., D. Qin, M. Manning, Z. Chen, M. Marquis, K.B. Averyt, ed. *Climate Change 2007: The Physical Science Basis. Contribution of Working Group I to the Fourth Assessment Report of the Intergovernmental Panel on Climate Change*. Cambridge, United Kingdom and New York, NY, USA: Cambridge University Press.

Luteyn, J.L., 1999. *Paramos: a checklist of plant diversity, geograpical distribution, and botanical literature*, New York: The New York Botanical Garden Press.

Luteyn, J.L., 1992. Páramos: why study them? In J. L. Balslev, H., Luteyn, ed. *Páramo: an Andean ecosystem under human influence*. London: Academic Press, pp. 1–14.

Maldonado, V., 2016. *Ecohydrology of the Andes Páramo Region*. Delft University of Technology.

Manciati, C. et al., 2014. Empirical mass balance modelling of South American tropical glaciers : case study of Antisana volcano , Ecuador. *Hydrological Sciences Journal*, 59(8), pp.1519–1535.

Mark, B.G., 2008. Tracing tropical Andean glaciers over space and time: Some lessons and transdisciplinary implications. *Global and Planetary Change*, 60(1–2), pp.101–114.

Mark, B.G. & Mckenzie, J.M., 2007. Tracing Increasing Tropical Andean Glacier Melt with Stable Isotopes in Water. *Environmental Science & Technology*, 41(20), pp.6955–6960.

Mark, B.G. & Seltzer, G.O., 2005. Evaluation of recent glacier recession in the Cordillera Blanca, Peru (AD 1962-1999): Spatial distribution of mass loss and climatic forcing. *Quaternary Science Reviews*, 24(20–21), pp.2265–2280.

Mark, B.G. & Seltzer, G.O., 2003. Tropical glacier meltwater contribution to stream discharge: A case study in the Cordillera Blanca, Peru. *Journal of Glaciology*, 49(165), pp.271–281.

Markovich, K., Maxwell, R. & Fogg, G., 2016. Hydrogeological response to climate change in alpine hillslopes. *Hydrological Processes*, 30, pp.3126–3138.

Messerli, B., 2001. The International Year of the Mountains (IYM), the Mountain Research Initiative (MRI) and PAGES, editorial. *Pages News*, 9(2).

Messerli, B., Viviroli, D. & Weingartner, R., 2004. Mountains Vulnerable of the World : Water Towers for the 21st Century. *AMBIO Special Report*, 13(December 2004), pp.29–34.

Morris, J.N., Poole, A.J. & Klein, A.G., 2006. Retreat of Tropical Glaciers in Colombia and Venezuela from 1984 to 2004 as Measured from ASTER and Landsat Images. In *63rd Eastern Snow Conference*. Newark, Delaware, USA, pp. 181–191.

Morueta-holme, N. et al., 2015. Strong upslope shifts in Chimborazo ' s vegetation over two centuries since Humboldt. *Proceedings of the National Academy of Sciences*,

112(41), pp.12741–12745.

Mosquera, G.M. et al., 2016. Combined Use of Isotopic and Hydrometric Data to Conceptualize Ecohydrological Processes in a High-Elevation Tropical Ecosystem. *Hydrological Processes*, 3008.

Podwojewski, P. et al., 2002. Overgrazing effects on vegetation cover and properties of volcanic ash soil in the pa. *Soil use and Management*, 18, pp.45–55. Available at: http://onlinelibrary.wiley.com/doi/10.1111/j.1475-2743.2002.tb00049.x/abstract.

Polk, M.H. et al., 2017. Exploring hydrologic connections between tropical mountain wetlands and glacier recession in Peru's Cordillera Blanca. *Applied Geography*, 78, pp.94–103.

Pourrut, P. et al., 1995. CLIMA DEL ECUADOR. In P. Pourrut & P. Pouyaud, eds. *El agua en el Ecuador : clima, precipitaciones, escorrentia*. Quito, Ecuador: Corporación Editora Nacional, Colégio de Geógrafos del Ecuador and ORSTOM, pp. 13–26.

Poveda, G. & Pineda, K., 2009. Reassessment of Colombia's tropical glaciers retreat rates: are they bound to disappear during the 2010–2020 decade? *Advances in Geosciences*, 22(2008), pp.107–116. Available at: http://www.adv-geosci.net/22/107/2009/.

Rabatel, a. et al., 2013. Current state of glaciers in the tropical Andes: a multi-century perspective on glacier evolution and climate change. *The Cryosphere*, 7(1), pp.81–102. Available at: http://www.the-cryosphere.net/7/81/2013/.

Ramírez, E. et al., 2001. Small glaciers disappearing in the tropical Andes: a case-study in Bolivia: Glaciar Chacaltaya (16o S). *Journal of Glaciology*, 47(157), pp.187–194. Available at: https://www.cambridge.org/core/product/identifier/S0022143000210897/type/journal_article.

Raup, B. et al., 2007. The GLIMS geospatial glacier database: A new tool for studying glacier change. *Global and Planetary Change*, 56(1–2), pp.101–110. Available at: http://linkinghub.elsevier.com/retrieve/pii/S0921818106001597.

Rhoades, R.E., Ríos Zapata, X. & Ochoa, J.A., 2008. Mama Cotacachi: History, Local Perceptions, and Social Impacts of Climate Change and Glacier Retreat in the Ecuadorian Andes. In B. Orlove, E. Wiegandt, & B. H. Luckman, eds. *Darkening Peaks: Glacier Retreat, Science, and Society*. Berkeley, CA: University of California Press, pp. 218–228.

Rozanski, K. & Araguas, L., 1995. Spatial and temporal variability of stable isotope composition of precipitation over the south american continent. *Bulletin de l'Institut Français d'Études Andines*, 24(3), pp.379–390.

Ryu, J.S., Lee, K.S. & Chang, H.W., 2007. Hydrochemistry and isotope geochemistry of Song Stream, a headwater tributary of the South Han River, South Korea.

Geosciences Journal, 11(2), pp.157–164.

Samaniego, P. et al., 2012. Eruptive history of Chimborazo volcano (Ecuador): A large , ice-capped and hazardous compound volcano in the Northern Andes. *Journal of Volcanology and Geothermal Research*, 221–222, pp.33–51. Available at: http://dx.doi.org/10.1016/j.jvolgeores.2012.01.014.

Schmidt, S.. et al., 2008. The earliest stages of ecosystem succession in high-elevation (5000 metres above sea level), recently deglaciated soils. *Proceedings of the Royal Society B: Biological Sciences*, 275(1653), pp.2793–2802. Available at: http://rspb.royalsocietypublishing.org/cgi/doi/10.1098/rspb.2008.0808.

Sicart, J.E. et al., 2011. Analysis of seasonal variations in mass balance and meltwater discharge of the tropical Zongo Glacier by application of a distributed energy balance model. *Journal of Geophysical Research*, 116(D13), p.D13105. Available at: http://doi.wiley.com/10.1029/2010JD015105.

Sicart, J.E. et al., 2007. Glacier mass balance of tropical Zongo glacier, Bolivia, comparing hydrological and glaciological methods. *Global and Planetary Change*, 59(1–4), pp.27–36.

Sidle, W.C., 1998. Environmental isotopes for resolution of hydrology problems. *Environmental Monitoring and Assessment*, 52(3), pp.389–410.

Smith, J.A., Mark, B.G. & Rodbell, D.T., 2008. The timing and magnitude of mountain glaciation in the tropical Andes. *Journal of Quaternary Science*, 23(6–7), pp.609–634. Available at: http://doi.wiley.com/10.1002/jqs.1224.

Somers, L. et al., 2016. Quantifying groundwater- surface water interactions in a proglacial valley, Cordillera Blanca, Peru. *Hydrological Processes*, 2929(June), pp.2915–2929.

Soulsby, C. et al., 2003. Identifying and assessing uncertainty in hydrological\npathways: a novel approach to end member mixing\nin a Scottish agricultural catchment. *Journal of Hydrology*, 274, pp.109–128.

Stumm, W. & Morgan, J.., 2013. *Aquatic Chemistry: Chemical Equilibria and Rates in Natural Waters* 3, revised ed., John Wiley & sons.

Tague, C. et al., 2008. Deep groundwater mediates streamflow response to climate warming in the Oregon Cascades. *Climatic Change*, 86(1–2), pp.189–210. Available at: http://link.springer.com/10.1007/s10584-007-9294-8.

Tappa, D.J. et al., 2016. Isotopic composition of precipitation in a topographically steep, seasonally snow-dominated watershed and implications of variations from the global meteoric water line. *Hydrological Processes*, 30(24), pp.4582–4592. Available at: http://doi.wiley.com/10.1002/hyp.10940.

Veettil, B.K. et al., 2014. Combined influence of PDO and ENSO on northern Andean glaciers: a case study on the Cotopaxi ice-covered volcano, Ecuador. *Climate Dynamics*, 43(12), pp.3439–3448.

Vergara, W. et al., 2007. Economic Impacts of Rapid Glacier Retreat in the Andes. *Eos, Transactions American Geophysical Union*, 88(25), pp.261–268.

Vimeux, F. et al., 2005. What are the climate controls on dD in precipitation in the Zongo Valley (Bolivia)? Implications for the Illimani ice core interpretation. *Earth and Planetary Science Letters*, 240(September 2017), pp.205–220.

Vuille, M. et al., 2008. Climate change and tropical Andean glaciers: Past, present and future. *Earth-Science Reviews*, 89(3–4), pp.79–96. Available at: http://linkinghub.elsevier.com/retrieve/pii/S0012825208000408.

Vuille, M. et al., 2003. Modeling delta d18O in precipitation over the tropical Americas: 2. Simulation of the stable isotope signal in Andean ice cores. *Journal Of Geophysical Research-Atmospheres*, 108(D6), p.4175. Available at: http://www.agu.org/pubs/crossref/2003/2001JD002039.shtml%5Cnpapers2://publication/doi/10.1029/2001JD002039.

Vuille, M., Bradley, R.S. & Keimig, F., 2000. Interannual climate variability in the Central Andes and its relation to tropical Pacific and Atlantic forcing. *Journal of Geophysical Research*, 105(D10), pp.12446–12460.

Vuille, M. & Keimig, F., 2004. Interannual Variability of Summertime Convective Cloudiness and Precipitation in the Central Andes Derived from ISCCP-B3 Data. *Journal of Climate*, 17, pp.3334–3348.

Wagnon, P. et al., 1999. Annual cycle of energy balance of Zongo Glacier, Cordiller Real, Bolivia. *Journal Of Geophysical Research*, 104(D4), pp.3907–3923.

Wagnon, P. et al., 2001. Anomalous heat and mass budget of Glaciar Zongo , Bolivia , during the 1997 / 98 El Nino year. *Journal of Glaciology*, 47(156), pp.21–28.

Walther, G.-R., Beißner, S. & Burga, C.A., 2005. Trends in the upward shift of alpine plants. *Journal of Vegetation Science*, 16(5), p.541. Available at: http://doi.wiley.com/10.1658/1100-9233(2005)16[541:TITUSO]2.0.CO;2.

Whymper, E., 1892. *Travels among the Great Andes of Ecuador*, New York: Charles Scribner's Sons.

Wickert, A.D., 2014. The ALog: Inexpensive, Open-Source, Automated Data Collection in the Field. *Bulletin of the Ecological Society of America*, 95(2), pp.166–176.

Williams, M. et al., 2002. Interpreting Climate Signals from a Shallow Equatorial Core: Antisana, Ecuador. In *The Patagonian Icefields*. p. 169.

Windhorst, D. et al., 2013. Impact of elevation and weather patterns on the isotopic composition of precipitation in a tropical montane rainforest. *Hydrology and Earth System Sciences*, 17, pp.409–419.

Wohl, E. et al., 2012. The hydrology of the humid tropics. *Nature Climate Change*, 2(9), pp.655–662. Available at: http://www.nature.com/doifinder/10.1038/nclimate1556.

Appendix A: Additional Figures

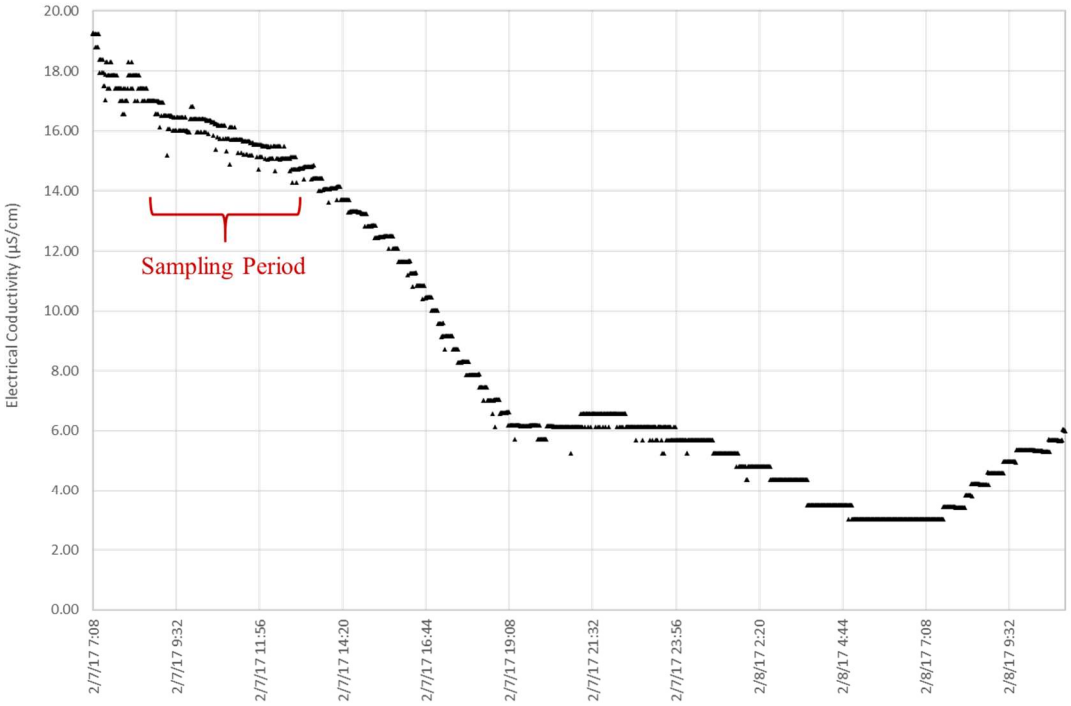

Figure 1 24 hours of calibrated, temperature corrected conductivity measurements in the Gavilan Machay stream. An Atlas Scientific EZO conductivity probe was used to collect conductivity measurements in the stream at the tongue of the Reschreiter Glacier. Measurements were made over the 24-hour period in which water samples were collected and confirmed that no significant change in water chemistry occurred during the sampling period. Additionally, it revealed that diurnal variability in conductivity (~ 16 µS/cm) was negligible when compared to conductivity variations at the watershed scale (~160 µS/cm).

Appendix B: June 2016 Example of HBCM Output for Confluence Cell

CELL 2: CONFLUENCE

HBCM 1,0
ETS, University of Quebec

before to start, you need to place the input matrix in B; the tracer column in T; the goundwaters in GW and the sampling point name in S

Please make sure that tracer values at the cell outflow and at least at one contributor must be above the detection limit of the analytical methods
test for tracers conservation? (o or n) o

out of range:
2 rejected tracers
2×1 cell array

'Na'
'HCO3'

lack of contrast between sources :
0 rejected tracers

Tracers remaining for the HBCM application to the present cell:
5×1 cell array

'Mg'
'Ca'
'SO4'
'Cl'
'd18O'

number of sources: 2
number of tracers remaining: 5

groundwater to be considered as water sources? (o or n) ***Note: o = oui (yes) & n = no**

→ n

Results for GW: 0
number of sources incling GW: 2

number of used tracers: 5

cumulated error sources tracers
Columns 1 through 7

10.7988e-003 933.2786e-003 66.7214e-003 1.0000e+000 2.0000e+000 3.0000e+000 4.0000e+000

Column 8

5.0000e+000

Results for GW: 0
number of sources incling GW: 2
number of used tracers: 4

cumulated error sources tracers
5.3792e-003 933.3128e-003 66.6872e-003 2.0000e+000 3.0000e+000 4.0000e+000 5.0000e+000
9.1740e-003 933.3227e-003 66.6773e-003 1.0000e+000 2.0000e+000 3.0000e+000 4.0000e+000
11.9924e-003 918.6945e-003 81.3055e-003 1.0000e+000 2.0000e+000 3.0000e+000 5.0000e+000
12.4860e-003 933.3310e-003 66.6690e-003 1.0000e+000 3.0000e+000 4.0000e+000 5.0000e+000
13.4531e-003 933.3294e-003 66.6706e-003 1.0000e+000 2.0000e+000 4.0000e+000 5.0000e+000

Results for GW: 0
number of sources incling GW: 2
number of used tracers: 3

cumulated error sources tracers
1.4078e-003 933.3376e-003 66.6624e-003 2.0000e+000 3.0000e+000 4.0000e+000
5.8235e-003 933.3272e-003 66.6728e-003 3.0000e+000 4.0000e+000 5.0000e+000
6.2455e-003 918.7056e-003 81.2944e-003 2.0000e+000 3.0000e+000 5.0000e+000
7.1119e-003 933.3317e-003 66.6683e-003 2.0000e+000 4.0000e+000 5.0000e+000
10.6321e-003 918.6913e-003 81.3087e-003 1.0000e+000 2.0000e+000 3.0000e+000

10.8840e-003 933.3313e-003 66.6687e-003 1.0000e+000 3.0000e+000
4.0000e+000
11.1075e-003 786.7455e-003 213.2545e-003 1.0000e+000 3.0000e+000
5.0000e+000
12.1754e-003 933.3166e-003 66.6834e-003 1.0000e+000 2.0000e+000
4.0000e+000
13.8502e-003 786.8636e-003 213.1364e-003 1.0000e+000 2.0000e+000
5.0000e+000
16.5899e-003 933.3345e-003 66.6655e-003 1.0000e+000 4.0000e+000
5.0000e+000

Results for GW: 0
number of sources incling GW: 2
number of used tracers: 2

cumulated error sources tracers
87.5686e-006 933.3325e-003 66.6675e-003 3.0000e+000 4.0000e+000
1.3306e-003 918.7014e-003 81.2986e-003 2.0000e+000 3.0000e+000
2.0217e-003 933.3322e-003 66.6678e-003 2.0000e+000 4.0000e+000
2.5489e-003 786.7032e-003 213.2968e-003 1.0000e+000 5.0000e+000
8.0381e-003 918.6871e-003 81.3129e-003 2.0000e+000 5.0000e+000
8.6094e-003 932.4172e-003 67.5828e-003 3.0000e+000 5.0000e+000
8.6463e-003 933.3326e-003 66.6674e-003 4.0000e+000 5.0000e+000
14.1139e-003 786.7966e-003 213.2034e-003 1.0000e+000 3.0000e+000
14.6175e-003 918.6804e-003 81.3196e-003 1.0000e+000 2.0000e+000
16.2396e-003 933.3293e-003 66.6707e-003 1.0000e+000 4.0000e+000

---
summary matrix

GW
numbers of tracers
5
4
3
2

minimum reached residue
10.7988e-003
5.3792e-003
1.4078e-003

87.5686e-006

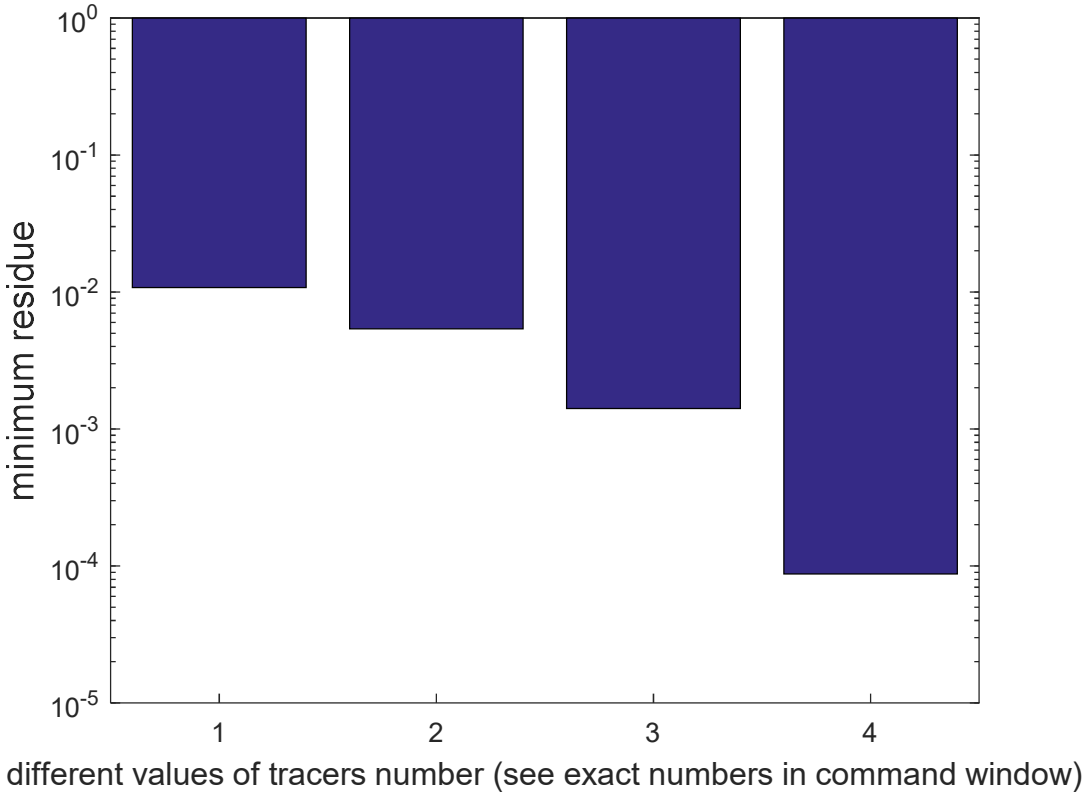
minimum residue
10^{0}
10^{-1}
10^{-2}
10^{-3}
10^{-4}
10^{-5}
1
2
3
4
different values of tracers number (see exact numbers in command window)

Appendix C: Hydrochemical Analysis Results for Major Ions & Isotopes for 2015-2017 Sampling Campaigns

June 2015																			
Sample Name	Sample Type	Elevation	pH	Specific Conductivity (µS/cm)	Date	$\delta^{18}O$ (‰)	$\delta^{2}H$ (‰)	D Excess	Na^{+}	K^{+}	Mg^{2+}	Ca^{2+}	F^{-}	Cl^{-}	SO_4^{2-}	HCO_3^{-}	ΣCations (meq/L)	ΣAnions (meq/L)	TDS (mg/L)
Melt-340	Glacier Melt	4471	5.76	30.3	06/12/15	-13.9	-99.3	12.2	0.047	0.022	0.075	0.104	0.040	0.041	0.042	0.260	0.425	0.425	29.788
GW-305	Spring	4000	5.89	59.4	06/15/15	-13.2	-93.9	11.4	0.241	0.066	0.260	0.211	0.050	0.090	0.024	1.061	1.249	1.249	93.009
GW-323	Spring	4245	4.13	92.6	06/12/15	-13.0	-94.8	8.9	0.194	0.038	0.180	0.190	0.035	0.058	0.029	0.820	0.973	0.973	72.724
GW-S3	Spring	4047	7.89	361.5	06/20/15	-13.1	-95.1	9.9	0.708	0.061	0.865	0.472	0.054	0.086	0.151	3.000	3.443	3.443	257.261
GW-S6	Spring	3992	8	100	06/20/15	-12.8	-91.2	11.5	0.176	0.057	0.165	0.141	0.037	0.077	0.025	0.679	0.844	0.844	62.509
GW-S15	Spring				06/12/15	-12.7	-92.5	9.2	0.325	0.064	0.377	0.313	0.026	0.056	0.038	1.609	1.767	1.767	134.360
GW-S16	Spring				06/20/15	-13.2	-93.9	11.7	0.382	0.053	0.493	0.347	0.039	0.041	0.087	1.860	2.115	2.115	158.955
GW-S17	Spring				06/20/15	-13.3	-94.7	11.6	0.771	0.066	1.088	0.543	0.045	0.118	0.225	3.485	4.098	4.098	304.279
GW-S19	Spring				06/20/15	-13.5	-97.0	10.9	0.417	0.054	0.449	0.303	0.049	0.066	0.065	1.728	1.974	1.974	147.989
Mix-110	Stream	3895	6.6	139.8	06/14/15	-13.0	-93.1	11.1	0.232	0.043	0.319	0.250	0.040	0.049	0.147	1.031	1.415	1.415	103.333
Mix-111	Stream	3912	6.65	144.1	06/15/15	-13.0	-91.5	12.6	0.245	0.044	0.351	0.262	0.040	0.055	0.170	1.081	1.517	1.517	110.359
Mix-124	Stream	3994			06/15/15	-12.6	-87.8	13.1	0.227	0.039	0.360	0.352	0.042	0.038	0.298	1.014	1.690	1.690	121.216
Mix-131	Stream	4061	7.8	129.2	06/15/15	-13.5	-94.3	13.6	0.231	0.043	0.244	0.193	0.042	0.044	0.048	0.969	1.149	1.149	85.720
Mix-301	Stream	3912	6.04	70.3	06/15/15	-14.2	-99.9	13.3	0.096	0.029	0.149	0.128	0.039	0.044	0.037	0.523	0.680	0.680	49.327
Mix-306	Stream	4000	6.83	64.1	06/15/15	-13.9	-99.3	12.2	0.090	0.030	0.145	0.139	0.041	0.043	0.038	0.529	0.689	0.689	50.032
Mix-330	Stream	4250	4.32	30.1	06/12/15	-13.5	-94.3	13.6	0.040	0.019	0.074	0.100	0.037	0.037	0.042	0.249	0.409	0.409	28.559
Mix-331	Stream	4275	4.15	15.7	06/12/15	-14.2	-99.9	13.3	0.043	0.020	0.074	0.101	0.039	0.037	0.043	0.251	0.413	0.413	28.841
Mix-332	Stream	4275	4	0	06/12/15	-13.2	-93.9	11.4	0.000	0.021	0.153	0.116	0.050	0.038	0.018	0.435	0.560	0.560	39.363
Mix-401	Stream	3960	7.23	145.3	06/12/15	-13.0	-94.8	8.9	0.094	0.031	0.248	0.324	0.028	0.040	0.543	0.115	1.269	1.269	83.396
Mix-501	Stream	4061	7.87	61.7	06/12/15	-12.4	-89.2	9.8	0.063	0.033	0.123	0.115	0.029	0.041	0.054	0.394	0.572	0.572	41.151

Table 1 June 2015 Results

June 2016																				
Sample Name	Sample Type	Elevation	pH	Specific Conductivity (µS/cm)	Date	$\delta^{18}O$ (‰)	$\delta^{2}H$ (‰)	D Excess	Na^{+}	K^{+}	Mg^{2+}	Ca^{2+}	F^{-}	Cl^{-}	SO_4^{2-}	HCO_3^{-}	ΣCations (meq/L)	ΣAnions (meq/L)	TDS (mg/L)	
HM-ice	Glacier Ice	5150	6.98	3.9	07/05/16	-13.7	-99.4	10.6	0.004	0.000	0.001	0.010	0.000	0.009	0.022	0.000	0.026	0.052	2.914	
HM-ice	Glacier Ice	5150	6.66	3.1	07/05/16	-14.7	-107.0	10.5	0.009	0.000	0.000	0.005	0.000	0.004	0.021	0.000	0.019	0.046	2.575	
HM-ice	Glacier Ice	5150	6.25	4.1	07/05/16	-14.3	-102.3	12.4	0.007	0.000	0.002	0.015	0.000	0.007	0.021	0.000	0.041	0.049	3.111	
R-Ice	Glacier Ice	4810	6.29	16.7	06/28/16	-15.2	-111.4	10.2	0.022	0.004	0.010	0.044	0.002	0.012	0.024	0.072	0.135	0.135	9.807	
R-Ice	Glacier Ice	4810	6.26	12.5	06/28/16	-15.3	-110.6	11.5	0.027	0.006	0.011	0.043	0.002	0.007	0.023	0.085	0.141	0.141	10.472	
R-Ice	Glacier Ice	4810	6.34	53	06/28/16	-13.7	-96.5	13.1	0.212	0.033	0.047	0.155	0.025	0.020	0.042	0.519	0.649	0.649	49.956	
Melt-340	Glacier Melt	4471	5.76	30.3	06/30/16	-12.9	-91.0	12.5	0.097	0.013	0.054	0.098	0.012	0.015	0.040	0.306	0.414	0.414	30.978	
Lake-S7	Lake	4480			06/28/16	-11.1	-81.5	7.3	0.062	0.033	0.025	0.015	0.014	0.055	0.027	0.053	0.175	0.175	11.855	
HM-precip	Precip	4780			07/06/16	-8.3	-53.9	12.3	NA	NA	NA	NA	NA	NA	NA	NA	NA	NA	NA	
BT-precip	Precip	3895	6	21.7	07/08/16	-9.4	-62.4	12.8	0.066	0.002	0.002	0.016	0.000	0.039	0.028	0.009	0.104	0.104	6.911	
R-precip	Precip	4360	6.03	13.7	06/28/16	-9.7	-57.0	20.2	0.028	0.015	0.001	0.023	0.000	0.038	0.022	0.010	0.091	0.091	6.188	
GW-323	Spring	4245	4.13	92.6	06/28/16	-12.2	-87.9	10.0	0.238	0.036	0.183	0.205	0.007	0.058	0.039	0.906	1.050	1.050	79.887	
GW-S1	Spring	4283	6.1	185.2	07/06/16	-13.4	-94.7	12.6	0.391	0.038	0.236	0.296	0.009	0.039	0.061	1.324	1.494	1.493	114.928	
GW-S101	Spring	3800	6.03	145.8	06/25/16	-12.5	-93.5	6.9	0.478	0.109	0.372	0.348	0.012	0.070	0.039	1.867	2.026	2.026	156.685	
GW-S2	Spring	4277	6	83.1	07/06/16	-13.6	-94.3	14.5	0.362	0.040	0.217	0.269	0.009	0.035	0.044	1.244	1.374	1.374	106.185	
GW-S20	Spring		8.34	136	06/26/16	-12.8	-89.8	12.8	0.343	0.048	0.325	0.323	0.008	0.037	0.061	1.504	1.686	1.670	129.118	
GW-S3	Spring	4047	7.89	361.5	06/26/16	-13.3	-89.8	16.9	0.693	0.060	0.795	0.471	0.011	0.086	0.141	2.894	3.283	3.272	247.546	
GW-S6	Spring	3992	8	100	06/26/16	-12.3	-83.9	14.6	0.198	0.047	0.166	0.137	0.009	0.067	0.035	0.700	0.850	0.846	64.012	
GW-S8	Spring	4500	7.64	42.5	07/06/16	-13.1	-90.7	13.7	0.133	0.003	0.023	0.075	0.005	0.056	0.051	0.168	0.332	0.332	23.840	
GW-S9	Spring	4320	7.1	93.5	07/06/16	-12.4	-87.2	12.2	0.173	0.041	0.134	0.163	0.009	0.064	0.044	0.646	0.807	0.806	60.746	
GW-S7	Spring	4475	5.61	80.3	06/28/16	-11.8	-80.9	13.7	0.107	0.025	0.300	0.089	0.009	0.039	0.024	0.816	0.911	0.911	67.075	
GW-305	Spring	4000	6.83	64.1	06/26/16	-13.4	-87.2	20.0	0.277	0.059	0.237	0.198	0.009	0.077	0.035	1.051	1.206	1.206	91.686	
Mix-306	Stream	4000	5.89	59.4	06/26/16	-13.2	-89.8	15.5	0.122	0.020	0.114	0.125	0.011	0.028	0.038	0.505	0.619	0.619	46.484	
Mix-110	Stream	3895	6.6	139.8	06/25/16	-12.1	-86.4	10.3	0.216	0.038	0.247	0.213	0.008	0.042	0.122	0.880	1.174	1.174	87.171	
Mix-111	Stream	3912	6.65	144.1	06/25/16	-12.2	-85.2	12.0	0.232	0.035	0.270	0.225	0.007	0.044	0.134	0.939	1.258	1.257	93.179	
Mix-120	Stream	3960	7.52	150	06/26/16	-12.6	-83.0	17.6	0.238	0.038	0.271	0.227	0.007	0.044	0.143	0.931	1.270	1.269	94.024	
Mix-121	Stream	3960	7.15	156.2	06/26/16	-12.5	-84.4	15.7	0.274	0.041	0.293	0.212	0.008	0.052	0.060	1.144	1.324	1.323	99.928	
Mix-130	Stream	4061	7.84	110.2	06/26/16	-12.2	-83.4	13.9	0.208	0.042	0.187	0.159	0.008	0.041	0.047	0.798	0.942	0.939	71.460	
Mix-131	Stream	4061	7.8	129.2	06/26/16	-12.1	-87.9	8.6	0.251	0.044	0.226	0.181	0.008	0.047	0.047	0.957	1.109	1.106	84.126	
Mix-155	Stream	4550	7.23	40.2	07/06/16	-12.0	-83.4	12.4	0.129	0.000	0.029	0.052	0.012	0.035	0.042	0.159	0.291	0.291	20.832	
Mix-301	Stream	3912	6.04	70.3	06/25/16	-12.3	-92.2	6.5	0.144	0.024	0.138	0.129	0.012	0.028	0.037	0.592	0.704	0.704	53.039	
Mix-321	Stream	4235	5.21	35.5	06/28/16	-13.1	-84.2	20.7	0.105	0.016	0.076	0.112	0.010	0.019	0.038	0.392	0.497	0.497	37.387	
Mix-330	Stream	4250	4.32	30.1	06/28/16	-12.3	-86.9	11.2	0.107	0.015	0.069	0.113	0.011	0.019	0.038	0.379	0.486	0.486	36.595	
Mix-331	Stream	4275	4.15	15.7	06/28/16	-12.5	-90.5	9.9	0.099	0.015	0.066	0.115	0.012	0.018	0.039	0.369	0.476	0.476	35.768	
Mix-332	Stream	4275	4	0	06/28/16	-11.5	-80.1	12.1	0.077	0.014	0.081	0.084	0.012	0.036	0.031	0.311	0.421	0.421	30.814	
Mix-401	Stream	3960	7.23	145.3	06/26/16	-11.4	-78.7	12.8	0.128	0.022	0.194	0.250	0.006	0.035	0.369	0.257	1.036	1.036	70.744	
Mix-501	Stream	4061	7.87	61.7	06/26/16	-11.5	-78.9	13.3	0.098	0.026	0.090	0.104	0.007	0.032	0.047	0.377	0.512	0.510	38.126	

Table 2 June & July 2016 Results

February 2017																			
Sample Name	Sample Type	Elevation	pH	Specific Conductivity (µS/cm)	Date	$\delta^{18}O$ (‰)	$\delta^{2}H$ (‰)	D Excess	Na^{+}	K^{+}	Mg^{2+}	Ca^{2+}	F^{-}	Cl^{-}	SO_4^{2-}	HCO_3^{-}	ΣCations (meq/L)	ΣAnions (meq/L)	TDS (mg/L)
Melt-340	Glacier Melt	4471	6.82	27.3	2/7/17	-14.0	-99.1	12.8	0.150	0.006	0.031	0.056	0.013	0.077	0.029	0.182	0.331	0.331	23.382
R-Precip	Precip/ Overland Flow	4360			2/5/17	-9.0	-65.6	6.1	0.072	0.023	0.048	0.027	0.026	0.078	0.047	0.047	0.245	0.245	15.379
GW-305	Spring	4000	7.4	94.5	2/7/17	-13.4	-94.3	13.0	0.362	0.062	0.267	0.225	0.011	0.118	0.028	1.219	1.406	1.405	106.584
GW-323	Spring	4245	6.92	118.8	2/7/17	-12.6	-90.9	9.7	0.312	0.040	0.210	0.214	0.010	0.074	0.031	1.056	1.202	1.201	91.617
GW-S1	Spring	4283			2/4/17	-13.9	-93.1	18.3	0.433	0.036	0.221	0.254	0.010	0.052	0.047	1.264	1.420	1.420	109.322
GW-S101	Spring	3800	6.42	123.4	2/4/17	-13.0	-87.3	16.9	0.549	0.099	0.392	0.338	0.013	0.101	0.030	1.934	2.107	2.107	162.305
GW-S2	Spring	4277			2/4/17	-13.7	-96.3	13.0	0.444	0.061	0.224	0.267	0.011	0.072	0.034	1.337	1.487	1.487	114.949
GW-S20	Spring		8.31	208.1	2/4/17	-12.7	-93.6	8.3	0.485	0.050	0.470	0.360	0.010	0.072	0.089	1.914	2.193	2.174	166.216
GW-S3	Spring	4047	8.05	341.4	2/4/17	-13.1	-93.9	10.6	0.851	0.065	0.881	0.488	0.012	0.122	0.151	3.201	3.655	3.637	275.306
GW-S6	Spring	3992	8.17	40.9	2/4/17	-12.2	-86.8	10.6	0.277	0.044	0.172	0.137	0.012	0.094	0.024	0.779	0.939	0.933	70.680
GW-S8	Spring	4500			2/4/17	-13.9	-92.6	18.8	0.209	0.004	0.026	0.074	0.008	0.077	0.041	0.246	0.413	0.413	30.119
GW-S9	Spring	4320			2/4/17	-13.1	-87.3	17.8	0.258	0.047	0.191	0.223	0.009	0.113	0.093	0.825	1.132	1.132	83.932
GW-S7	Spring	4475	5.64	40	2/6/17	-12.0	-85.2	10.4	0.176	0.033	0.087	0.044	0.015	0.090	0.020	0.326	0.471	0.471	34.186
Mix-110 A	Stream	3895	7.8	161.7	2/4/17	-12.8	-91.2	11.3	0.364	0.044	0.346	0.205	0.010	0.084	0.169	1.075	1.510	1.507	110.809
Mix-110 B	Stream	3895			2/7/17	-12.4	-88.6	10.9	0.390	0.040	0.339	0.272	0.011	0.091	0.172	1.206	1.652	1.652	121.975
Mix-111 A	Stream	3912	7.93	178.8	2/4/17	-12.7	-88.6	12.7	0.351	0.050	0.354	0.256	0.010	0.052	0.119	1.316	1.621	1.615	121.596
Mix-111 B	Stream	3912	8.06	174.2	2/7/17	-12.4	-84.3	15.1	0.436	0.046	0.315	0.231	0.010	0.074	0.133	1.217	1.574	1.567	117.787
Mix-120	Stream	3960	8.03	177.9	2/4/17	-12.3	-90.0	8.1	0.372	0.047	0.378	0.289	0.010	0.073	0.193	1.277	1.753	1.746	129.487
Mix-121	Stream	3960	8.11	177.2	2/4/17	-13.0	-88.9	15.2	0.429	0.054	0.406	0.268	0.011	0.112	0.071	1.557	1.833	1.823	137.675
Mix-130	Stream	4061	8.16	126	2/4/17	-13.1	-88.9	16.2	0.338	0.060	0.250	0.206	0.010	0.068	0.049	1.127	1.310	1.302	99.857
Mix-131	Stream	4061	8.21	139.1	2/4/17	-13.4	-89.9	17.5	0.242	0.036	0.198	0.197	0.011	0.068	0.031	0.921	1.068	1.061	80.941
Mix-155	Stream	4550			2/7/17	-12.4	-82.7	16.1	0.226	0.010	0.045	0.073	0.011	0.056	0.026	0.351	0.470	0.470	35.328
Mix-301 A	Stream	3912	7.74	58.3	2/4/17	-14.4	-98.4	16.5	0.234	0.013	0.119	0.101	0.014	0.083	0.026	0.538	0.688	0.686	50.885
Mix-301 B	Stream	3912	8.1	58.8	2/7/17	-14.1	-95.6	17.0	0.164	0.013	0.119	0.098	0.013	0.046	0.026	0.498	0.611	0.608	45.546
Mix-306	Stream	4000	7.74	48.6	2/7/17	-14.1	-95.2	17.6	0.187	0.010	0.087	0.086	0.012	0.090	0.028	0.384	0.543	0.542	39.457
Mix-321	Stream	4235	7.5	30.6	2/7/17	-13.6	-96.6	12.1	0.159	0.006	0.032	0.046	0.012	0.060	0.054	0.141	0.322	0.322	22.586
Mix-330	Stream	4250	7.38	28.6	2/7/17	-13.8	-97.2	12.9	0.157	0.002	0.034	0.068	0.013	0.076	0.029	0.214	0.362	0.362	25.857
Mix-331	Stream	4275	7.2	27.8	2/7/17	-14.1	-97.1	16.0	0.204	0.003	0.030	0.053	0.014	0.081	0.030	0.219	0.374	0.374	26.841
Mix-332	Stream	4275	7.53	54.6	2/7/17	-12.3	-82.7	15.5	0.144	0.032	0.140	0.109	0.014	0.091	0.016	0.537	0.674	0.673	49.619
Mix-401	Stream	3960	7.79	180.4	2/4/17	-12.5	-83.6	16.1	0.378	0.093	0.522	0.688	0.009	0.062	0.606	1.605	2.892	2.888	209.803
Mix-501	Stream	4061	8.07	71.9	2/4/17	-12.8	-84.9	17.3	0.207	0.028	0.134	0.122	0.010	0.060	0.056	0.561	0.746	0.743	55.536
Mix-310	Stream	4145	7.6	39.4	2/7/17	-13.5	-98.3	9.8	0.184	0.003	0.062	0.075	0.014	0.071	0.028	0.319	0.461	0.460	33.508
Mix-311	Stream	4150	7.52	35	2/7/17	-13.8	-96.2	14.3	0.165	0.001	0.049	0.071	0.014	0.049	0.027	0.289	0.406	0.405	29.833
Mix-312	Stream	4150	7.34	120	2/7/17	-13.0	-90.0	13.7	0.265	0.058	0.286	0.156	0.012	0.095	0.022	1.053	1.205	1.204	90.495
Mix-320	Stream	4210	7.5	31.7	2/7/17	-13.9	-96.6	15.0	0.167	0.001	0.041	0.064	0.015	0.067	0.028	0.240	0.378	0.377	27.173

Table 3 February 2017 Results